BIOMEDICAL ENGINEERING

Understanding the pathology of dystonia by hardware emulation

By

Won Joon Eric Sohn

submitted to the

Department of Biomedical Engineering.

FACULTY OF THE USC GRADUATE SCHOOL

UNIVERSITY OF SOUTHERN CALIFORNIA

In Partial Fulfillment of the Requirements for the Degree

DOCTOR OF PHILOSOPHY

Principal Investigator: Terence D. Sanger

August 2015

To my parents,

For their unwavering support and love.

Acknowledgements

I would like to express my gratitude to many people who encouraged and helped me along the way, by walking beside me, to come to the journey of life this far. In particular, I am immensely indebted to my advisor Terence Sanger for his generous encouragement and guidance throughout my Ph.D. studies. His intellectual input and encouragement was sufficient to propel me to bring this study forward and helped me to defend the thesis. I am also thankful that he provided me a model for an excellent academic leader. I sincerely thank C. Minos Niu, friend, coworker and a mentor, for his inspiration and guidance throughout my doctoral studies. My successful thesis completion cannot be explained without his contribution. I would also like to express my gratitude to Francisco Valero-Cuevas for his whole-hearted support for this study and his personal encouragement. I take this opportunity to thank Alice Parker and Viktor Prasanna for not only serving as my dissertation committee members but also for generously spending their time to review this study. I wish to acknowledge the collaborative work of this study provided by Sirish Nandyala. I would like to thank my colleagues Matteo Bertucco, Diana Ferman, Aprille Tongol, Shanie Liyanagamage, Enrique Arguelles, Amber Dunning, Adam Feinman, Cassie Borish, Francesca Lunardini, Nasir Bhanpuri, Scott Young for their tremendous support and contribution to build a friendly and warm working environment, which should not be taken for granted. My gratitude also goes to Junseob Shin and people in the Light Ministry for their companionship in walking the narrow road of life. I am grateful for the support from the James S. McDonnel Foundation and National Institute of Neurologic Disorders and Stroke (R01-NS069214) and Biomedical Engineering Department from University of Southern California. I dedicate this work to my family for their endless love and patiently supporting me. I would like to mention my sincere gratitude for Hyemi Kim for her tremendous patience, love, inspiration and support. Lastly, I thank God for His providence. From the beginning of the doctoral study to this moment, I lacked nothing and I confess that His grace was sufficient for me.

Table of Contents

Table of Figures

Summary

Movement disorders are neurological conditions that affect speed, fluency, quality, and ease of movement in a negative direction. In that regard, investigating the neurological underpinning of the cause of the movement disorder is desirable. In case of secondary dystonia due to cerebral palsy, which causes involuntary movements, postures and prolonged muscle contraction, great difficulties in understanding the mechanism of the disorder have been posed by physiologically limited methods to conduct studies investigating the underlying neurological mechanism in human body. The emulation study presented here is one of the alternative responses to overcome the limitation posed by human studies. Centered on understanding the dystonia, three emulation studies were conducted. The first study proposes two plausible neurological mechanisms that lead to behavioral characteristics of dystonia and the outcomes from the emulation are compared with available data from subjects with dystonia (**chap 3**). The second study investigates the origin and development of motor overflow in focal hand dystonia in the context of spike-based plasticity mechanism (**chap 4**). The third study investigates the mechanism of constraint-induced therapy, a popular rehabilitative method in impaired biological systems with spike-based plasticity mechanism (**chap 5**). The studies utilize extremely fast and customizable hardware, which provides a unique benefit of accelerated emulation of the development of neurological system under tested circumstances. The first study is published in Journal of Neural Engineering. The second and third studies will be submitted to relevant journals (undecided at this point). The engineering technique and general methodology behind the use of programmable hardware (**chap 2**) is published in neural information processing systems (NIPS).

1 Introduction

1.1 Specific aim

There is currently no quantitative model of how the functions of neurons affect the specific abnormalities observed in movement disorders. Although clinical experience has provided insight in making qualitative prediction of how certain kinds of injury might lead to particular outcome, qualitative clinical insight itself is of little use if the goal is to make a specific prediction on the effect of particular impairment–whether they are neuronal or anatomic in nature, based on specific quantifiable physiological measures in individual patients. In order to study the causal relationship between a particular neuronal injury and the resultant immediate or long term biomechanical effect on the movement of a patient, we designed a multi-purpose high-speed emulation platform in scalable hardware. In this project, the platform is designed to emulate a subset of human sensorimotor nervous system that is speculated to be responsible for many movement disorders when it is impaired. Technical preparation section (chap 2) is dedicated for the methodological considerations. The structures of fundamental building blocks of the monosynaptic spinal stretch reflex pathway, including spiking neurons, spindle, muscle, and synapse, etc., as well as how fast computation are achieved in customizable hardware are described. Although the thesis is centered on understanding the pathology of dystonia, the third study (chap 5) extends the use of the technology to understand the mechanism for the popular rehabilitative method called constraint-induced therapy.

1.2 Background

Dystonia is a movement disorder in which involuntary sustained or intermittent muscle contractions cause twisting and repetitive movements, abnormal postures, or both (Fahn, 1988; Sanger *et al.*, 2003). Dystonia may involve one body region such as neck, face, leg or hand (focal dystonia), involve contiguous body regions (segmental dystonia) or involve broad regions of the body (generalized dystonia). Dystonia is called primary if the origin is known to be genetic or hereditary, and secondary if it results from structural damages or environmental factor that provided insult to the brain. Statistics shows that dystonia affects men, women, and children of all ages and backgrounds. It is estimated that there are 250,000 cases of idiopathic dystonia in the

U.S., 1:3,000 ratio, but the true prevalence could rise much above the reported number. Focal dystonia, 300 per millions, has 9 times the prevalence of generalized dystonia, among them cervical dystonia (CD) is the most frequent form among focal dystonia, writer's cramp (graphospasm) may be the most prevalent form of dystonia in the general population.

Dystonia causes a wide degree of disabilities and pain ranging from mild to severe. Dystonia can have a devastating impact on the quality of life of a patient and their family in that it debilitates physical and mental wellbeing as well as social function of a person, not to mention it can have a stigmatizing effect of living with such a visible disorder. At present there is no known cure, but only selective treatment options exist.

It is worth mentioning the term cerebral palsy (CP) in relation to dystonia since it is a blanket term for a group of movement and posture disorders that occur as a consequence of damages in the brain which is acquired at an early age when the brain is still developing – before birth, during birth and immediately after birth. Typically, dystonia is one feature or symptom associated with the syndrome of dyskinetic CP (a type of CP featuring variable movement that is involuntary) when it involves twisting and repetitive movements with fixed postures. Dyskinetic movement is called athetosis when it involves slow and 'stormy' movements, chorea when it involves dance-like irregular, unpredictable movements and so on.

In focal task-specific dystonia, a type of dystonia that is characterized by excessive muscle contraction producing abnormal posture during selective motor activity that often involve highly skilled, repetitive movements, is best known for focal hand dystonia, writer's cramp, musician's cramp or occupational dystonia because it interferes with the performance of the common tasks such as writing or playing a musical instrument. The origin and development of focal hand dystonia is emulated in the second study (chap 4).

In this project, we attempt to emulate some of the well-known characteristic features of dystonia including:

- hypertonia, an increased resistance to a passive perturbation
- prolonged time required to relax previously-contracted muscles
- reduced active range of motion
- development and perpetuation of motor overflow in focal hand dystonia

And also we attempt to emulate the mechanism of constraint-induced therapy in the hemiplegic CP.

In doing so, physiological evidence of dystonia will be cross-examined with clinical data.

1.3 Pathophysiology of dystonia

Neurophysiological mechanisms that lead to the clinical manifestations of dystonia are largely unknown. The exact cause of dystonia may be highly heterogeneous due to the variety of injuries identified in clinical examinations. It is classified as primary dystonia when no abnormality in the brain is observed and secondary dystonia when observable damage or lesion in the brain is seen which can be detected in the advanced neuroimaging techniques.

In specific, lesions in the basal ganglia, thalamus, or brain stem is likely to associate with secondary dystonia (Kahn *et al.*, 1985); and although not common, dystonia can sometimes appear after trauma or peripheral nerve injuries (Jankovic, 2001). Structural lesion could be a result from brain trauma, tumor, stroke, oxygen deprivation, infection, drug reactions, poisoning caused by lead or carbon monoxide (webmd.com). Brain injuries eventually develop into symptoms of dystonia, perhaps through the ensuing abnormality in the motor cortex. For example, injuries in basal ganglia have been found to increase the activity of the primary motor cortex (Playford *et al.*, 1993; Ceballos-Baumann, 1994), which could be attributable to impaired cortical inhibition (Hallett, 2011; Beck *et al.*, 2008; Ridding *et al.*, 1995). Clinical treatments also support the linkage between cortical injury and dystonia through the effect of motor cortex: high frequency stimulation and ablative surgeries in thalamus and GPi, the main basal ganglia outflow nucleus inhibitory to motor cortex, has been practiced to reduce cortical overactivity in dystonia patients. Moreover, long-latency stretch reflex (LLSR) has been found hyperactive during voluntary movements in childhood dystonia. Due to the possible linkage between motor cortical activity and stretch reflex (Suminski *et al.*, 2007; Morimoto *et al.*, 1984; Evarts and Tanji, 1976), it is possible that dystonia is not specific to injuries but can be sufficiently caused by a hyperactive LLSR pathway. Here we focus on testing this possibility using hardware emulation.

The causes of focal task-specific dystonia are unknown, but it is conjectured that the disorder is likely the combination of genetic and environmental factors. There is an evidence from studies in monkeys of disorganization of sensory cortical representation. In particular, monkeys with focal hand dystonia had neurons in the primary sensory cortex responded to tactile stimulation in more than one finger, in other words with a confused receptive field. It has been shown that the coupled use of two fingers for a long time could develop a de-differentiation in the cortical representational map in the primary sensory cortex. As such, the conjecture is that sensory abnormalities could contribute to the motor abnormality observed in dystonia. A previous study (Sanger and Merzenich, 2000) provided a computational model that explains how the sensory abnormalities could lead to motor manifestations of dystonia. Sanger hypothesized that task-specific dystonia such as writer's cramp has to do with an abnormally high gain in the sensorimotor loop that could take years to develop.

1.4 Impact of an early treatment of dystonia

In many cases the causes of CP are unknown and thus it is hard to prevent it. Because early signs of CP usually appear before a child reaches 3 years of age, physical impairment such as a problem in walking, lack of muscle coordination, hearing loss, speech and language disorders can cause severe developmental problem. Often children with CP develop into intellectual disability. Therefore, the treatment is aimed at helping child's motor and cognitive development and to prevent the occurrence of secondary injury (Sanger et al. 2008).

> For example, reduction in arm dystonia may permit improved handwriting, which may in turn allow better participation in school and thereby contribute to improved intellectual ability later in life. Thus, the neurologist can work with the child, the family, and other clinicians to facilitate and ensure developmental progress. Just as a physical therapist's efforts may be required to obtain maximum benefit from a neurologist's tone-reducing medication, a neurologist's efforts may be required to provide medications that permit continued progress in physical therapy (Sanger 2008)

Currently, there is no cure for CP, but there are many treatments that can increase the quality of life for kids with CP. In dystonia, pharmacologic therapies including treating Levodopa, anticholinergic medication, baclofen, clonazepam as well as nonpharmacological therapies such

as desensitization, limb immobilization which aim at restructuring the cortical map with learning based on the principle of neuroplasticity. Injection of botulinum toxin, which targets local muscle with a several months of short-lasting period, is currently a mainstay of treatment for most focal dystonia. Surgical treatment is not often suggested due to its risk factors but targeting the anatomical source of a disturbance with deep brain stimulation, pallidotomy has been successfully performed for many decades.

1.5 The value of emulation in studying injury in nervous system leading to abnormal motor behavior

1. Emulation study allows us to answer questions about the *sufficient* mechanism responsible for the movement disorders that have a neurological origin.
2. We can emulate specific disease hypotheses without emulating whole brain by building a neural circuit around a structure that is relatively well-known, such as stretch reflex pathway.
3. We can conduct experiment that is generally prohibited in human studies due to practical and ethical reasons.
4. We can use the emulator to study not only the immediate effects of a change in physiological parameter to account for any behavior abnormalities but also the long-term plasticity effect of certain injury or intervention to the system.
5. The only way to test and characterize the high-level behavior of a brain model is to actually build the closed loop between the artificial nervous system and the body (plant) acting in an environment and to interrogate the model through a well-designed experiment.
6. Once the general purpose emulation platform is built, we can identify the causal mechanism by manipulating specific brain regions, such as simulating the effect of brain lesion, neuronal injury, cell death, pharmacologic treatment, rehabilitation, etc.

2 Technical preparation

Disclaimer: This section is originally published in neural information processing systems (NIPS). C.M. Niu, S. Nandyala, W.J. Sohn, and T.D. Sanger, Multi-scale Hyper-time Hardware Emulation of Human Motor Nervous System Based on Spiking Neurons using FPGA. Advances in Neural Information Processing Systems 25 (2012) 37-45.

Our central goal in building a high-speed emulation platform in hardware is to quantify the long-term progression of pediatric neurological diseases, such as a typical 10-15 years progression of child dystonia. To this purpose, quantitative models are convincing only if they can provide multi-scale details ranging from neuron spikes to limb biomechanics. The models also need to be evaluated in hyper-time, i.e. significantly faster than real-time, for producing useful predictions. We designed a platform with digital VLSI hardware for multiscale hyper-time emulations of human motor nervous systems. The platform is constructed on a scalable, distributed array of Field Programmable Gate Array (FPGA) devices. All devices operate asynchronously with 1 millisecond time granularity, and the overall system is accelerated to 365x real-time. Each physiological component is implemented using models from well documented studies and can be flexibly modified. Thus the validity of emulation can be easily advised by neurophysiologists and clinicians. The following sections present the methodology of building FPGA modules in correspondence to components of a monosynaptic spinal loop. Results of emulated activities are shown. The paper also discusses the rationale of approximating neural circuitry by organizing neurons with sparse interconnections. In conclusion, our platform allows introducing various abnormalities into the neural emulation such that the emerging motor symptoms can be analyzed. It compels us to test the origins of childhood motor disorders and predict their long-term progressions.

2.1 Challenges of studying developmental motor disorders

There is currently no quantitative model of how a neuropathological condition, which mainly affects the function of neurons, ends up causing the functional abnormalities identified in clinical examinations. The gap in knowledge is particularly evident for disorders in developing human nervous systems, i.e. childhood neurological diseases. In these cases, the ultimate clinical effect of cellular injury is compounded by a complex interplay among the child's injury, development, behavior, experience, plasticity, etc. Qualitative insight has been provided by clinical experiences into the association between particular types of injury and particular types of outcome. Their quantitative linkages, nevertheless, have yet to be created — neither in clinic nor in cellular physiological tests. This discrepancy is significantly more prominent for individual child patients, which makes it very difficult to estimate the efficacy of treatment plans. In order to understand the consequence of injury and discover new treatments, it is necessary to create a modeling toolset with certain design guidelines, such that child neurological diseases can be quantitatively analyzed.

Perhaps more than any other organ, the brain necessarily operates on multiple spatial and temporal scales. On the one hand, it is the neurons that perform fundamental computations, but neurons have to interact with large-scale organs (ears, eyes, skeletal muscles, etc.) to achieve global functions. This multi-scale nature worth more attention in injuries, where the overall deficits depend on both the cellular effects of injuries and the propagated consequences. On the other hand, neural processes in developmental diseases usually operate on drastically different time scales, e.g. spinal reflex in milliseconds versus learning in years. Thus when studying motor nervous systems, mathematical modeling is convincing only if it can provide multi-scale details, ranging from neuron spikes to limb biomechanics; also the models should be evaluated with time granularity as small as 1 millisecond, meanwhile the evaluation needs to continue trillions of cycles in order to cover years of life.

It is particularly challenging to describe the multi-scale nature of human nervous system when modeling childhood movement disorders. Note that for a child who suffered brain injury at birth, the full development of all motor symptoms may easily take more than 10 years. Therefore the millisecond-based model needs to be evaluated significantly faster than real-time, otherwise

the model will fail to produce any useful predictions in time. We have implemented realistic models for spiking motoneurons, sensory neurons, neural circuitry, muscle fibers and proprioceptors using VLSI and programmable logic technologies. All models are computed in Field Programmable Gate Array (FPGA) hardware in 365 times real-time. Therefore one year of disease progression can be assessed after one day of emulation. This section presents the methodology of building the emulation platform. The results demonstrate that our platform is capable of producing physiologically realistic multi-scale signals, which are usually scarce in experiments. Successful emulations enabled by this platform will be used to verify theories of neuropathology. New treatment mechanisms and drug effects can also be emulated before animal experiments or clinical trials.

2.2 Methodology of multi-scale neural emulation

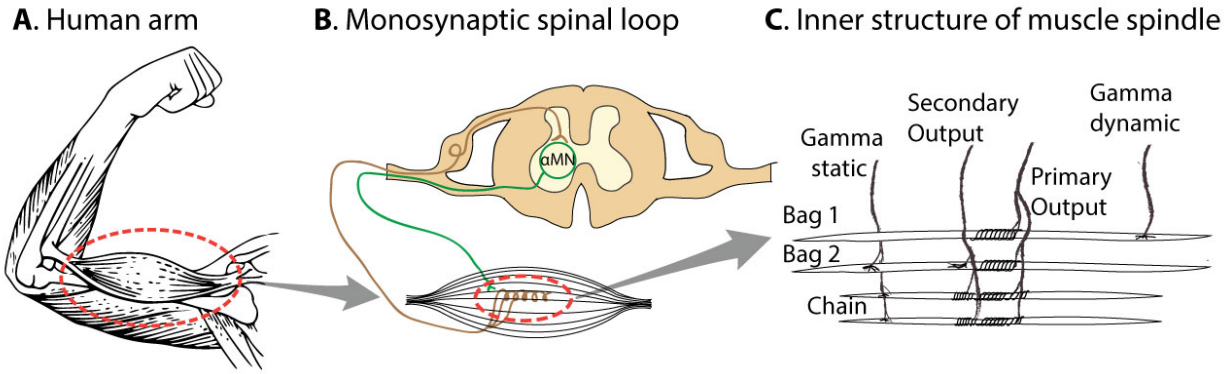

Figure 1: Illustration of the multi-scale nature of motor nervous system.

The motor part of human nervous system is responsible for maintaining body postures and generating voluntary movements. The multi-scale nature of motor nervous system is illustrated in **Error! Reference source not found.**. When the elbow (**Error! Reference source not found.**A) is maintaining a posture or performing a movement, the involved muscle produces force based on how much spiking excitation is delivered from its motoneurons (**Error! Reference source not found.**B). The motoneurons are regulated by their own sensory input, which in-turn comes from the proprioceptors residing in the muscle. As the primary sensory organ found in skeletal muscles, a muscle spindle is another complex system that has its own microscopic Multiple-Input-Multiple-Output structure (**Error! Reference source not found.**C). Spindles continuously provide information about the length and lengthening speed of the muscle fiber. This section uses the monosynaptic spinal loop as an example for explaining the methodology of multi-scale hyper-time neural emulation in hardware. Additional structures can be added to the backbone platform using similar methods described here.

2.2.1 Modularized architecture for multi-scale models

Decades of studies on neurophysiology provided an abundance of models characterizing different components of the human motor nervous system. The functional differentiation between physiological components allowed us to model the motor nervous system as

concatenated structures, each of which maps input signals to the output. In particular, in a monosynaptic spinal loop illustrated in **Error! Reference source not found.**B, stretching the uscle will elicit a chain of physiological activities as: muscle stretch ⇒ spindle ⇒ sensory neuron ⇒ synapse ⇒ motoneuron ⇒ muscle contraction. The adjacent components must have compatible interfaces, and the interfacing variables must also be physiologically realistic. In our design, each component is mathematically described in Table 1:

Table 1: Functional definition of neural models

COMPONENT	MATHEMATICAL DEFINITION
Neuron	$S(t) = f_{\text{neuron}}(I, t)$
Synapse	$I(t) = f_{\text{synapse}}(S, t)$
Muscle	$T(t) = f_{\text{muscle}}(S, L, \dot{L}, t)$
Spindle	$A(t) = f_{\text{spindle}}(L, \dot{L}, \Gamma_{\text{dynamic}}, \Gamma_{\text{static}}, t)$

As can be seen, all components are modeled as black-box functions that map the inputs to the outputs. The meanings of these mathematical definitions are explained below. This design allows existing physiological models to be easily inserted and switched. In all models the input signals are time-varying, e.g. I = I(t); L = L(t) , etc. The argument of t in input signals are omitted throughout this paper.

2.2.2 Selection of models for emulation

Models were selected in consideration of their computational cost, physiological verisimilitude, and whether it can be adapted to the mathematical form defined in Table 1.

Model of Neuron

Neurons take post-synaptic current I as the input, and produce a binary spike train S in the output. The neuron model adopted in the emulation was developed by Izhikevich (Izhikevich, 2003b):

$$v' = 0.04v^2 + 5v + 140 - u + I \quad (1)$$

$$u' = a(bv - u) \quad (2)$$

$$\text{if } v = 30 \text{ mV}, \text{ then } v \leftarrow c,\ u \leftarrow u + d$$

where the output is the action potential v, which directly produces a binary spike train; a; b; c; d are model parameters that need to be tuned based on the neuron's firing properties. Note that in Izhikevich model the action potential v is in millivolts and the time is in milliseconds. Since all other models require SI units the coefficients in eq.1 need to be adjusted.

Model of Synapse

When a pre-synaptic neuron fires, i.e. S(0) = 1, an excitatory synapse subsequently produces an Excitatory Post-Synaptic Current (EPSC) that drives the post-synaptic neuron. Neural recording of hair cells in rats (Glowatzki and Fuchs, 2002) provided evidence that the time profile of EPSC can be well characterized using the equations below:

$$I(t) = \begin{cases} V_m \times \left(e^{-\frac{t}{\tau_d V_m}} - e^{-\frac{t}{\tau_r V_m}}\right) & \text{if } t \geq 0 \\ 0 & \text{otherwise} \end{cases}$$

The key parameters in a synapse model is the time constants for rising (τr) and decaying (τd). In our emulation τr = 0.001s and τr = 0.003s.

Model of Muscle force and electromyograph (EMG)

The primary effect of skeletal muscle is converting the motoneuron spikes S into a force T depending on the instantaneous length L and lengthening speed $\dot{L}$ of the muscle itself. We used Hill's muscle model in the emulation with parameter tuning described in (Shadmehr and Wise, 2005). Another measurable output of muscle is electroencephalograph (EMG). EMG is the small skin current polarized by motor unit action potential (MUAP) when it travels along muscle fibers. Models exist to describe the typical waveform picked by surface EMG electrodes. In this project we chose to implement the one described in (Fuglevand *et al.*, 1993b). We further implement the muscle to produce the recruitment order and size principles observed in real physiological data. It has been well known that when a voluntary motor command is sent to the motoneuron pool, the motor units are recruited in an order that small ones get recruited first followed by the big ones (Henneman, 1957). Further detail can be found in Figure 4 and Figure 6.

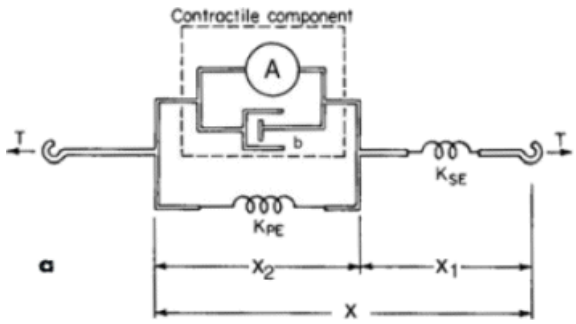

$$\dot{T} = \frac{K_{SE}}{b}\left(K_{PE}\Delta x + b\dot{x} - (1 + \frac{K_{PE}}{K_{SE}})T + A \right)$$

Hill's muscle model is mathematically described as the differential equation above. Recaptured in Shadmehr and Arbib (1992).

T Muscle Tension.

A Active tension applied by stimulation of membrane voltage.

K_{se} Serial spring constant (SE).

K_{pe} Parallel spring constant (PE).

B Damping Coefficient.

X Muscle Length.

Model of Proprioceptor

Spindle is a sensory organ that provides the main source of proprioceptive information. As can be seen in Fig.1C, a typified spindle model produces two afferent outputs (primary Ia and secondary II) according to its gamma fusimotor drives ($\Gamma_{dynamic}$ and Γ_{static}) and muscle states (L and $\dot{L}$). Spindle model needs to account for various types of stretch inputs, which requires complex dynamic model. The complexity originated from the non-linear nature of muscle fibers and their coupling with spike generating spots. On representative model that numerically approximates the spindle dynamics was developed by Mileusnic et al. (Mileusnic *et al.*, 2006b). The model used differential equations to characterize a typical cat soleus spindle. Eqs.3-9 present a subset of this model for spindle bag1 fiber:

$$\dot{x_0} = \left(\frac{\Gamma_{\text{dynamic}}}{\Gamma_{\text{dynamic}} + \Omega^2_{\text{bag1}}} - x_0 \right) / \tau \quad (3)$$

$$\dot{x_1} = x_2 \quad (4)$$

$$\dot{x_2} = \frac{1}{M} \left[T_{SR} - T_B - T_{PR} - \Gamma_1 x_0 \right] \quad (5)$$

where

$$T_{SR} = K_{SR}(L - x_1 - L_{SR0}) \quad (6)$$

$$T_B = (B_0 + B_1 x_0) \cdot (x_1 - R) \cdot CSS \cdot |x_2|^{0.3} \quad (7)$$

$$T_{PR} = K_{PR}(x_1 - L_{PR0}) \quad (8)$$

$$CSS = \left(\frac{2}{1 + e^{-1000 x_2}} \right) - 1 \quad (9)$$

2.2.3 Neuron connectivity with sparse interconnections

Although the number of spinal neurons (~1 billion) is significantly less compared to that in the brain cortex (~100 billion), a fully connected spinal network still means approximately 2 trillion synaptic endings (Gelfan *et al.*, 1970). Implementing such a huge number of synapses imposes a major challenge, if not impossible, given limited hardware resource. In this platform we approximated the neural connectivity by sparsely connecting sensory neurons to motoneurons as parallel pathways. We do not attempt to introduce the full connectivity. The rationale is that in a neural control system, the effect of a single neuron can be considered as mapping current state x to change in state x through a band-limited channel. Therefore when a collection of neurons are firing stochastically, the probability of _ x depends on both x and each neuron's firing behavior s (s = 1 when spiking, otherwise s = 0), as such:

$$p(\dot{x}|x, s) = p(\dot{x}|s = 1)p(s = 1|x) + p(\dot{x}|s = 0)p(s = 0|x)$$

Eq.10 is by definition a master equation that determines a probability flow on the state. From the Kramers-Moyal expansion we can associate this probability flow with a partial differential equation for the change in probability density:

$$\frac{\partial}{\partial t} p(x,t) = \frac{\partial}{\partial x} \left(D_1(x) p(x,t) \right) + \frac{\partial^2}{\partial x^2} \left(D_2(x) p(x,t) \right) + \cdots \quad (11)$$

It has been shown in (Sanger, 2010, 2011b) that when higher order (>2) fluctuations in the probability density are ignored, according to the Fokker-Planck equation, the probability flow can be deterministically described using a linear operator L:

$$\frac{\partial}{\partial t}p(x,t) = \mathcal{L}p(x,t) \tag{12}$$

Due to the linearity, various Ls can be superimposed to achieve complex system dynamics (illustrated in **Error! Reference source not found.**A)

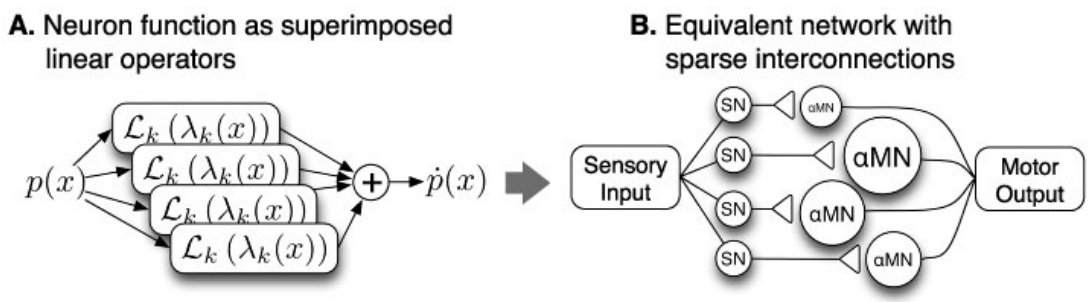

Figure 1.5. Functions of neuron population can be described as the combination of linear operators (A). Therefore the original neural function can be equivalently produced by sparsely connected neurons formalizing parallel pathways (B).

As a consequence, the statistical effect of two fully connected neuron populations is equivalent to ones that are only sparsely connected, as long as the probability flow can be described by the same L. In particular, in a movement task it is the statistical effect from the neuron ensemble to skeletal muscles that determines the global behavior. Therefore we argue that it is feasible to approximate the spinal cord connectivity by sparsely interconnecting sensory and motor neurons (Fig.1.5B). Here a pool of homogenous sensory neurons projects to another pool of homogeneous motoneurons. Pseudorandom noise is added to the input of all homogeneous neurons within a population. It is worth noting that this approximation significantly reduces the number of synapses that need to be implemented in hardware.

2.2.4 Hardware implementation on FPGA

We select FPGA as the implementation device due to its inherent parallelism that resembles the nervous system. FPGA is favored over GPU or clustered CPUs because it is relatively easy to network hundreds of nodes with customizable protocols. The platform is distributed on multiple nodes of Xilinx Spartan-6 devices. The interfacing among FPGAs and computers is created using OpalKelly development board XEM6010. The dynamic range of variables is tight in the selected models of Izhikevich neuron, synapse and EMG, which helps maintaining the accuracy even when evaluated in 32-bit fixed-point arithmetics. The spindle model, in contrast, requires floating-point arithmetics due to its wide dynamic range and complex calculations (see eq.3-9). Hyper-time computations with floating-point numbers are resource consuming and therefore need to be implemented with special attentions.

2.2.5 Floating-point arithmetics in combinational logic

Our arithmetic implementations are compatible with IEEE-754 standard. Typical floating-point arithmetic IP cores are either pipe-lined or based on iterative algorithms such as CORDIC, all of which require clocks to schedule the calculation. In our platform, no clock is provided for model evaluations thus all arithmetics need to be executed in pure combinational logic. Taking advantage of combinational logic allows all model evaluations to be 1) fast, the evaluation time depends entirely on the propagating and settling time of signals, which is on the order of microseconds, and 2) parallel, each model is evaluated on its own circuit without waiting for any other results.

Our implementations of adder and multiplier are inspired by the open source project "Free FloatingPoint Madness", available at http://www.hmc.edu/chips/. Please contact the authors of this paper if the modified code is needed.

Fast combinational floating-point division

Floating-point division is even more resource demanding than multiplications. We avoided directly implementing the dividing algorithm by approximating it with additions and multiplications. Our approach is inspired by an algorithm described in (Lomont, 2003), which

provides a good approximation of the inverse square root for any positive number x within one Newton-Raphson iteration:

$$Q(x) = \frac{1}{\sqrt{x}} \approx x(1.5 - \frac{x}{2} \cdot x^2) \quad (x > 0) \tag{13}$$

Q(x) can be implemented only using floating-point adders and multipliers. Thereby any division with a positive divisor can be achieved by concatenating two blocks of Q(x):

$$\frac{a}{b} = \frac{a}{\sqrt{b} \cdot \sqrt{b}} = a \cdot Q(b) \cdot Q(b) \quad (b > 0) \tag{14}$$

This algorithm has been adjusted to also work with negative divisors (b < 0).

Numerical integrators for differential equations

Evaluating the instantaneous states of differential equation models require a fixed-step numerical integrator. Euler's Method was chosen to balance the numerical error and FPGA usage:

$$\dot{x} = f(x,t) \tag{15}$$

$$x_{n+1} = x_n + Tf(x_{n+1}, t_{n+1}) \tag{16}$$

where T is the sampling interval. f(x, t) is the derivative function for state variable x.

2.2.6 Asynchronous spike-based communication between FPGA chips

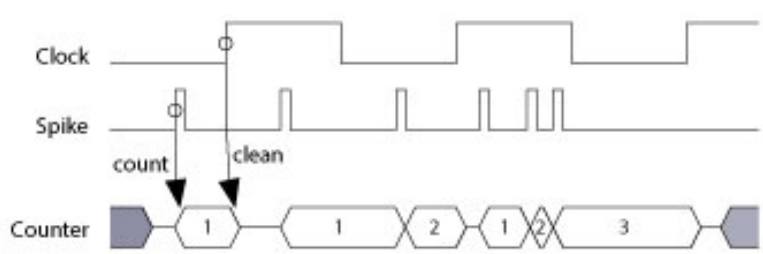

Figure 2: Timing diagram of asynchronous spike-based communication

FPGA nodes are networked by transferring 1-bit binary spikes to each other. Our design allowed the sender and the receiver to operate on independent clocks without having to synchronize. The timing diagram of the spike-based communication is shown in fig. 2. The sender issues Spike on with a pulse width of $1/(365 \times F_{emu})$ second. Each Spike then triggers a counting event on the receiver, meanwhile each Clock first reads the accumulated spike count and cleans the counter afterwards. Note that the phase difference between Spike and Clock is not predictable due to asynchronicity. Although it is possible to lose a spike during the setup time of latching the counter, it only loses a spike per clock cycle at most, which is effectively negligible considering the nature of robustness in spike-modulated signal transmission.

2.2.7 Serialize neuron evaluations within a homogeneous population

Different neuron populations are instantiated as standalone circuits. Within in each population, however, homogeneous neurons mentioned in Section 2.5 are evaluated in series in order to optimize FPGA usage. Within each FPGA node all modules operate synchronously, meaning that all updating events are triggered by a central clock. Therefore the maximal number of neurons that can be serialized (N_{serial}) per block is restrained by the following relationship:

$$F_{fpga} = C \times N_{serial} \times 365 \times F_{emu} \tag{17}$$

Here F_{fpga} is the fastest clock rate that a FPGA can operate on; C = 4 is the minimal clock cycles needed for updating and storing each state variable in the block RAM; F_{emu} = 1 kHz is the time granularity of emulation (1 millisecond), and $365 \times F_{emu}$ represents 365x real-time. Consider that Xilinx Spartan-6 FPGA devices peaks at 200MHz central clock frequency, the theoretical maximum of neurons that can be serialized per neuron block is:

$$N_{serial} \leqslant 200\ \text{MHz}/(4 \times 365 \times 1\ \text{kHz}) \approx 137 \tag{18}$$

In the current design we choose N_{serial} = 128.

2.3 Results: emulated activities of motor nervous system

Figure 3 shows pictures of a working FPGA node, two networked nodes and a screenshot of the software front-end. Each FPGA node is able to emulate monosynaptic spinal loops consisting of

1,024 sensory neurons and 1,024 motor neurons (which is 8 blocks of neurons). The spike-based asynchronous communication is successful between two FPGA nodes. Note that the emulation has to be significantly slowed down for on-line plotting. When the emulation is at full speed (365x real-time) the software front-end is not able to visualize the signals due to limited data throughput.

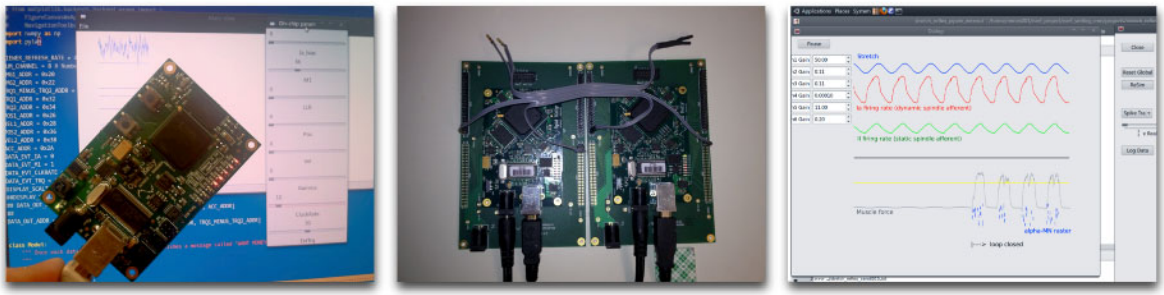

Figure 3. The neural emulation platform in operation. Left: One working FPGA node. Center: Two FPGA nodes networked using asynchronous spiking protocol. Right: Software front-end displaying multi-scale signals.

The emulation platform successfully created multi-scale information when the muscle is externally stretched (Figure 4A). We also tested if our emulated motor system is able to produce the recruitment order and size principles observed in real physiological data. It has been well known that when a voluntary motor command is sent to the motoneuron pool, the motor units are recruited in an order that small ones get recruited first followed by the big ones (Henneman, 1957). The comparison between our results and real data are shown in Figure 4B, where the top panel shows decoded motor unit activities from real human EMG (De Luca and Hostage, 2010), and the bottom panel shows 20 motor unit activities emulated using our platform. No qualitative difference was found.

2.4 Discussion and future work

We designed a hardware platform for emulating the multi-scale motor nervous activities in hypertime. We managed to use one node of single Xilinx Spartan-6 FPGA to emulate monosynaptic spinal loops consisting of 2,048 neurons, associated muscles and proprioceptors.

The neurons are organized as parallel pathways with sparse interconnections. The emulation is successfully accelerated to 365x real-time. The platform can be scaled by networking multiple FPGA nodes, which is enabled by an asynchronous spike-based communication protocol. The emulated monosynaptic spinal loops are capable of producing reflex-like activities in response to muscle stretch. Our results of motor unit recruitment order are compatible with the physiological data collected in real human subjects. There is a question of whether this stochastic system turns out chaotic, especially with accumulated errors from Backward Euler's integrator. Note that the firing property of a neuron population is usually stable (Sanger, 2011b) even with explicit noise, and spindle inputs are updated by measurement continuously so the integrator errors are corrected at every iteration. To our knowledge, the system is not critically sensitive to the initial conditions or integrator errors. This question, however, is both interesting and important for in-depth investigations in the future.

It has been shown (Raphael *et al.*, 2010) that replicating classic types of spinal interneurons (propriospinal, Ia-excitatory, Ia-inhibitory, Renshaw, etc.) is sufficient to produce stabilizing responses and rapid reaching movement in a wrist. Our platform will introduce those interneurons to describe the known spinal circuitry in further details. Physiological models will also be refined as needed. For the purpose of modeling movement behavior or diseases, Izhikevich model is a good balance between verisimilitude and computational cost. When testing drug effects along disease progression, however, neuron models are expected to cover sufficient molecular details including how neurotransmitters affect various ion channels. With the advancing of programmable semiconductor technology, it is expected to upgrade our neuron model to Hodgkin-Huxley's. For the muscle models, Hill's type of model does not fit the muscle properties accurately enough when the muscle is being shortened. Alternative models will be tested.

Other studies showed that the functional dexterity of human limbs – especially in the hands – is critically enabled by the tendon configurations and joint geometry (Valero-Cuevas *et al.*, 2007). As a result, if our platform is used to understand whether known neurophysiology and biomechanics are sufficient to produce able and pathological movements, it will be necessary to use this platform to control human-like limbs. Since the emulation speed can be flexibly adjusted

from arbitrarily slow to 365x real-time, when speeded to exactly 1x real-time the platform will function as a digital controller with 1kHz refresh rate.

The main purpose of the emulation is to learn how certain motor disorders progress during childhood development. This first requires the platform to reproduce motor symptoms that are compatible with clinical observations. For example it has been suggested that muscle spasticity in rats is associated with decreased soma size of motoneurons (Brashear and Elovic, 2010), which presumably reduced the firing threshold of neurons. Thus when lower firing threshold is introduced to the emulated motoneuron pool, similar EMG patterns as in (Levin and Feldman, 1994) should be observed. It is also necessary for the symptoms to evolve with neural plasticity. In the current version we presume that the structure of each component remains time invariant. In the future work spike-timing-dependent plasticity (STDP) will be introduced such that all components are subject to temporal modifications.

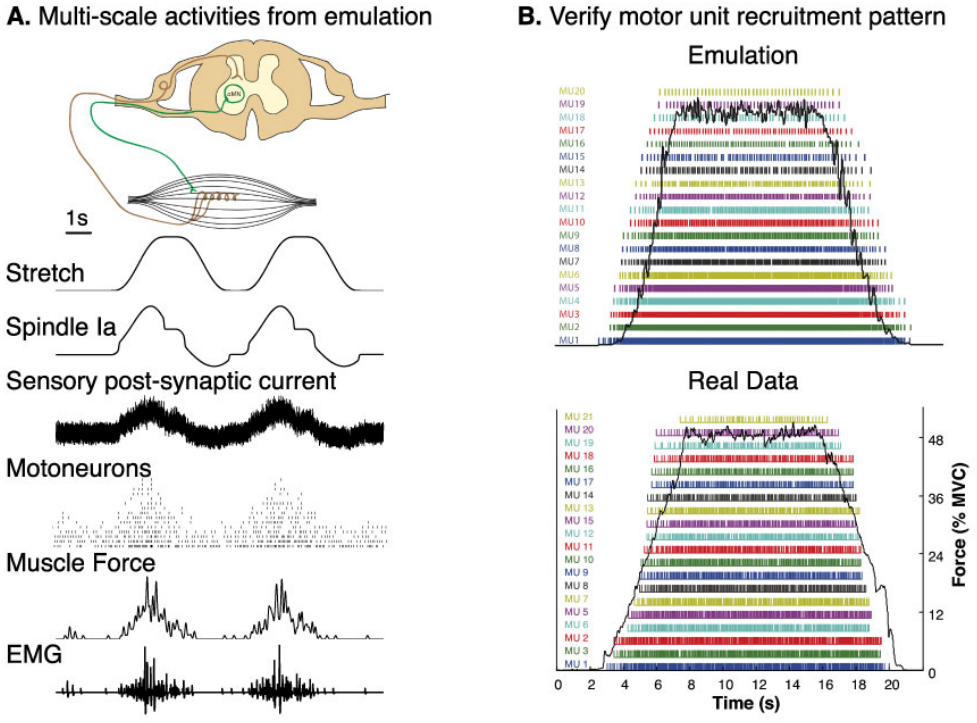

Figure 4: A) Physiological activity emulated by each model when the muscle is sinusoidally stretched. B) Comparing the emulated motor unit recruitment order with real experimental data.

3 Study 1: What is the mechanism of childhood secondary dystonia due to cerebral palsy?

Publication Citation:

W.J. Sohn, C.M. Niu, and T.D. Sanger, Increased long-latency reflex activity as a sufficient explanation for childhood hypertonic dystonia: a neuromorphic emulation study. Journal of neural engineering 12 (2015) 036010.

Increased long-latency reflex activity as a sufficient explanation for childhood hypertonic dystonia: a neuromorphic emulation study

Won J. Sohn[1†], Chuanxin M. Niu[4†], Terence D. Sanger[1,2,3*]

† The authors equally contributed to the study

[1]Department of Biomedical Engineering, [2]Biokinesiology, and [3]Neurology, University of Southern California, 1042 Downey Way, Los Angeles, California, 90089
[4]Department of Rehabilitation, Ruijin Hospital, School of Medicine, Shanghai Jiao Tong University, Shanghai, China

*** E-mail:** tsanger@usc.edu

Abstract. *Objective.* Childhood dystonia is a movement disorder that interferes with daily movements and can have a devastating effect on quality of life for children and their families. Although injury to basal ganglia is associated with dystonia, the neurophysiological mechanisms leading to the clinical manifestations of dystonia are not understood. Previous work suggested that long-latency stretch reflex (LLSR) is hyperactive in children with hypertonia due to secondary dystonia. We hypothesize that abnormal activity in motor cortices may cause an increase in the long-latency stretch reflex leading to hypertonia. *Approach.* We modelled two possibilities of hyperactive LLSR by either creating a tonic involuntary drive to cortex, or increasing the synaptic gain in cortical neurons. Both models are emulated using programmable Very-Large-Scale-Integrated-circuit (VLSI) hardware to test their sufficiency for producing dystonic symptoms. The emulation includes a joint with two Hill-type muscles, realistic muscle spindles, and 2,304 Izhikevich-type spiking neurons. The muscles are regulated by a monosynaptic spinal pathway with 32ms delay and a long-latency pathway with 64ms loop-delay representing transcortical/supra-spinal connections. *Main results.* When the limb is passively stretched, both models produce involuntary resistance with increased antagonist EMG responses similar to human data; also the muscle relaxation is delayed similar to human data. Both

models predict reduced range of motion in voluntary movements. *Significance.* Although our model is a highly simplified and limited representation of reflex pathways, it shows that increased activity of the long-latency stretch reflex is by itself sufficient to cause many of the features of hypertonic dystonia.

3.1 Introduction

Dystonia is an involuntary alteration in the pattern of muscle activation during voluntary movement or maintenance of posture (Sanger *et al.*, 2003). In secondary dystonia, symptoms are often caused by injury to cortex, thalamus or basal ganglia (Colton *et al.*, 2002; Sanger *et al.*, 2003; Breakefield *et al.*, 2008), but the link between injury to these areas and the resulting clinical symptoms remains unclear. Previous work suggested that the long-latency stretch reflex (LLSR) is abnormally increased in childhood hypertonia due to secondary dystonia (Kukke and Sanger, 2011). We do not know whether the elevated LLSR is a cause of dystonia or merely an associated phenomenon. To explore this question, we test using simulation whether elevation of LLSR in a highly simplified model is sufficient to cause features of hypertonic dystonia, including resistance to passive stretch, delayed muscle relaxation, and reduced range of motion in voluntary movement.

The eventual manifestation of secondary dystonia may be attributable to increased activity in the motor cortex. Brain imaging provides the direct evidence of increased motor cortical activity in secondary dystonia (Ceballos-Baumann, 1994); other studies using transcranial magnetic stimulation (TMS) over motor cortex also show increased corticospinal excitability (Trompetto *et al.*, 2012; Kojovic *et al.*, 2013). In other forms of dystonia, it was found that patients exhibit reduced intracortical inhibition (Ridding *et al.*, 1995; Edwards *et al.*, 2003; Quartarone *et al.*, 2003; Prescott *et al.*, 2013) and increased cortical plasticity (Quartarone *et al.*, 2003; Edwards *et al.*, 2006; Weise *et al.*, 2006; Prescott *et al.*, 2013). The association between increased motor cortex activity and secondary dystonia could be due to an inhibitory effect of basal ganglia over motor cortex, possibly through thalamocortical pathways (DeLong and Wichmann, 2007; Hallett, 2011). This association is supported by clinical treatments for patients of dystonia, where dystonic symptoms were alleviated after ablative surgeries (Imer *et al.*, 2005; Hashimoto *et al.*, 2010) or deep brain stimulations (McIntyre *et al.*, 2004; Vidailhet *et al.*, 2005; Krauss, 2010; Air *et al.*, 2011) in the globus pallidus internus (GPi). Therefore in this emulation study we focus on how different cortical parameters lead to abnormal reflex behaviors similar to dystonia.

One possible outcome of increased motor cortex excitability is to elevate LLSR due to the role of primary motor cortex in reflex modulation (Evarts and Tanji, 1976; Lee *et al.*, 1983; Morimoto *et al.*, 1984; Capaday *et al.*, 1991; Matthews, 1991; Palmer and Ashby, 1992;

Pruszynski *et al.*, 2011). Therefore loss of inhibition in the motor cortex may leak an uncontrolled drive that either lowers the threshold of cortical cells or amplifies their response to afferent input. In both cases the activity of LLSR is expected to increase. In our previous studies, children with secondary dystonia showed increased reflex activity (van Doornik *et al.*, 2009) with long-latency responses (Kukke and Sanger, 2011), which could potentially cause hypertonia in this population. Taken together, existing evidence suggests that the hypertonic manifestation of secondary dystonia may be directly caused by elevated LLSR, which potentially results from many insults including increased motor cortex excitability after injuries in basal ganglia, cerebellum, thalamus, or sensory cortices.

To determine whether this is a plausible mechanism for hypertonic dystonia and not merely an epiphenomenon, we emulate the effect of increased cortical drive or increased afferent input to cortex. The term "emulation" is used to disambiguate from numerical simulations (usually slower than real-time) in software. We do not include a model of the basal ganglia, because we seek to test whether any structure projecting to and causing uncontrolled firing of motor cortical areas could potentially be a cause of dystonia. Other possible areas with oligosynaptic connectivity to motor cortices include prefrontal cortex, primary sensory cortex, thalamus, and cerebellum. We choose the synthetic analysis approach primarily because it allows flexible ways of introducing abnormalities that are physiologically plausible but difficult to obtain from human subjects in laboratory. It also provides information about physiological components at drastically different physical and temporal scales, including millisecond time-scale action potentials in microscopic neurons, and seconds-long contractions in whole muscles. We leverage the recently available technology of programmable Very-Large-Scale-Integrated-circuit (VLSI), which allows us to create emulations of neurons that communicate using spikes, with the ability to increase the number of emulated neurons without sacrificing speed. With VLSI, the neural circuitry and connectivity is also easily modifiable. In this study, we first built a small set of structures to create a non-impaired system with functioning reflexes including a short-latency loop representing the spinal monosynaptic reflex pathway, and a long-latency loop representing the supra-spinal/transcortical pathway. Due to the aforementioned contribution of motor cortex to long-latency response, we selectively increase the activity of the transcortical pathway to emulate a hyperactive LLSR. We hypothesize two possible causes of hyperactive LLSR. First, the cortical neurons may receive a tonic drive that is either sub- or supra-threshold but overall

depolarizing. This *TONIC* model makes the cortical neurons easier to fire or achieve high firing rate, even when receiving the same level of excitatory post-synaptic current (EPSC) from sensory feedback. Second, the synaptic gain of cortical neurons may uniformly increase, which augments the excitability of cortical neurons. This *HI-GAIN* model amplifies the EPSC provided by ascending sensory feedback, which eventually elevates the overall activity of the transcortical pathway. These two mechanisms are the major categories of abnormality that can lead to increases in LLSR at the cellular level, so we modeled both. We argue it is important to test if different mechanisms are both sufficient to produce dystonia, which may eventually help sub-categorizing secondary dystonia. In both models, the spinal pathway remains intact and therefore only the long-latency component in the reflex pathway is elevated.

We focus on changes in EMG or movement kinematics by comparing both TONIC and HI-GAIN models with the non-impaired condition. There are three experiments in this study:

1. passive back-and-forth stretch
2. voluntary relaxation of force
3. voluntary back-and-forth movement

In the first two experiments, data from human subjects are available and thus compared to verify the sufficiency of our model for producing dystonia; human data are not yet available for the last experiment, therefore the results can be used as testable hypotheses for future experiments.

3.2.Materials and methods

We focus on using spike-based emulation to determine the functional role of sensorimotor components, especially their sufficiency for causing clinical symptoms in abnormal conditions. The hardware emulation of the spiking neurons and sensorimotor components is constructed using Field Programmable Gate Arrays (FPGA, Xilinx Spartan-6), a programmable version of VLSI electronic chips. We favor FPGAs over pipelined hardware such as GPUs (Graphic Processing Units) or clustered CPUs (Central Processing Units) due to their inherent parallelism that resembles neural circuitry. We also found that when networking multiple units for large-scale disease emulation, FPGAs allow significantly more flexibility than custom-built hardware

for communication protocols such as neuromorphic transmission protocols that directly transmit neuron-like spikes.

The activity of the emulated sensorimotor system is recorded using a dedicated data-logging computer. The FPGA communicates with the data-logging computer through a high-speed USB channel and the OpalKelly development kit and interface software (XEM6010, OpalKelly Inc.). The technical details can be located in the previous study (Niu *et al.*, 2014). The biomechanics of the limb is simulated in software. The biomechanical simulation updates its states by first polling muscle force from the FPGAs, followed by sending muscle kinematic variables (length and velocity of lengthening) back to the FPGAs. This hybrid setup containing both hardware and software is slower than pure hardware emulation, but it simplifies the coordination between flexor and extensor FPGA chips.

3.2 Models for the sensorimotor system and increased LLSR

We study a sensorimotor system that includes a limb joint comprising two opposing monoarticular muscles (flexor and extensor), muscle spindles, spindle afferents, alpha-motoneurons and associated supraspinal structures (Figure 5A). The hardware emulates parallel proprioceptive pathways including monosynaptic connections with 32ms loop-delay representing the spinal proprioceptive pathway, and oligosynaptic pathways with 64ms loop-delay representing the supra-spinal/transcortical components of the stretch reflex loop. The delays were chosen both to approximate known conduction delays and also for efficiency of hardware emulation. Our previous work suggests that in sensorimotor systems, the statistical effect of two fully connected neuron populations is equivalent to ones that are only sparsely connected (Sanger, 2011a), therefore we connect the spindle afferents to motoneurons using parallel connections instead of implementing the full connectivity among neurons. In this study we do not introduce inhibitory mechanisms such as Renshaw cells or reciprocal inhibition. Both gamma dynamic and gamma static drive are set to 80Hz, which is a moderate intensity of fusimotor stimulus in the classic experiment chosen for modeling the muscle spindle (Emonet-Denand *et al.*, 1977). No alpha-gamma coactivation is introduced. This provides a baseline system for the non-impaired behavior before introducing the disease model.

On top of the non-impaired system, we model two possible mechanisms to increase LLSR: the TONIC model and HI-GAIN model. In the TONIC model (Figure 5B), we superimpose a

tonic input on the voluntary commands via a depolarizing synapse. The tonic input lowers the threshold of the cortical neuron pool and therefore facilitates the transcortical pathway when stimulated by proprioceptive feedback. In the HI-GAIN model (Figure 5C), the synaptic gain of afferent inputs to the cortical neuron pool is increased by augmenting the excitatory postsynaptic potential (EPSC) in response to afferent input. Therefore the TONIC model is an additive excitatory drive that is present even in the absence of afferent input, while the HI-GAIN model is a multiplicative drive that is present only when afferent input is present. Both TONIC and HI-GAIN models increase the excitability of cortical neuron pools to afferent input, either by lowering threshold or by increasing the effect of the input. We test both models because either or both mechanisms could be active in childhood dystonia.

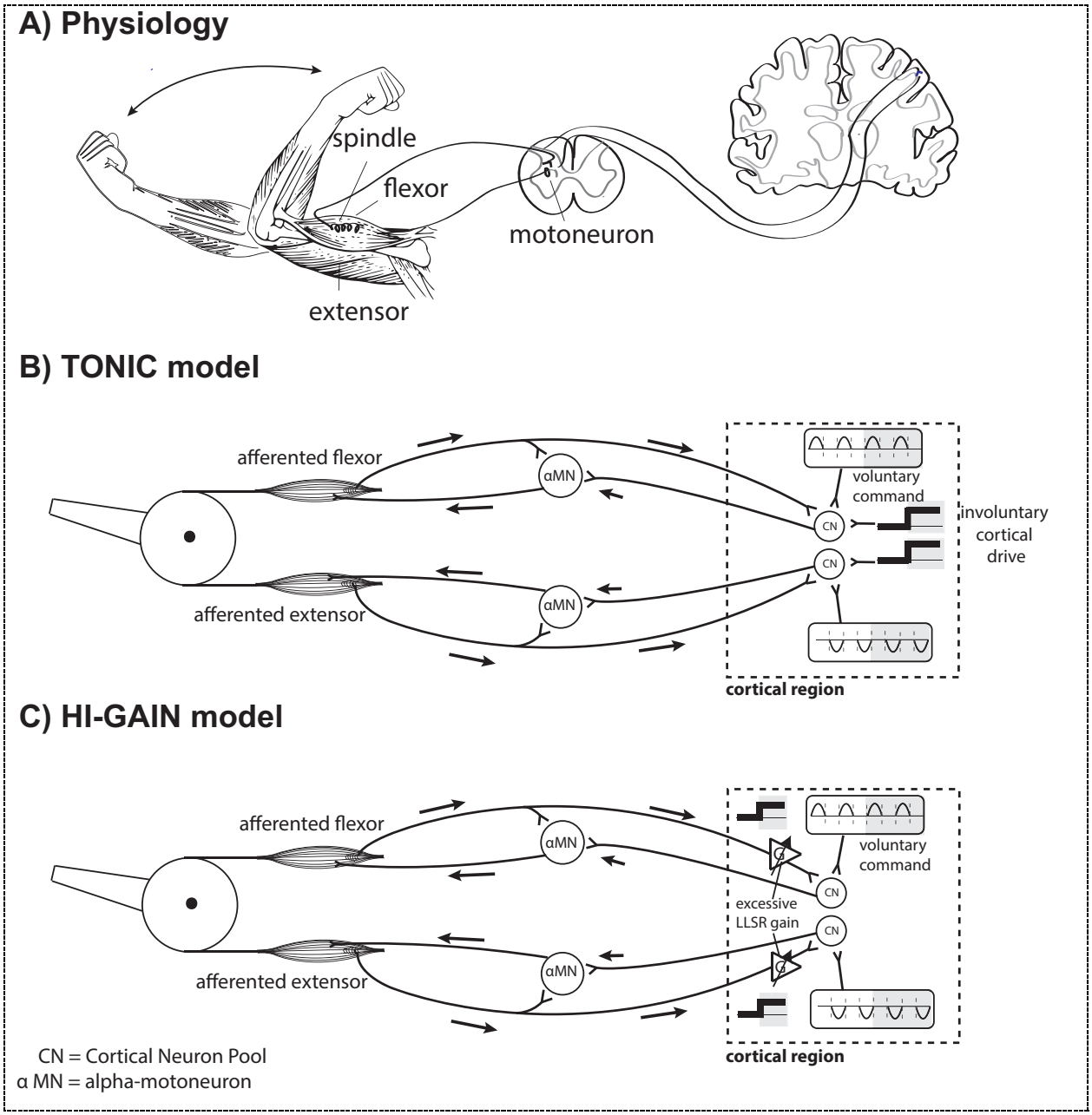
A) Physiology
spindle
flexor
motoneuron
extensor
B) TONIC model
afferented flexor
αMN
voluntary
command
CN
involuntary
cortical
drive
CN
αMN
afferented extensor
cortical region
C) HI-GAIN model
afferented flexor
αMN
voluntary
command
CN
excessive
LLSR gain
CN
αMN
afferented extensor
cortical region
CN = Cortical Neuron Pool
α MN = alpha-motoneuron

Figure 5. A) Components of human sensorimotor system model. The system includes a limb joint comprising two opposing monoarticular muscles (flexor and extensor), muscle spindles, spindle afferents, alpha-motoneurons, and associated spinal and supraspinal structures. Our model includes a monosynaptic reflex arc with a 32ms loop-delay and a supra-spinal transcortical reflex pathway with a 64ms loop-delay. B) The TONIC model of dystonia. The dashed box shows the procedure of introducing involuntary *tonic* activity. Before the disease onset (unshaded area), the system executes the voluntary commands received from antagonistic cortical inputs; after the disease onset (shaded area), the voluntary descending commands are superimposed on a tonic input. C) The HI-GAIN model of dystonia. The synaptic gain associated with the afferent cortical projection becomes higher after the disease onset (shaded areas), which directly increases the loop-gain of the transcortical feedback loop.

3.2.1 Implementation of sensorimotor system on hardware

An adult elbow joint is simulated in software as a 34cm beam freely rotating around a single D.O.F. axis, the mass of the beam is 1.52kg as an approximation to a human fore arm (Scheidt and Ghez, 2007); the moment arm of muscle is simplified as constant 30mm, which is in the middle range of moment arm measured from human biceps (Murray *et al.*, 1995). The joint is driven by a pair of antagonistic muscles following Hill-type model (Hill, 1938). The sensorimotor components that interact with the simulated joint are arranged on FPGA hardware as shown in Figure 6. Each muscle is controlled by 128 spindles as modeled by Mileusnic *et al.* (2006a), simple spiking neurons developed by Izhikevich (Izhikevich, 2003a), and a motor-unit action potential (MUAP) model similar as (Fuglevand *et al.*, 1993a; Rodriguez *et al.*, 2007; Krutki *et al.*, 2008) producing a surface electromyogram. Izhikevich neurons are used because they permit use of biologically realistic variables including transmembrane currents, yet they can be implemented much more efficiently in hardware than the more complex Hodgkin-Huxley equations that they approximate. A total of 768 alpha-motoneurons were divided into 6 groups representing motor units with various sizes, so that the size principle (Henneman *et al.*, 1965) is present when motor units are recruited. The parameters are tuned such that at maximal spiking rate of the alpha-motoneuron pool, the muscle exerts approximately 5N tangential force at the tip of the joint. In the transcortical loop, the spindle afferent information travels through a

population of 128 cortical neurons representing the primary sensory and motor cortices. The main focus of modeling cortex is to enable a longer loop-delay compared to spinal pathways, therefore we accept a pool of 128 neurons as a model of cortex even though it is a clear oversimplification of the real biology. Due to the limited capacity of each FPGA unit, the system must be distributed on multiple FPGAs as indicated by the blocks. The entire system uses 6 interconnected FPGA boards to emulate 2 muscles and 2,304 spiking neurons.

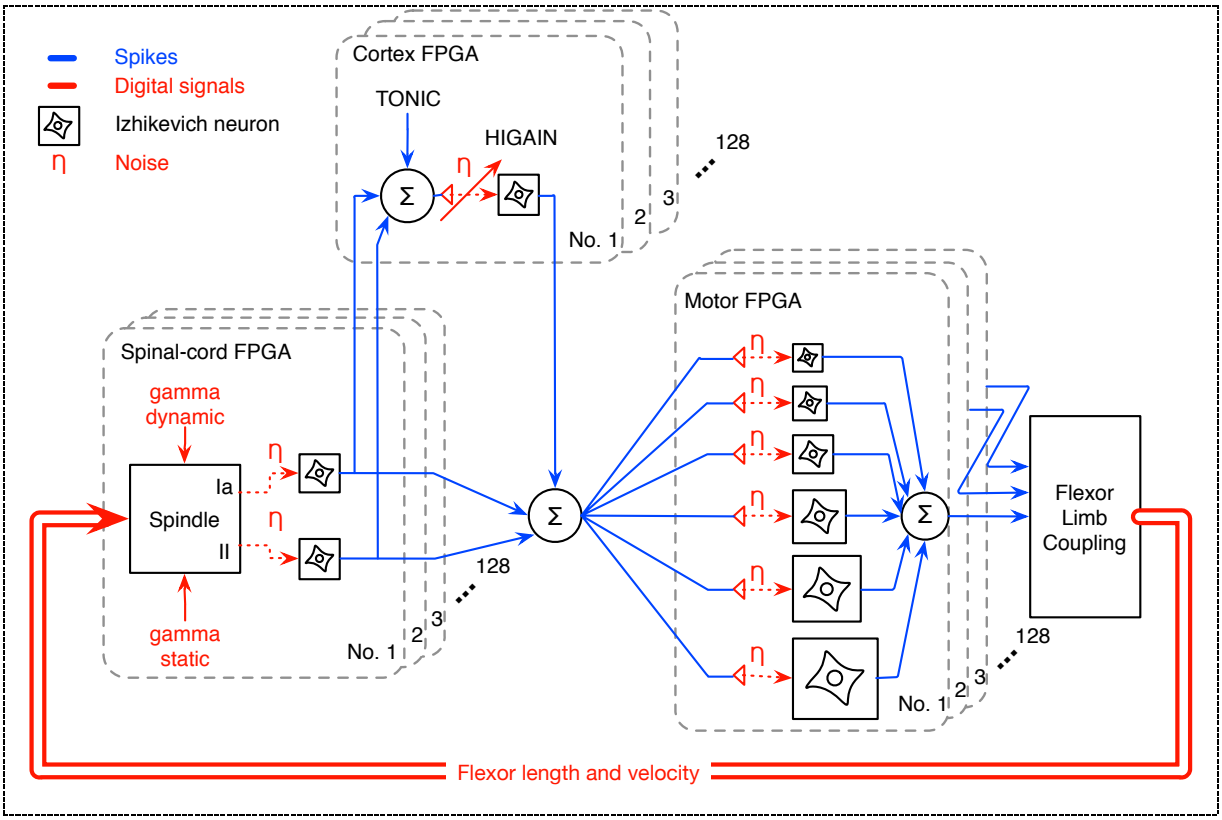

Figure 6. Detailed configuration of the motor nervous system on neuromorphic hardware. The components are implemented separately for the flexor and extensor, which simultaneously drive the joint modeled as a beam freely rotating around the endpoint (simulated in software outside FPGAs). For each muscle (flexor or extensor), the muscle force is calculated from a Hill-type muscle model activated by 6 motoneuron pools with 6 different motoneuron sizes, each pool comprising of 128 identical motoneurons modeled by Izhikevich (Izhikevich, 2003a). The motoneuron pools receive excitatory input from both the spinal loop and transcortical loop. In the spinal loop, the sensory feedback is provided by muscle spindles implemented as Mileusnic and colleagues did (Mileusnic *et al.*, 2006a), which include both the Primary (Ia) and Secondary (II) afferents to provide the dynamic and static proprioceptive information about the muscle. A total of 128 spindles are implemented for each muscle, thus providing 256 independently spiking afferents. In the transcortical loop, the spindle afferents synapse on a population of 128 cortical neurons representing the primary sensory and motor cortex. The cortical part is clearly an oversimplification of the cortex but it enables an additional 32ms conduction delay in the proprioceptive feedback loop, which is the main focus of this study rather than modeling a full cortex. In the cortex, spindle afferents may join additional inputs modeling the voluntary motor command. The TONIC model is implemented by adding to the cortical drive a tonic component that is independent from the voluntary drive or the sensory feedback. The HI-GAIN model is implemented by increasing the synaptic gain of the spindle afferents prior to activating the cortical neuron pool. Due to the limited capacity of each FPGA unit, the system must be distributed on multiple FPGAs as indicated by the blocks. The entire system uses 6 FPGA boards enabling 2 muscles with 2,304 neurons. Only half of the system (flexor) is shown.

3.2.2 Experiments

We have verified the sufficiency of both the TONIC and HI-GAIN models for dystonic symptoms in the following three experiments:

3.2.2.1 Experiment 1: Passive back-and-forth stretch

We replicate the experiment where a sinusoidal perturbation was applied to a joint of a child with hypertonic arm dystonia (van Doornik *et al.*, 2009). In the original study, the subject was instructed to rest, and the right arm was rotated manually by the experimenter following an approximately sinusoidal time profile with frequency varying from 0.2 Hz up to 2 Hz.

We use the same waveform as in the original study to stretch the emulated system. A pre-recorded waveform of joint displacement is applied to the software-simulated joint. We keep the voluntary command at zero during the passive stretch to capture the fact the subject was at rest. It was found that patients with dystonia failed to relax the muscles and produced cyclic EMG responses to the stretch. The models of dystonia are validated based on their abilities to qualitatively explain human data. To this purpose, we calculate the phase angle between the model-generated EMG and the joint angle using the same approach as in van Doornik et al. (2009). The range of phase angle reflects which kinematic variable could be the main cause of the EMG response. For example, a phase angle of 0° means the EMG response is in line with the joint angle, thus making the EMG position-dependent; while -90° means the EMG response is velocity-dependent; any phase angle between -180° and -90° suggests that the EMG response has acceleration-dependent components; any phase angle between 0° and 180° means that the EMG is active during muscle shortening.

During model validation, we first introduce a small TONIC input (TONIC model) to the cortical neuron pool or a small cortical gain (HI-GAIN model) sufficient to produce dystonic symptoms, i.e. an observable phase angle. Then we progressively increase the intensity of dystonia until the phase angle stopped changing significantly, mainly due to the saturation of neurons. We consider a model sufficient to explain human data if the parameter-scan produces a wide range of phase angle that includes those from human patients.

3.2.2.2 Experiment 2: Voluntary relaxation of muscle

One of the common manifestations of childhood dystonia is that the voluntary relaxation of muscle contraction is delayed (Sanger *et al.*, 2003). We replicate the experiment that documented this delay by comparing normal subjects to patients with secondary dystonia (Ghez *et al.*, 1988).

Both muscles were first activated at 50% maximum voluntary contraction (MVC), followed by a step decrease in the voluntary command. This experiment simulated when the subject attempts to rapidly relax the co-contracted muscles following a cue signal (Ghez *et al.*, 1988). It was shown that the EMG decreased more slowly in patients with secondary dystonia, and thus the overall duration of muscle relaxation was delayed.

We quantify the rate of muscle relaxation by fitting the filtered EMG to a sigmoid function defined below:

$$EMG_{sigmoid}(t) = EMG_{min} + \frac{(EMG_{max} - EMG_{min})}{1 + e^{\tau t}}$$

where the free parameter τ denotes the rate at which the EMG decreases during muscle relaxation. The relationship between τ and the severity of dystonia was tested using a similar parameter-scan as in Experiment 1.

3.2.2.3 Experiment 3: Reduced range of motion in voluntary movements

In clinic, it is commonly observed that patients with dystonia apply great efforts in order to achieve a normal range of movement; otherwise the range of motion in voluntary movements is reduced. These phenomena are, however, not well documented in experimental studies. It is reported that the range of motion is reduced in neck and knee for patients with primary dystonia (Carpaneto *et al.*, 2004; Lebiedowska *et al.*, 2004). We hypothesize that similar reduction in range of motion is likely to occur in secondary dystonia. In addition, we test if the reduced range of motion can be improved by amplifying the voluntary command, which is a straightforward engineering approach to compensate a less responsive system.

The two cortical neuron pools regulating flexor and extensor receive half-wave rectified sinusoidal waveforms (180 degrees out of phase), which produces a back-and-forth joint swinging movement. The peak-to-peak amplitudes of joint angle resulting from these inputs are analyzed. If the amplitude of joint angle is reduced in dystonia models, we linearly increase the sinusoidal voluntary commands to test if the reduction can be compensated.

3.2.2.4 Data acquisition and processing

All data are sampled at 1kHz. The EMG signals are first high-pass filtered using 10Hz cut-off frequency (Butterworth, 3rd order), followed by rectification and a low-pass filter at 120Hz cut-off frequency (Butterworth, 3rd order). Phase angle analysis and the nonlinear fitting of the sigmoid function (for quantifying muscle relaxation, explained below) are performed using Matlab (Mathworks, Inc.).

3.3 Results

3.3.1 Non-impaired stretch reflex and hypertonia with increased LLSR

We first verify the quality of emulation by passively stretching the joint and monitoring the reflex behavior elicited by the stretch. The joint was passively extended by 45 degrees within 0.2 seconds from the software interface. The sensorimotor information recorded in response to a virtual stretch in the non-impaired condition is shown in Figure 7A, including the spindle afferents (group Ia and II), motoneuron rasters, muscle force and EMG. As can be seen, the hardware emulation is capable of producing concurrent multi-scale information during a virtual behavior.

We further compared the stretch reflex between the non-impaired condition and our two dystonia models. The joint was briefly stretched using a short torque pulse (5N for 20ms, Figure 7B), which extended the flexor by approximately 40% of L_0 (the resting length of muscle). Hypertonia can be seen from the increased flexor force in the dystonia conditions compared to the non-impaired condition (Figure 7B, Muscle force). The EMG response is divided into R1 (30-50ms), R2 (50-80ms), and R3 (80-100ms) regions representing the short-, long-, and longer-latency responses. By overlapping the non-impaired condition and our models of dystonia (Figure 7B, EMG), it can be seen that R2 responses are increased by both TONIC and HI-GAIN model, i.e. LLSR is increased in both models.

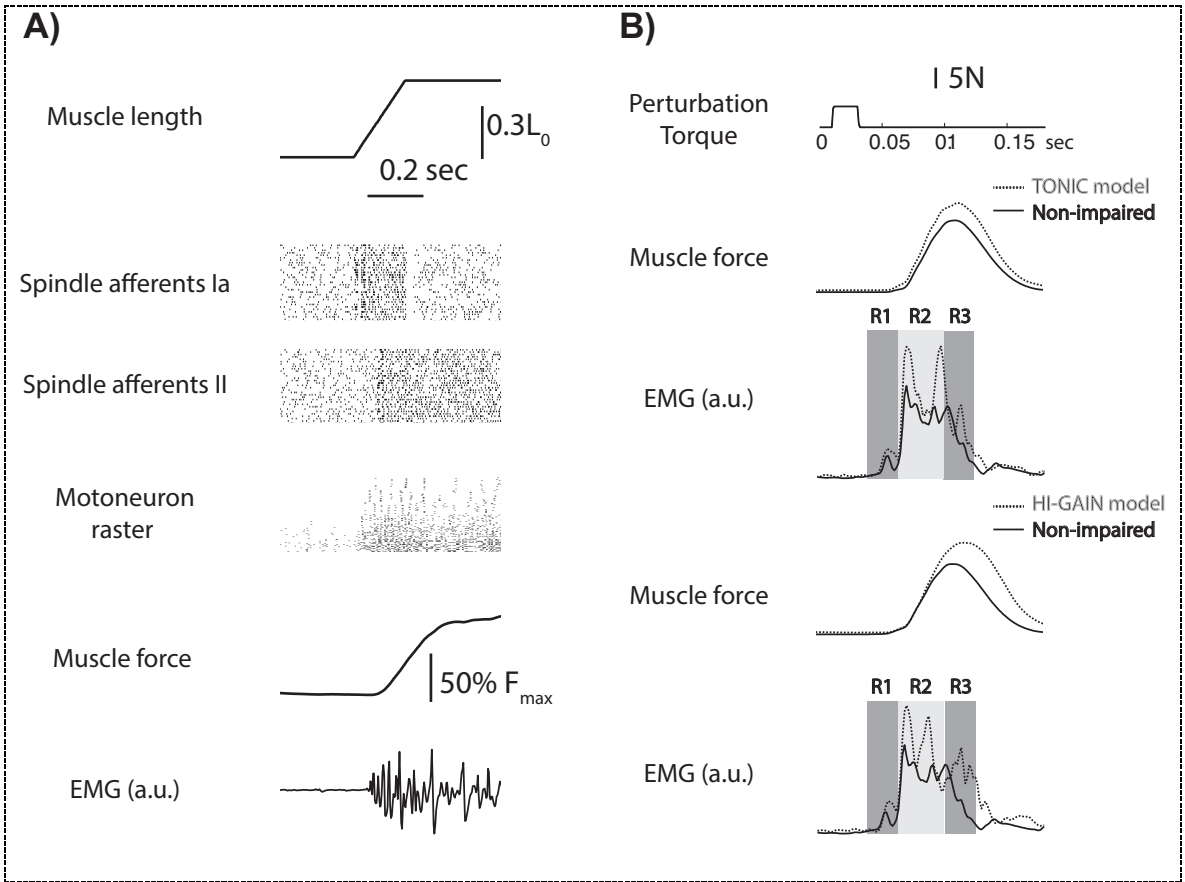

Figure 7. The emulated stretch reflex in the non-impaired condition and models of increased LLSR. A) EMG responses to a stretch-and-hold perturbation in the non-impaired condition. The joint flexor was stretched by approximately 40% of L_0. The emulated EMG showed a burst in response to the stretch. The motoneuron raster showed patterns compatible with both the early burst in EMG response and the subsequent tonic components. B) Emulated hypertonia and increased LLSR. The muscle force increases from baseline in both TONIC and HI-GAIN model, which implemented the increased muscle resistance to passive muscle stretch commonly observed in hypertonic dystonia. EMG responses to a torque pulse perturbation (5N for 20ms) in both the non-impaired condition and the models of dystonia. R1 (30-50ms), R2 (50-80ms), and R3 (80-100ms) regions represent the short-, medium-, and long-latency responses. In both TONIC and HI-GAIN model the R2 response was increased compared with the non-impaired condition.

3.3.2 Experiment 1: Involuntary responses to passive joint stretch

The dystonic subjects showed phasic EMG responses to the manual sinusoidal stretch in their biceps (Fig.8A). In the emulation, the virtual arm was passively rotated with the identical waveform as shown in Fig.8 A. Our emulated result showed that in both TONIC (Fig.8B) and HI-GAIN (Fig.8C) models, the flexor EMG activity modulates with the joint angle similarly to the original human experiment.

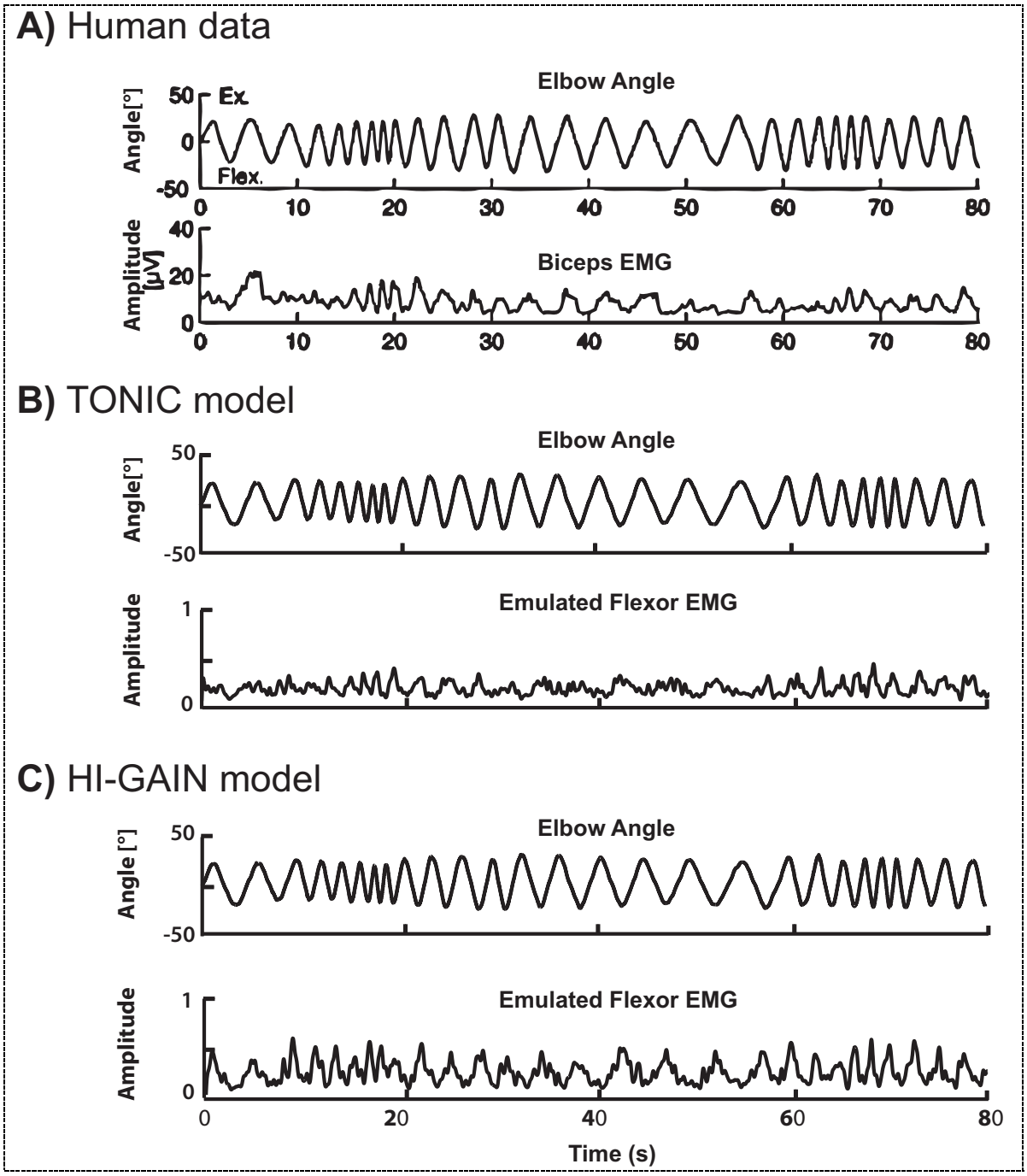
A) Human data
Elbow Angle
Angle[°]
50
0
-50
Ex.
Flex.
0
10
20
30
40
50
60
70
80
Amplitude [µV]
40
20
0
Biceps EMG
B) TONIC model
Elbow Angle
Angle[°]
50
-50
Amplitude
1
0
Emulated Flexor EMG
C) HI-GAIN model
Elbow Angle
Angle [°]
50
-50
Amplitude
1
0
Emulated Flexor EMG
0
20
40
60
80
Time (s)

Figure 8. Biceps EMG during arm rotation in a child with hypertonic arm dystonia (A) created based on the data in van Doornik et al. (2009). When the subject was instructed to rest, the right arm was rotated manually by the experimenter following approximately a sinusoidal time profile with frequency varying from 0.2 Hz up to 2 Hz. The biceps showed phasic EMG responses to the manual stretch. In the emulation, the virtual joint was passively rotated with the identical waveform under two models of dystonia. The voluntary command is set to zero to represent the subject being "at rest". In the TONIC model (B), the EMG is not silent when the joint is passively rotated and shows similar phasic patterns as the human EMG recording. In the HI-GAIN model (C), similar non-silent EMG responses are observed with increased magnitude in phasic response.

The 8 patients with dystonia from human experiments (van Doornik *et al.*, 2009) showed a wide range of phase angle between -101° and 17° (Table 2, van Doornik *et al.*, 2009). There were 2 patients (Subjects 4 and 5) with dyskinetic cerebral palsy (CP) who showed positive phase angles, suggesting EMG responses during muscle shortening (a "shortening reaction" more frequently seen in Parkinsonism). These 2 patients were excluded from the model validation, since their mechanisms were unlikely the same as the other 6 patients who were non-dyskinetic. As can be seen from Fig.9, 5 out of 6 patients showed phase angles between -90° and 0° (combination of position- and velocity-dependent); 1 out of 6 patients showed a joint angle below -90° (with acceleration-dependent components).

We validate our models of dystonia by testing whether the reported phase angles in human can be achieved in emulation. In the TONIC model, we scan the tonic EPSC with fixed increments from 40pA up to 280pA. We stop at 280pA since further increases did not significantly change the phase angle mainly due to the saturation of cortical neurons. The scan of tonic EPSC produces phase angles from -32°to -53°, which explains only 1 out of 6 patients (dark gray area, Fig.9A). In the HI-GAIN model, we start the scan by selecting a unit gain that amplifies the non-impaired EPSC by 4 times, then we progressively increase the gain to 19 times of a unit. We stop at the gain of 19 for the same reason of saturation. This process produces phase angles from -29° to -147°, which covers the reported phase angles of all 6 subjects (dark gray area, Fig.9B).

We infer the upper and lower limits of phase angle by setting the emulation to boundary conditions (light gray area in Fig.9). The upper limit of phase angle is obtained by de-afferenting the secondary fibers (group II) and keeping the loop gain high; and the lower limit is obtained by de-afferenting the primary fibers (group Ia) and keeping the loop gain low. The boundary conditions are constructed based on the factors that may affect the phase shift, e.g. loop delay, loop gain, and the relative contribution between position- and velocity-dependent components, etc. See Discussion for further considerations. The overall range of phase angle (-9° to -169°) is larger than both TONIC and HI-GAIN models.

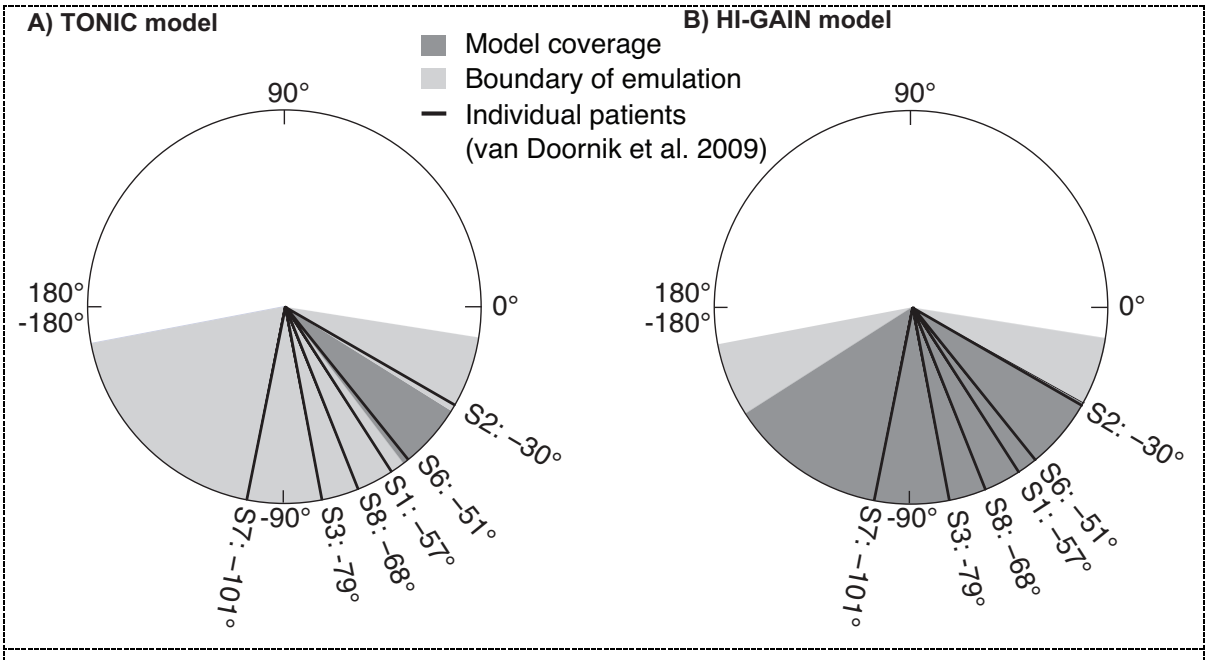

Figure 9. The phase angle calculated from emulation and human data. The thick lines show the phase angles of 6 patients with hypertonic arm dystonia. (A) The TONIC model produces phase angles from -32° to -53° (dark gray area), which includes 1 out of 6 patients. (B) The HI-GAIN model produces phase angles from -29° to -147° (dark gray area), which includes all 6 patients. The boundary of emulation is tested by de-afferenting either the primary (group Ia) or the secondary (group II) spindle fiber, resulting in the minimum phase angle of -169° and the maximum of -9° (light gray area).

The sensitivity of phase angle to the intensity of emulated dystonia in each model is shown in Fig.10. In the TONIC model, the phase angle decreases with increased tonic current input

following a significant linear correlation (Fig.10A, slope $= -0.074, p < 0.0001, r^2 = 0.59$, 4 repetition for each level of TONIC input). In the HI-GAIN model, similar linear correlation is observed (Fig.10B, slope $= -6.50, p < 0.0001, r^2 = 0.78$, 4 repetitions for each level of HI-GAIN). Overall, the HI-GAIN model can capture more variance in phase angle than could the TONIC model. The results suggest that in terms of phase angle, the HI-GAIN model can explain more data than the TONIC model, although both models produce results qualitatively similar to the human data.

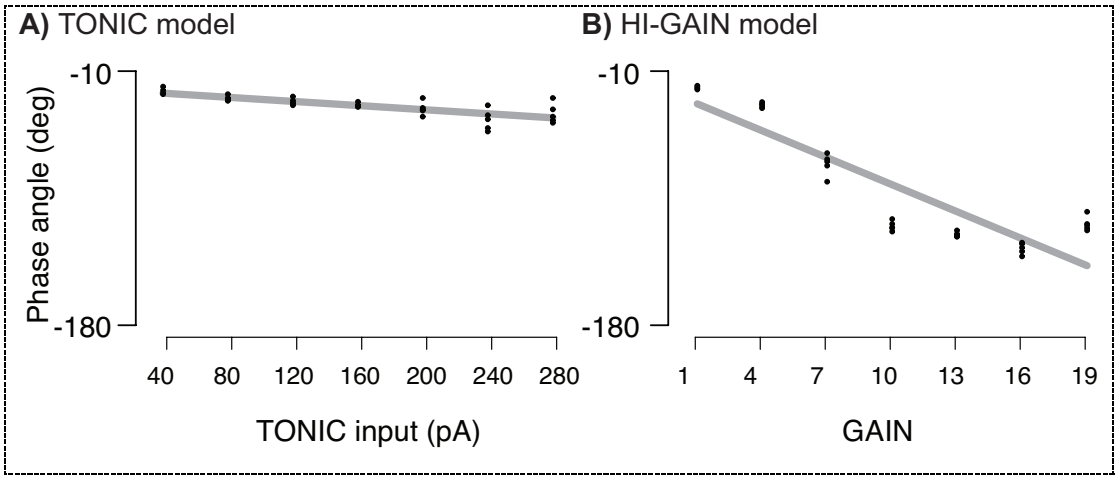

Figure 10. The sensitivity of phase angle to the intensity of emulated dystonia in each model. In the TONIC model, we scan the TONIC input from 40pA to 280pA with fixed increments. The average phase angles produced by these TONIC inputs range from -32° to -53°, where a higher TONIC input significantly reduces the phase angle (slope $= -0.074, p < 0.0001, r^2 = 0.59$, 4 repetition for each level of TONIC input). The linear trend tends to saturate when the TONIC input exceeds 240pA. In the HI-GAIN model, we start the scan of cortical gain by selecting a unit gain that amplifies the non-impaired EPSC by 4 times. The gain is increased to 19 times of a unit with fixed increments. The average phase angles produced by the HI-GAIN model range from -29° to -147°, where a higher cortical gain significantly reduces the phase angle (slope $= -6.50, p < 0.0001, r^2 = 0.78$, 4 repetitions for each level of HI-GAIN). The linear trend tends to saturate when the TONIC input exceeds 16 units. These results suggest that in terms of phase angle, the HI-GAIN model can explain more human data than the TONIC model.

3.3.3 Experiment 2: Delayed relaxation of muscle force

Fig.11 shows that both the TONIC and HI-GAIN models suffice to delay muscle relaxation compared with the non-impaired condition. The phenomenon is qualitatively similar to human data.

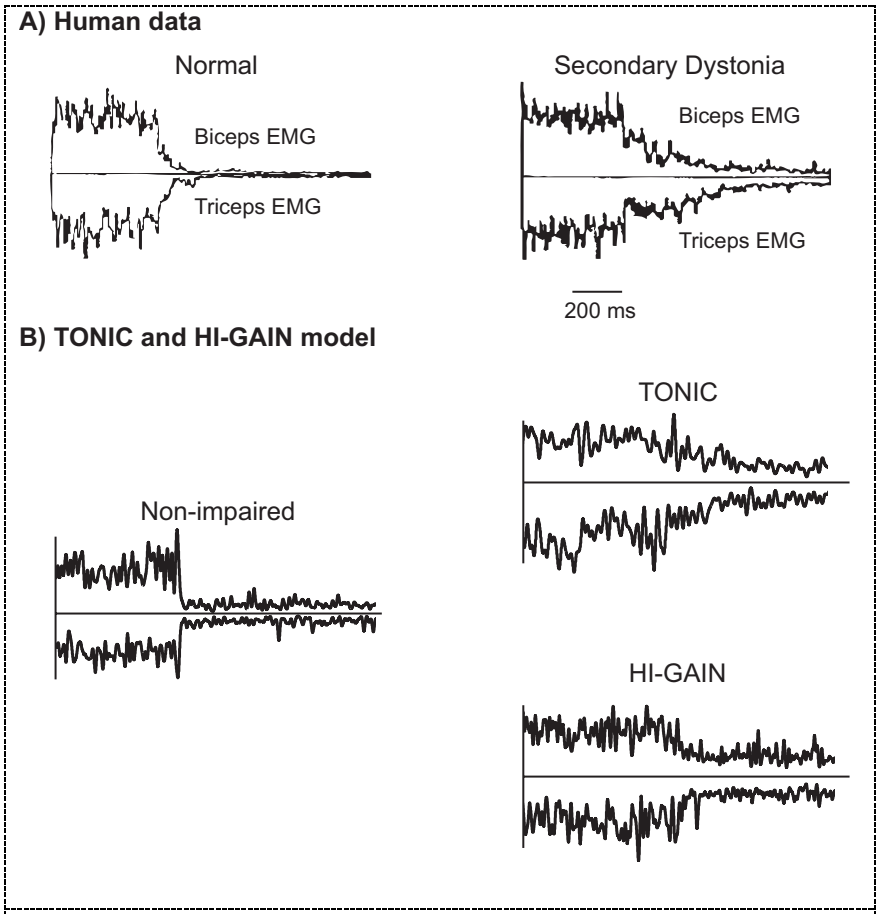

Figure 11. Relaxation of muscle activity from a state of co-contraction in biceps and triceps in a normal subject and a patient with secondary dystonia (A), created based on the data in Ghez et al. (1988). Subjects were first required to maximally co-contract the biceps and triceps muscles and upon a visual cue relax the muscle as fast as possible. The duration for muscle relaxation in the patient with secondary dystonia (right) was elongated compared to the normal subject (left). In emulation (B), both TONIC and HI-GAIN models showed delayed EMG relaxation compared with the non-impaired condition, when the voluntary descending command that co-contracts biceps and triceps were abruptly shut off. Single representative trials are shown.

The rate of relaxation (τ) was calculated both from human data and emulated results for model validation. Due to the limited human data, we could only obtain two values of τ based on the original EMG time series in Ghez et al. (1988). The τ calculated from the normal subject almost tripled that from the patient with secondary dystonia ($\tau_{normal} = 0.044, \tau_{dystonia} = 0.015$), which is compatible with the visual pattern of delayed relaxation (Fig.11A). These two values of τ are plotted in Fig.12 (dotted and dashed lines) for comparison with emulated τ.

In the TONIC model, the level of TONIC input was scanned using the same set-up as in Experiment 1. The emulated τs were all lower than τ_{normal} (Fig.12A), and $\tau_{dystonia}$ was included in the emulated range of τ. When the TONIC input increases, the delay of relaxation is significantly longer ($slope = -0.00012$, $p < 0.00001$, $r^2 = 0.65$, 4 repetitions for each level of TONIC input). In the HI-GAIN model, the emulated τs were also lower than τ_{normal} (Fig.12B). But the linear correlation between τ and model intensity is much weaker, represented by modest significance and lower r^2 value (Fig.12B, $slope = -0.00051$, $p = 0.046$, $r^2 = 0.11$, 4 repetitions for each level of HI-GAIN). In contrast to Experiment 1, results from Experiment 2 suggest that the TONIC model can explain more data than the HI-GAIN model.

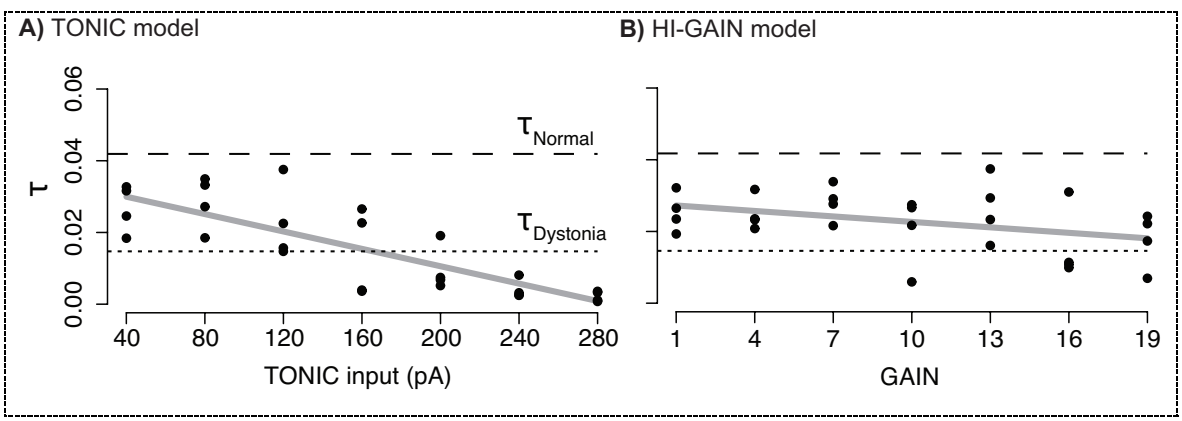

Figure 12. Relationship between the rate of relaxation (τ) and the intensity of either the TONIC or the HI-GAIN model. In both models, the intensity of dystonia is scanned the same as in Experiment 1. Two reference αs calculated from human data are shown, the rate in the normal subject ($\tau_{\text{normal}} = 0.044$, dashed line) represents faster relaxation compared to the patient with secondary dystonia ($\tau_{\text{dystonia}} = 0.015$, dotted line). In the TONIC model (A), the emulated τs are all lower than τ_{normal}, and their range includes τ_{dystonia}. When the TONIC input increases, the delay of relaxation is significantly longer (slope $= -0.00012$, $p < 0.00001$, $r^2 = 0.65$, 4 repetitions for each level of TONIC input). In the HI-GAIN model, the emulated τs are also lower than τ_{normal} (B). But the linear correlation between τ and model intensity is much weaker, represented by modest significance and lower r^2 value (slope $= -0.00051$, $p = 0.046$, $r^2 = 0.11$, 4 repetitions for each level of HI-GAIN).

3.3.4 Experiment 3: Reduced range of motion in voluntary movements

In this experiment, we aimed to predict how dystonia affects movement kinematics. In the TONIC model, just adding a middle level TONIC input is sufficient to reduce the peak-to-peak amplitude of voluntary movement (Fig.13). The reduced range of motion can almost fully recover if we amplify the voluntary commands, suggesting that patients can compensate the reduced range of motion by increasing voluntary effort. Similar results are produced using the HI-GAIN model. In this experiment, both models predicted similar kinematic consequences using anecdotal parameters. More human data are required to distinguish between these two models.

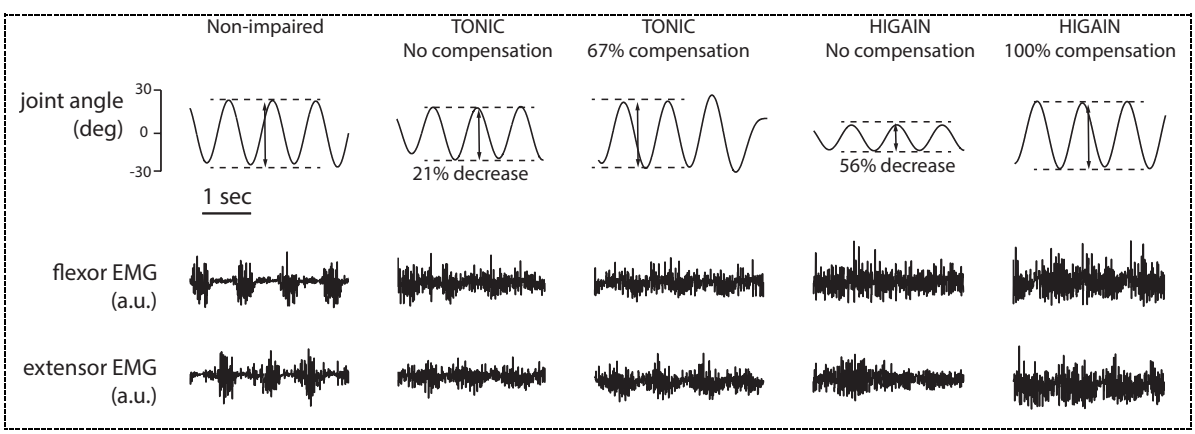

Figure 13. Dystonia models predict that the range of motion in voluntary arm-swing movement should be reduced in dystonia; with certain level of compensation by increasing the voluntary command, the range of movement can be recovered. In the non-impaired condition, the joint was voluntarily swinging at 1Hz with approximately 50° range of movement; the muscles are activated using alternating descending commands at 1Hz as depicted in Fig. and thus generate alternating EMG bursts. In the TONIC model, we maintained the level and frequency of the 1Hz voluntary command, but added a tonic input with 80% of the peak-to-peak magnitude of the voluntary command. This reduces the movement range by 21%, which can be recovered by compensating the voluntary command by 67% of its original magnitude. In the HI-GAIN model, a 4.7 times increase in the synaptic gain of cortical neuron pool decreased the movement range by 56%, which can be recovered by compensating the voluntary command by 100%.

3.4 Discussion

Using our recently developed technique of neuromorphic emulation in hardware, we tested the hypothesis that increased long-latency stretch reflexes, created by excessive activity in the motor cortex, are sufficient to induce forces and EMGs with similar patterns to those seen in patients with secondary dystonia. In particular, we verified that when the limb is passively stretched as in van Doornik *et al.* (2009), both an additive tonic input in the cortical neuron pool (TONIC model) and an elevated synaptic gain in the motor cortex (HI-GAIN model) suffice to induce EMG responses in the absence of a voluntary command. The HI-GAIN model explains a wider range of phase angle from human data than does the TONIC model. Furthermore, we verified that both TONIC and HI-GAIN models suffice to delay muscle relaxation similar to the results of Ghez et al. (1988). The rate of relaxation could be better explained by TONIC model than the HI-GAIN model. Our models also predict that the range of movement should be reduced if the magnitude of the voluntary command remains the same in dystonia. Alternatively, we predict that dystonia increases the voluntary effort required to make movements of the same magnitude.

3.4.1 Relationship between LLSR and secondary dystonia

Our results suggest that increased LLSR may be an intermediate mechanism linking brain injuries and the clinical manifestations of hypertonic dystonia. That is, even though the injuries

may occur in various parts of the brain (e.g. thalamus, basal ganglia, cortex, etc.), all these injuries could produce hypertonic dystonia due to excess activity in the motor cortex via elevated LLSR. We show that both TONIC and HI-GAIN models are sufficient for explaining the dystonic symptoms in the demonstrated cases. Nevertheless, the manifestation of these two models could differ when the severity of dystonia increases (Fig.10); it is also suggested that hypertonia due to tonic input may have a stronger effect than high synaptic gain on the delay in muscle relaxation (Fig.12). In theory, the TONIC model can be interpreted as a non-intrinsic abnormal drive to the motor cortex, originated from other parts of the brain; while the HI-GAIN model suggests that there is some intrinsic deficit in the motor cortex that amplifies its overall activity. These differences suggest testable hypotheses in future studies to distinguish the heterogeneous causes of dystonia.

Elevated LLSR is not exclusively observed in dystonia but also reported in other disorders such as rigidity. It is possible that dystonia and rigidity may share similarities in mechanism, although due to very different causes. It was not our intent to study rigidity, which is rare in children, but from our prior work (van Doornik *et al.*, 2009) we have noted that even within dystonia there appears to be a continuum between spring-like hypertonia and viscous hypertonia. Rigidity is primarily viscous and it is tempting to conjecture that rigidity may result from increased LLSR involving primarily velocity-dependent (rapidly adapting) afferents, whereas dystonia may result from elevated LLSR involving primarily position-dependent (slowly adapting) afferents.

3.4.2 Rationale of model validation

When validating our models against human data, we focused on whether varying a single parameter in the model could produce a wide range of outcome measures compatible with the human data. We did not, however, focus on the exact matching between emulated time series and human data. This is because dystonia has been known as a disease with high inter-patient variability, and data from humans are limited. As a result, we argue it is not that useful if the model aims at matching exactly to the physiological signals of human patients. Take Experiment 1 as an example, the power of the HI-GAIN model comes from its ability to explain the phase angle of any of the 6 patients using the same disease structure. Given more data from patients

with secondary dystonia, the range of outcome measures also provides an experimentally testable criterion to distinguish different models.

3.4.3 Thoughts on the two mechanisms of elevated LLSR

Either abnormality modelled by the two models can lead to elevated LLSR. This is important because intuitively it might appear that only the HI-GAIN model would increase the gain of the LLSR. Our results suggest that changes in threshold due to tonic drive can also achieve similar effects. It is possible that there is more than one mechanism of dystonia, and this points out that there may be multiple causes of similar phenomenology. For example, disorders of intrinsic excitability of motor areas (genetic or chemical) can produce dystonia, but so could disorders of other areas that project to primary motor areas. Therefore dystonia could result either from disorders of primary motor areas or from disorders of upstream areas, yet the manifestations will be difficult to distinguish on clinical grounds (although there are some differences).

Another utility of the modeling TONIC and HI-GAIN models is that they potentially represent different etiologies. In particular, a multiplicative increase in the loop gain (HI-GAIN model) cannot be implemented by an additive component added to the system, such as a leak in the trans-membrane current. In consequence, if the experimental data favors one model over the other, it suggests that the clinical diagnosis of dystonia should reflect the characteristics of the favored model, e.g. progressively increased phase angles or delayed relaxation.

3.4.4 Factors that may affect the phase angle in Experiment 1

Since phase angle is determined by the nonlinearity of a system and also its intrinsic delay, several factors in our neuromorphic emulation could directly affect the phase angle, including 1) the relative contribution between the primary (group Ia, both velocity- and position-dependent) and secondary (group II, mainly position-dependent) afferents of spindle, 2) the relative contribution between short- and long-latency pathway, and 3) the overall loop delay. Within the range from -180° and 0°, higher activity in the primary spindle fiber makes the system more velocity-dependent, resulting in lower phase angles; while higher activity in the secondary spindle fiber increases the phase angle. When scanning the intensity of dystonia we keep the activity similar between primary and secondary spindle afferents. When constructing the boundary condition of emulation, the secondary spindle fibers are removed such that the system

is the least position-dependent, which theoretically provides the smallest phase angle, and vise versa for the largest phase angle. The effect of loop delay on the phase angle is much weaker compared to fiber type, therefore loop delay is not considered when building the boundary conditions.

3.4.5 EMG response during muscle shortening

Two patients (Subject 4 and 5, van Doornik *et al.*, 2009) are excluded from the model since their positive phase angles suggest their muscles were activated by muscle shortening. This "shortening reaction" is mostly seen in Parkinsonism, but it is uncommon in normal afferented muscles since most of the proprioceptive spinal pathways are excitatory. Inhibitory pathways (e.g. Renshaw cells or reciprocal inhibition connections) are capable of reducing the EMG but usually not producing shortening reactions. One possible explanation for these two subjects is that there exists an overflow from the opposing muscle. Our models do not include inhibitory pathways or motor overflow. More experimental and modeling work is required to explain the positive joint angles attested in these two patients.

3.4.6 Advantage and limitation of neuromorphic hardware emulation

The use of hardware emulation provides a powerful tool for understanding the minimal model complexity for producing normal and pathological behaviors. It is clear that the hardware emulation could not accommodate all the physiological details involved in real behavior. For example, we emulated the closed-loop reflex of a joint with spinal pathways and simplified transcortical pathways. The cortical neuron pool only includes a single layer of 128 neurons that are far from the realistic anatomy in the primary sensory and motor cortices. Nevertheless, this simplified reconstruction of the cortex allows us to adjust only the long-latency component of the proprioceptive feedback independent from the functioning short-latency loop. Compared to studying the real biological system, hardware emulation is advantageous since it allows a precise and physiologically tenable intervention on the non-impaired system.

It is also an important issue whether our simplification of the sensorimotor system would lead to a locally correct conclusion that, however, cannot be generalized. It has been found that reflex of shoulder joint is concurrently modulated by the elbow joint (Pruszynski *et al.*, 2011). This suggests that a standalone reflex loop of a single joint, as modeled in this study, may overlook

the contribution from adjacent loops that would increase the LLSR and eventually worsen dystonia. On the contrary, our model did not include inhibitory pathways such as reciprocal inhibition, Renshaw cells, etc., which suggests that a more complex model may decrease LLSR and thus alleviate dystonia. In short, the model is *sufficient* to create some features of dystonia, but there could certainly be other contributors. It is unlikely that the inclusion of more joints would prevent the occurrence of dystonia, but it is likely to change its nature. It would be important to model dystonia in a multi-joint scenario.

3.5 Conclusion

In summary, we have shown through neuromorphic emulation that there are at least two possible mechanisms of cortical abnormality that could cause increased long-latency stretch reflexes and result in the clinical phenomenon of dystonia. While an emulation of this type does not prove that this is the mechanism of dystonia, it does provide evidence that a mechanism of this type is sufficient to cause the clinical features of dystonia, and is therefore worthy of further study. We hope that these results provide both insight and guidance for future clinical studies to test whether reducing the long-latency stretch reflex may alleviate symptoms of dystonia.

3.6 Author Contributions

Designed the experiment: WS CN. Performed the experiments: WS. Developed the hardware and software environment: WS CN. Analyzed the data: WJ CN. Wrote the paper: WS CN. Reviewed manuscript: WS CN TS.

4 Study 2. What causes motor overflow in focal hand dystonia?

Motor overflow in focal hand dystonia develops and perpetuates under correlated sensory inputs in neuromorphic emulation

Won J. Sohn[1†], Chuanxin M. Niu[4†], Terence D. Sanger[1,2,3*]

† The authors equally contributed to the study

[1]Department of Biomedical Engineering, [2]Biokinesiology, and [3]Neurology, University of Southern California, 1042 Downey Way, Los Angeles, California, 90089
[4]Department of Rehabilitation, Ruijin Hospital, School of Medicine, Shanghai Jiao Tong University, Shanghai, China

*** E-mail:** tsanger@usc.edu

Abstract. *Objective*. Motor overflow is a common and obstinate symptom of dystonia, manifested as unintentional muscle contraction that occurs during an intended voluntary movement. Although it is suspected that motor overflow is due to sensory cortical disorganization in some types of dystonia (e.g. focal hand dystonia), it remains elusive which mechanisms could initiate and, more importantly, perpetuate motor overflow. We hypothesize that distinct motor units have low risk of motor overflow if their inputs remain statistically independent. But when provided with confused sensory inputs, pre-existing crosstalk among motor units will grow under spike-timing-dependent-plasticity (STDP) and eventually produce irreversible motor overflow. *Approach*. We emulated a simplified neuromuscular system comprising 2 anatomically distinct muscles innervated by 2 layers of spiking neurons with STDP. The synaptic connections between layers included crosstalk connections. The motor units received either independent or correlated inputs during 4 days of continuous excitation. The emulation is critically enabled and accelerated by our neuromorphic hardware created in previous work. *Main results*. When driven by correlated inputs, the crosstalk synapses gained weight and produced prominent motor overflow; the growth of crosstalk synapses resulted in enlarged sensory representation reflecting cortical reorganization. The overflow failed to recede when the motor inputs resumed their original uncorrelated statistics. In the control group, no motor overflow was observed. *Significance*. Although our model is a highly simplified

and limited representation of the human neuromuscular system, it shows that correlated input to anatomically distinct muscles is by itself sufficient to cause motor overflow. Among many possible abnormal patterns of neural activity in patients with dystonia, our results suggest that the statistical independence of motor drives may be crucial for the specificity of voluntary movements.

Keywords: Overflow, Dystonia, Motor Control, Spike-timing-dependent plasticity (STDP), Electromyography (EMG)

4.1 Introduction

Motor overflow reflects a deficit in the specificity of motor commands. It describes a phenomenon with a leak in motor signals from one part of the body to other parts, producing extraneous movements, which accompany, but are incidental to, the voluntary action (Soska *et al.*, 2012). Motor overflow is commonly observed in dystonia (Gordon *et al.*, 2006; Albanese *et al.*, 2013), including cervical dystonia (REF), childhood dystonia due to brain injury (Young *et al.*, 2011), and commonly in focal hand dystonia (FHD) (Sitburana and Jankovic, 2008). Being one of the characteristic features of FHD, motor overflow activity has been thought to have bearing on the loss of inhibition at multiple levels in the central nervous system, abnormal plasticity and abnormal sensory function (Hallett, 2006), but the exact pathogenesis and pathophysiology are far from being well understood.

Although the neural basis of motor overflow in FHD is not well understood, there is evidence that sensory deficits, especially a decreased precision of tactile and proprioceptive perception, could be an important cause (Bara-Jimenez *et al.*, 2000a; Bara-Jimenez *et al.*, 2000b; Sanger and Merzenich, 2000). It was originally thought that once the sensory cortical map is established no further change occurs. However, several studies in the past decades have shown that the organization of somatotopic sensory cortex is plastic such that the map can be reorganized in response to sensory experience, and dramatic shifts can happen due to stroke or injury (Kaas and Florence, 1997; Nelles *et al.*, 1999; Chen *et al.*, 2002; Nudo, 2013). In FHD, the somatotopic map of hand region is believed to be altered through a process of neuroplasticity. Multiple studies suggest that there are occurrences of severe degradation in finger representation in somatosensory cortex (Elbert *et al.*, 1998; Bara-Jimenez *et al.*, 1998). In primate models of focal hand dystonia, de-differentiation in somatosensory cortex is created by excessive repetitive associative stimulation of a skin region on different digits not normally stimulated conjointly (Byl *et al.*, 1996). There were also a "smearing" of receptive fields in FHD (Byl *et al.*, 1996). In patients with Writer's cramp and Musician's cramp, enlarged and overlapping receptive fields in the somatosensory and primary motor cortex were observed. Supporting the sensory dysfunction in the pathology of dystonia, a decreased performance in spatial and temporal discrimination tests was consistently reported in patients with focal hand dystonia (Tinazzi *et al.*, 1999; Bara-Jimenez *et al.*, 2000a; Bara-Jimenez *et al.*, 2000b; Sanger *et al.*, 2001; Scontrini *et al.*, 2009)

Despite the physiological evidence of sensory deficits, developmental mechanisms of motor overflow in FHD have yet to be clarified. The prolonged, repetitive use of the hand may be a significant contributing factor in the development of the sensory abnormality in FHD. Studies with primates show that temporally correlated sensory input activity plays a key role in the establishment of modification in receptive fields and sensory topography through a hebbian-like plasticity (Bara-Jimenez *et al.*, 1998; Blake and Merzenich, 2002). In humans, associative pairing of tactile stimuli to the digits induces organizational changes in the sensory cortex (Godde *et al.*, 1996). In patients with writer's cramp, stimulation-induced reorganization in the corticospinal motor system is more rapid and pronounced compared to that in healthy controls and the brain's response to paired associative stimulation (PAS) was exaggerated and its spatial specificity was reduced in writer's cramp (Quartarone *et al.*, 2003). Considering the fact that somatosensory dysfunction has a direct link to motor disorder (Konczak and Abbruzzese, 2013) the loss of spatial specificity in sensory regions could lead to the loss of specificity in motor regions. Furthermore, it is known that altered sensorimotor connections to motor cortex may impair motor function because the somatosensory cortex has an important influence on the motor system (Hoon *et al.*, 2009; Sanger and Merzenich, 2000).

This evidence supports the temporal correlation hypothesis of cortical dynamic processing—the temporal coincidence of neural events from various sensory modalities induces plastic changes in cortical topography. Thus, we postulate that if there are correlated movements among fingers that generate sensory input statistics that are dependent on each other, it is likely to cause confusion in the sensory topography and eventually produce irreversible motor overflow. However, understanding the underlying neural mechanisms linking the characteristic sensory input statistics and the manifestation of motor overflow symptoms has been limited by methodological availability of *in-vivo* neurophysiology. Therefore, we attempt to overcome the limitation by leveraging a neuromorphic high-speed hardware emulation platform.

The rate-based computational model of the development of focal had dystonia was previously developed (Sanger and Merzenich, 2000). As predicted by Sanger and Merzenich(Sanger and Merzenich, 2000), and demonstrated by Merzenich and Byl (Byl *et al.*, 1996), correlated sensory inputs lead to sensory disorganization and have the potential to produce motor dysfunction. The innovation of this study is the use of spike-based simulation and high-speed emulation with a more physiologically accurate model of synaptic plasticity. In the motor overflow in FHD, we

speculate that temporally correlated sensory inputs between two digits could lead to the growth in synaptic connections that are not normally strengthened such that they cause the loss of spatial specificity and motor overflow between the two digits. In this study, we test a hypothesis that correlated input activity in two adjacent sensory regions is sufficient to develop and perpetuate motor overflow if spike-timing-dependent-plasticity (STDP) is simulated. The perpetuation of motor overflow in FHD is an emergent phenomenon when the crosstalk synapses gain weight due to the correlated inputs and produce prominent motor overflow; the overflow failed to recede even when the motor inputs subsequently became uncorrelated. We used programmable Very-Large-Scale-Integrated (VLSI) hardware to simulate four days of intensified development of synaptic strength at high speed. Our model demonstrates (1) the enlargement of the cortical finger representation and increase in receptive field of the digits by growth of crosstalk synapses under correlated sensory inputs, and (2) the perpetuation of motor overflow after the synchronized input activity has ended. Although our model is a highly simplified and limited representation of sensorimotor cortex, it allows us to explain how synchronized sensory inputs could lead to the development and perpetuation of overflow of motor commands due to plasticity.

4.2 Materials and methods

We emulated a two-layer neuronal network using our recently developed neuromorphic hardware. The emulation included 4 spiking neurons using Izhikevich's approximation to the classic Hodgkin-Huxley neurons (Izhikevich, 2003a). Izhikevich neurons are used because they permit use of biologically realistic variables including transmembrane currents, yet they can be implemented much more efficiently in hardware than the more complex Hodgkin-Huxley equations that they approximate (Izhikevich, 2003a). Our emulation using Very-Large-Scale-Integrated-circuit (VLSI) technology allows us to describe the change of synaptic weight under the influence of each individual spike, especially their relative timing compared to adjacent spikes. This is critical for evaluating whether the correlation between sensory inputs will have an effect on the output. We were capable of accelerating the emulation to 190x real-time. Therefore we are able to test hypotheses about the spatial specificity in adjacent sensorimotor system due to correlated or uncorrelated sensory input over long-term period. In this study, we did not make use of the parallel implementation of neuron populations because the major aim was to

investigate the phenomena arising from the fundamental properties of simplified neuron structure described in the next section.

Neural structure

We modeled a subset of sensorimotor system as a layer of adjacent sensory neurons projecting to the layer of neurons in the sensory cortex (Fig.15B). This is a simplified representation of the sensory-motor connections in cerebral cortex. The two input neurons (n0, n2) in the input layer, representing sensory neurons, project to two output neurons (n1, n3) in the output layer, representing sensory cortex. Among the four synaptic connections present in the structure, the strength of the connection is represented by the size of the weight in the connecting synapse. In the healthy state, the horizontal synaptic connection has a dominant connection and the crosstalk (diagonal) connection bears minimum weight to ensure high spatial specificity. In the network, all signals are encoded by neurons as spikes, which travel to the next level of neurons via synapses. The timing of the presynaptic and postsynaptic spikes determines the strengthening and weakening of the connection according to the spike timing dependent plasticity (STDP) rule (Bi and Poo, 2001; Froemke and Dan, 2002) (Fig.14A). The standard additive update with all-to-all scheme (Pfister and Gerstner, 2006) where all pairwise combinations of presynaptic and postsynaptic spikes contribute the update (Fig.14B). In this STDP implementation, maximum time difference between spike pairs is 64ms due to hardware restrictions. The number of points in the curve is adjusted to preserve the ratio of area under LTP and LTD. The STDP implementation does not include naturally occurring synaptic decay which is not a necessary requirement to demonstrate the result in this study but to additionally demonstrate that homosynaptic LTD is not an inevitable property of synapses under certain condition, as exemplified in the homeostatic synaptic level in the STPD demo (Fig.16C). In case of presynaptic spikes causing postsynaptic spikes to fire, causally correlated pre-post firing activity facilitates long-term potentiation (LTP) in the synapse under certain presynaptic frequency range (<20Hz) in the simulation. Stochastic current input to the neuron is used as an activity generator. Input current to the neuron ([0.6*I_th < I_input < 1.7*I_th], I_th: neuron firing threshold) has random variation with fixed mean value that causes presynaptic firing rate to be about 15Hz. This represents constant sensory stimulation over time, and is the combined current due to all sensory inputs to each neuron.

The equations that govern the update of the postsynaptic current and the synaptic weight are as follows:

$$\tau_{SCD}\frac{dI(t)}{dt} = I(t) + \delta(t - t_0)g(t)$$

$$g(t+1) = g(t) + f\left(t_{post} - t_{pre}\right)$$

Equation 1

First equation is a rule for updating the postsynaptic current. The postsynaptic current has an exponential decay ($\tau_{SCD} \cong 15ms$) and incoming presynaptic spike adds to a current the size of the strength of the synapse. Synaptic strength ($g(t)$) is updated according to the STDP kernel (f) additively (Fig. 14). The area under the STDP curve is larger in LTD curve than LTP curve by approximately 1.4 fold. In our implementation, discretized curve has a time resolution of 1ms. Fig. 14B is an illustration of the all-to-all scheme in STDP. All pairwise combination of presynaptic and postsynaptic spikes contributes to plasticity. In this implementation, a maximum time difference between of spike pairs is 64ms due to hardware restriction. The number of points in the curve is adjusted to preserve the ratio of area under LTP and LTD.

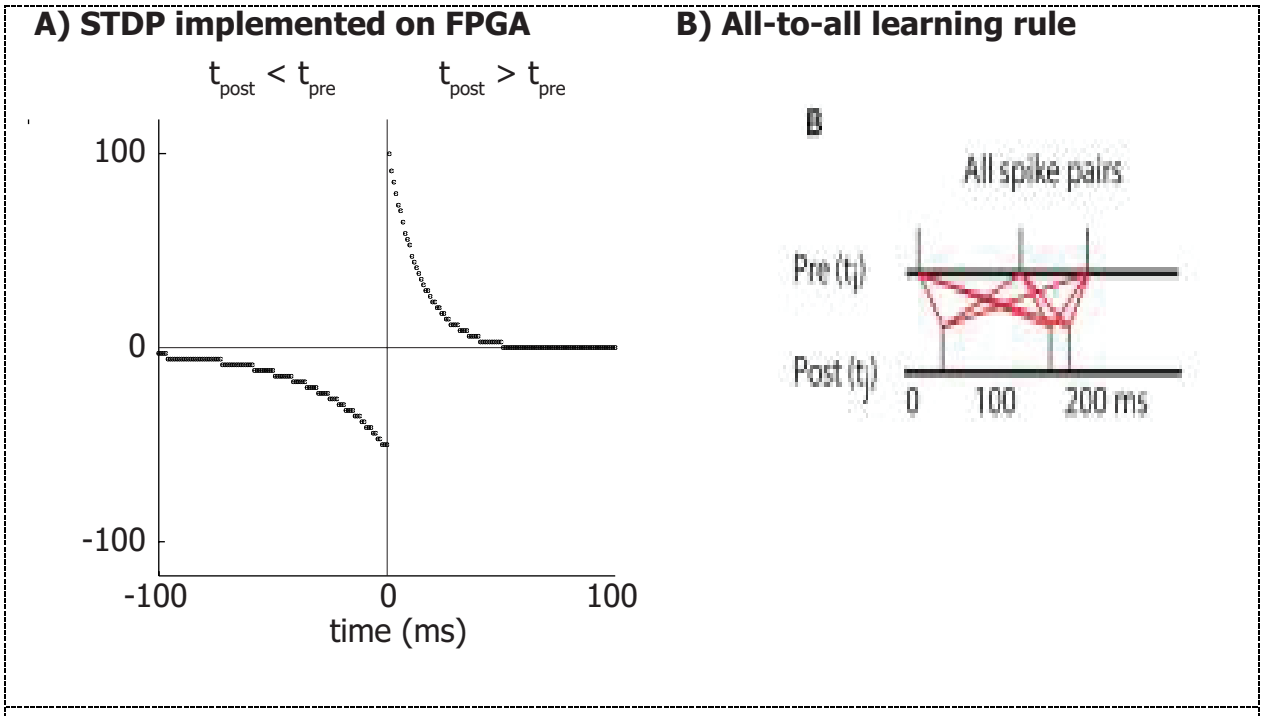

Figure 14. STDP demo. A) Spike timing dependent plasticity curve implemented on FPGA. Synapse potentiates when postsynaptic spike arrives a few milliseconds after presynaptic spike arrives and depresses if the order is reversed. The parameters A+= 103%, A- = -51%, tau+ = 0.014 sec, tau- = 0.034 sec are taken from Froemke and Dan (2002). The area under the curve is larger in LTD curve than LTP curve by approximately 1.4 fold. In our implementation, discretized curve has time resolution of 1ms. B) Illustration of all-to-all algorithm, a common method in STDP. All pairwise combination of presynaptic and postsynaptic spikes contributes to plasticity. In this implementation, maximum time difference between of spike pairs is 64ms due to hardware restriction. The number of points in the curve is adjusted to preserve the ratio of area under LTP and LTD.

4.2.1 Experimental procedure

The experiment is designed to test whether transient correlated sensory inputs may lead to the development of motor overflow. Experiment is divided into three phases according to the type of current profile to the input neurons in order to single out the effect of correlated sensory input as an inserted intervention in the middle of the experiment. In the control, there is no inserted intervention phase. In the first phase, two input neurons receive two different and statistically

independent currents, which represents two adjacent sensory neurons receiving distinct pattern of inputs from each other. Two different stochastic currents guarantee that the two are uncorrelated. In the second phase, current from an identical source is drawn to both input neurons in synchronous way such that inputs are fully correlated. In the third phase the input profile is the same as the first phase in order to observe how the hysteresis effect by second phase is carried on further. The hardware acceleration allows simulation in 30 minutes in real time to represent 95 hours worth continuous sensory stimulation.

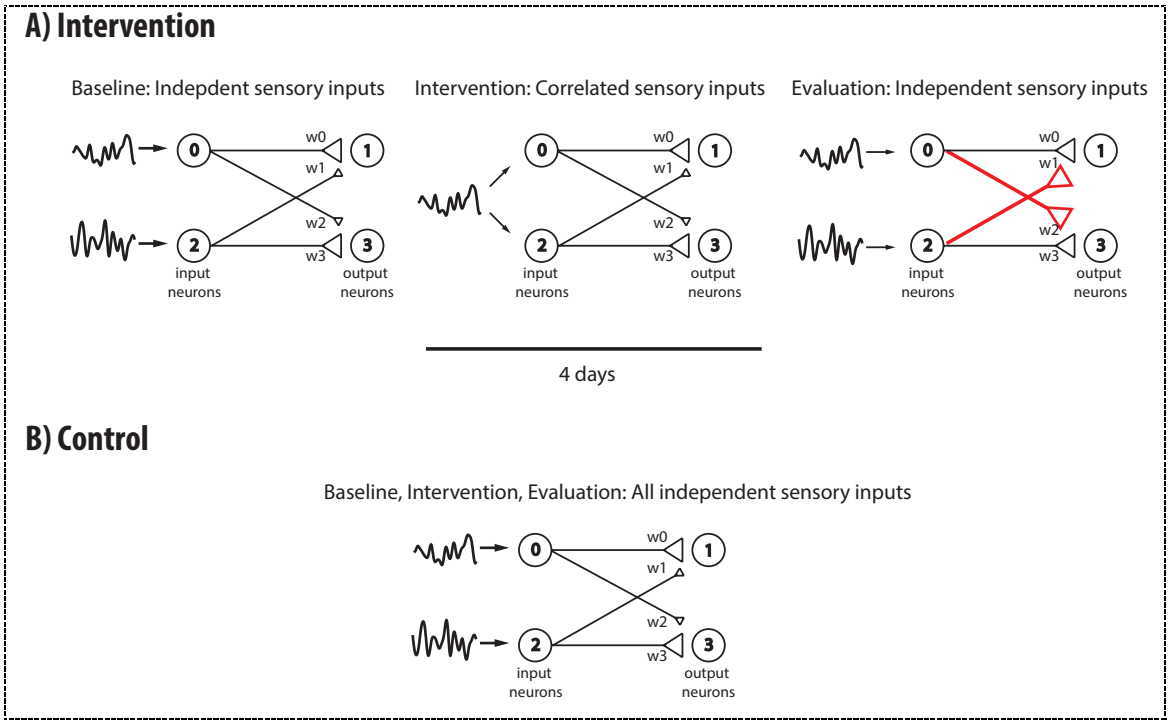

Figure 15. The experimental design testing whether confused (correlated) sensory inputs may lead to motor overflow. Experiment is divided into three phases according to the type of current profile to the input neurons. In the first phase, two input neurons receive different currents, which represents two adjacent sensory neurons receiving distinct pattern of inputs from each other. Two different stochastic current generators guarantee that the two are uncorrelated. In the second phase, current from a single source is drawn to both input neurons in synchronous way such that inputs are fully correlated. This goal of this phase is to observe the effect of two adjacent sensory neurons receiving correlated pattern of inputs. In the third phase the input profile is the same as the first phase in order to observe the perpetuated effect by second phase in long term. The hardware acceleration allows simulation in 30 minutes (real time) to represent 96 hours worth continuous sensory stimulation.

4.3 Results

4.3.1 Demo of plasticity effect under STDP

We first demonstrate the functionality of the implemented STDP by tracking the long-term effects of stochastic current input to the synaptic weight in homosynaptic connection (Fig.16A). When stochastic current drives the input neuron that generates ~15Hz of presynaptic firing rate, the postsynaptic spikes are generated from the postsynaptic current. The STDP rule dictates that causal correlation between pre- and postsynaptic spikes will initiate long-term potentiation (LTP) of the synapse. As weight increases, presynaptic spike causes a burst of postsynaptic spikes which gets denser and longer due to the increasing postsynaptic current and therefore works as a positive feedback to further weight increase. The time course of synaptic weight change demonstrated shows the synaptic growth by LTP dominant stage (between day1 and day 16) and homeostatic stable stage by the balance between LTP and LTD (after day 16). Increased postsynaptic firing rate due to synaptic growth increases LTD, which prevents the synapse to grow infinitely by forming a plateau of synaptic strength. The STDP implementation does not include naturally occurring synaptic decay. It is to demonstrate that homosynaptic LTD is not an inevitable property of synapses with STDP, and it exemplifies that decay may not be necessary to implement the homeostatis in the synaptic strength under homosynaptic stimulation.

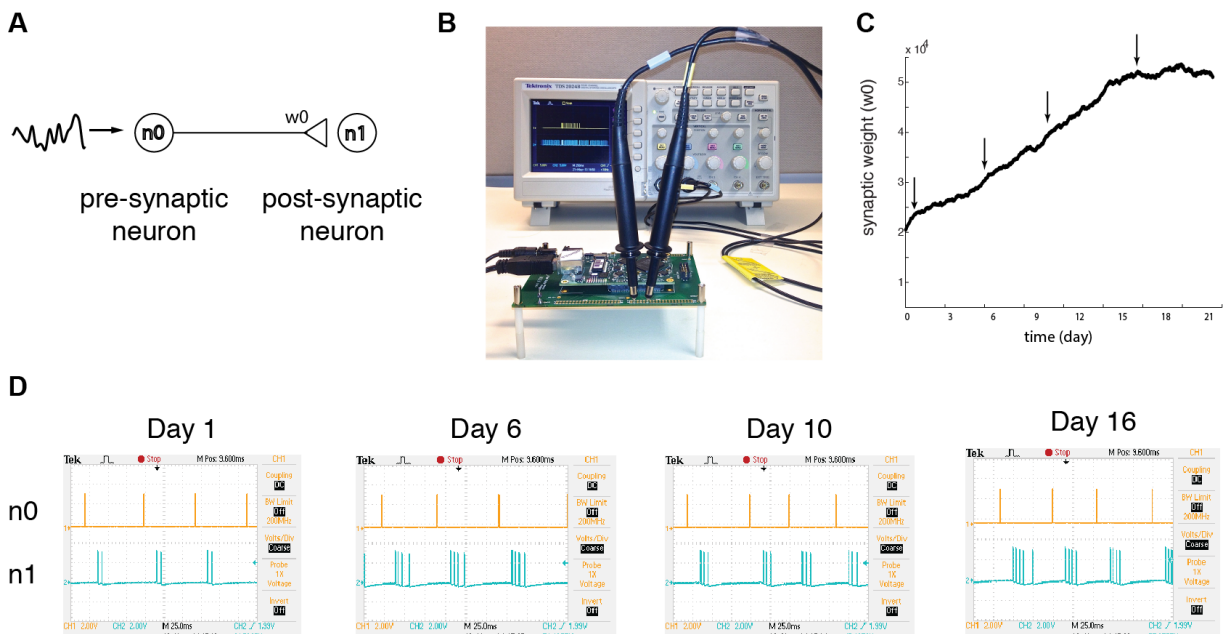

Figure 16. Validation of STDP implemented using neuromorphic hardware. We emulated a homosynaptic connection between 2 neurons (A), of which the pre-synaptic neuron received a continuous pseudo-white-noise input for an equivalence of 21 days. The neuromorphic hardware (B) accelerated the emulation by 190x real-time so the emulation took about 2 hours and 30 minutes, neuromorphic hardware also allows for onboard measurement of neuron spikes. The longitudinal change of synaptic weight across 21 days (C) shows a gradual increase between day 0 and day 14 followed by a plateau. When the pre-synaptic neuron produced spike trains at a constant rate, the increase and plateauing of post-synaptic spiking rate confirmed the longitudinal change of synaptic weight. Snapshots from oscilloscope are shown (D). Increased bursting after a single spike is observed as the synaptic weight increases. This is because the postsynaptic current has a weight dependent update rule (Equation 1).

4.3.2 Development and perpetuation of motor overflow

The initial condition of the network is set to have weak crosstalk connections and strong healthy horizontal connections (Fig.17A). This condition represents a healthy state. In the first phase, non-correlated input to the two input neurons is unable to grow the crosstalk (diagonal) synapses. This is because presynaptic spikes are weakly correlated with crosstalk postsynaptic spikes such that LTD dominates over LTP in the STDP curve. The first phase lasts until 18th hour. In the second phase, synchronized currents drive the two input neurons and the crosstalk gradually grows so long as the inputs were correlated. This is because presynaptic spikes are fully correlated with postsynaptic spikes such that LTP dominates in the STDP curve for both crosstalk and direct connections. The second phase lasted up to the 46th hour. The slight variation in the duration of this phase comes from the variation in time to grow the synapse due to the stochastic input current profile. The duration of the second phase is arbitrary but is set to be long enough to observe the growth of crosstalk synapses. In the third phase, non-correlated input currents were applied, but the network perpetuated the state of significant crosstalk. This is because presynaptic spikes from the input neurons are partially, but not negligibly, correlated with the postsynaptic spikes in the output neurons located diagonally due to the significantly grown crosstalk synapse such that contribution from LTP and LTD balances out in the crosstalk synapses. The third phase lasted up to the 4th day (95 hours). The shaded area in the plot represents the mean ± standard deviation for 6 trials.

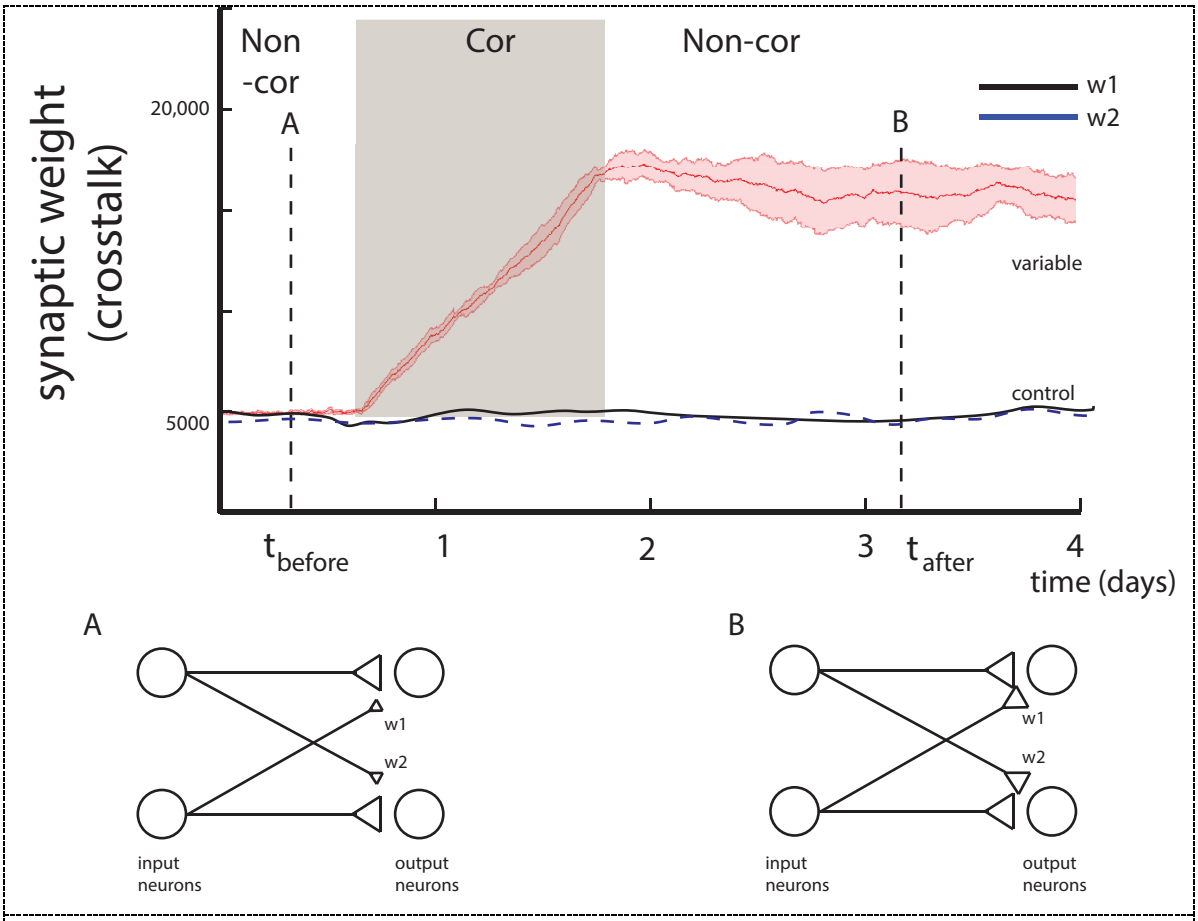

Figure 17. Development and perpetuation of the motor overflow. Change of synaptic weight of the crosstalk is plotted. A) Healthy state: the size of the crosstalk-synapses (w1, w2) are kept minimal and they do not grow under non-correlated input profile to the input neurons. B) Crosstalk synapses have grown after the correlated phase and the grown states are perpetuated even after the correlated phase has ended.

4.3.3 Enlarged sensory representation and increase in receptive field

We quantified the growth of crosstalk, enlarged cortical representation, increase in receptive field size in the following way. At time point A and B in Fig. 17, we sampled the input and output signals to analyze the change made before and after the intervention in the second phase. To quantify the growth of crosstalk and enlarged cortical representation, electromyogram (EMG) is generated from the postsynaptic signals as an output measure to represent the synaptic strength. Increased EMG response due to the growth of crosstalk represents the sensory deficit being

propagated to the motor abnormality. The size of the cortical representation is measured from the sum of EMG responses in the two output neurons due to the activity in one input neuron (Fig. 18). For the change in receptive field size, we count the number of input nodes that produce EMG activity in output neuron D (Fig. 18) over a specified threshold.

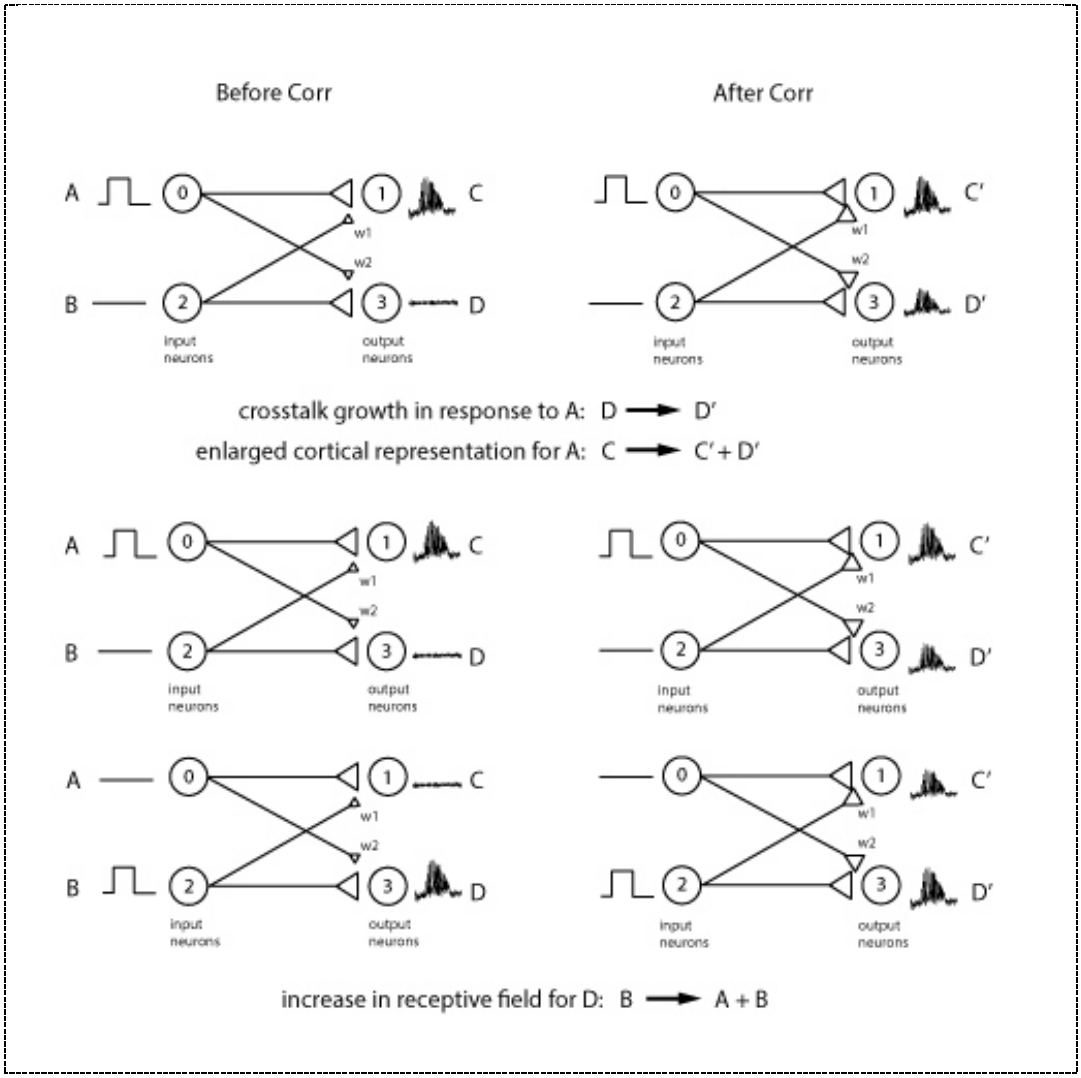

Figure 18. Visual aid for the enlarged cortical representation, increase in receptive field and growth in crosstalk. We also see a decrease in spatial specificity due to a growth of crosstalk.

Growth of crosstalk in response to input in A is represented by the difference between D and D' (Fig.18A)

Enlarged cortical representation for part A is represented by the difference between C and C' + D' (Fig.18B).

Increase in receptive field size for neuron D is represented by the A and A + B (Fig.18C)

Fig.19 shows a comparison between human overflow data and our emulation data. The human data (left) are from the study of motor overflow in patients with dystonic symptoms at hand (Young *et al.*, 2011). Human data show representative EMG recordings of two muscles during 60s trials. The participants were instructed to track the target on the screen that is controlled by EMG modulated signal from a task finger. EMG from a non-task finger is also recorded to measure the overflow. In the 2x2 matrices, if the signals are only in the diagonal window it means there is no overflow. If there is an activity in the non-diagonal window it signifies the existence of overflow of muscle activity from the muscle in the task finger to the muscle in the non-task finger. The comparison is made between control and dystonia. Similar to the human data, our emulation data (60s) sampled before and after the correlated input phase are plotted in the 2x2 matrices (Fig.19, right). Activity in the non-diagonal window signifies the overflow of activity due to crosstalk. Growth of crosstalk is measured from the change in mean EMG level in output node D in response to an input in A (Fig.18A). Normalized crosstalk is 0.08 (=0.0054/0.0720) in human control and 1.78 in human dystonia (+1.70, increased crosstalk), and 0.20 in emulated control and 0.31 (+0.11, increased crosstalk) in emulated dystonia. Enlarged cortical representation is measured from the change in sum of mean EMG levels in the two output nodes C and D (Fig.18B). Normalized cortical representation is 1.08 (=(0.0054+0.0720)/0.0720) in human control and 2.78 in human dystonia (+1.70, enlarged

cortical representation), and 1.20 in emulation control and 1.31 in emulation dystonia (+0.11, enlarged cortical representation). Increase in receptive field size is quantified by recording the number of input neurons that elicit a response in output node D (Fig.18C). Discrete number of receptive field is 1 in human control and 2 in human dystonia (+1, increased receptive field), and 1 in emulation control and 2 in emulation dystonia (+1, increased receptive field).

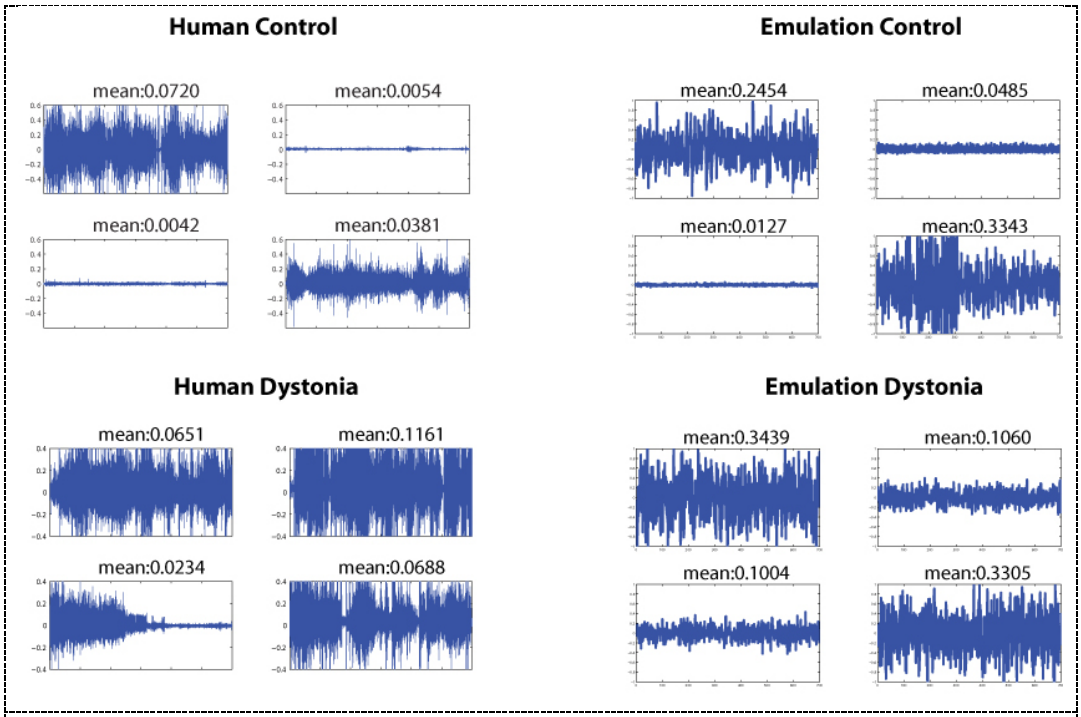

Figure 19. Comparison of motor overflow between human and emulated data. Signals only at diagonal windows represent healthy human control. In dystonia, signals in the non-diagonal windows increases due to motor overflow. Similar pattern is observed between emulation of control and dystonia (right).

4.4 Discussion

The purpose of this study was to use neurmorphic emulator to understand the origin and development of focal hand dystonia (FHD) because developmental mechanisms of motor overflow in FHD have yet to be clarified. We started from physiological evidences of sensory deficits found in FHD and speculated that the correlated sensory activity could a direct cause for

the development of motor overflow in FHD. In other words, this is to emulate prolonged, repetitive use of the hand as a significant contributing factor in the development of the sensory abnormality in FHD. Considering the fact that somatosensory dysfunction has a direct link to motor disorder (Konczak and Abbruzzese, 2013), and the somatosensory cortex has an important influence on the motor system (Hoon *et al.*, 2009; Sanger and Merzenich, 2000) we assumed that emulating the development of sensory disorganization would directly imply the disorganization in motor system, leading to motor overflow. In order to emulate the dynamic growth of strength in the neural structure, we implemented spike-timing-dependent plasticity (STDP) in customizable hardware to build a biologically realistic high-speed emulation platform to test the temporal correlation hypothesis of cortical dynamic processing in FHD—namely we postulate that correlated movements two adjacent fingers is sufficient to cause confusion in the sensory topography and eventually produce irreversible motor overflow between the two fingers. The hypothesis as an extension from the rate-based computational model of the development of focal had dystonia that was previously developed (Sanger and Merzenich, 2000). The innovation of this study is the use of spike-based simulation and high-speed emulation with a more physiologically accurate model of synaptic plasticity. Our model demonstrates (1) growth of crosstalk synapses and (2) the enlargement of the cortical finger representation and (3) increase in receptive field of the digits under correlated sensory inputs. Another emerging phenomenon of using STDP was the perpetuation of motor overflow after the synchronized input activity has ended.

4.4.1 Relevance of the simulated neural structure to the biology

The two-layer neural structure is used to represent simplistic sensorimotor system in the cortex. Four synaptic connections from input neuron substrate to output neuron substrate represent the normal and crosstalk connection between two sensory digit representations. Although admittedly the neural structure is an oversimplification of the complex system encompassing from sensory neurons to the sensory representational map in the cortex, our model allows us to explain how synchronized sensory inputs could lead to the development and perpetuation of overflow of motor commands due to plasticity.

4.4.2 Sensitivity of the result to other synaptic learning models

The question could be asked of how sensitive the result will be to the various synapse learning models. Although it is not of our interest in this study to test the different effects of various implementations of STDP update mechanisms, it can be said that the result is generalizable if 1) update mechanisms dictate that correlated pre- and postsynaptic spikes causes potentiation and uncorrelated pre- and postsynaptic spikes causes depression of the synaptic weight, 2) postsynaptic firing rates are *not* in the range that results in net depression. Our implementation has asymmetric STDP curve, and is all-to-all (Pfister and Gerstner, 2006) and standard additive. Variation in curve shape, nearest-neighbor implementation instead of all-to-all, multiplicative in stead of additive update will still generate the same results in this study if the above conditions are met.

4.4.3 Implication of the emulated result in clinical treatment of FHD

The emulation of the FHD suggests how to minimize the risk of development or possibly prevent the development of FHD. Since the synchronous sensory activity is the direct cause that makes the crosstalk synapse to grow, the first caution should be taken not to get heavily involved in effortful exercises that generate correlated sensory movements—forced grips or any simultaneous contraction of hand muscles, e.g. in labored writing. It is equally important that the potential patients must limit their duration of exercising any synchronous activity, if they must do some. For musician who are at a risk of developing musician's cramp, limiting the play time will help to prevent the crosstalk to grow beyond a point that will make the effective treatment harder due to the perpetuating nature of the overflow. Among the list of currently available treatment options in FHD, Botulinum toxin is proven to have a benefit but many patients discontinue due to dissatisfactions with the result. Sanger and Merzenich's model (Sanger and Merzenich, 2000) implies that some of the beneficial effect of injecting the toxin may be due to reducing the overall gain of the sensorimotor loop by reducing the sensory afferents. Present study implies that once the FHD is fully developed there may not be an easy way to return to the healthy initial state by eliminating the crosstalk connections. One of the possible rehabilitation methods might involve completely inactivating the affected hand for long enough time to hope for the cortical representational map of the hand to shrink in size (or un-mapping process) such that the remapping can be done easily.

The fact that we observe a rapid change in cortical organization upon stimulation also suggests higher-than-normal plasticity in patients with focal hand dystonia. It would be interesting future work to emulate the effect of learning rate in developing focal hand dystonia.

4.5 Conclusion

The purpose of this study was to understand the pathology of developing focal hand dystonia by using biologically realistic neural structure to test our temporal correlation hypothesis. As predicted by Sanger and Merzenich (Sanger and Merzenich, 2000), and demonstrated by Merzenich and Byl (Byl *et al.*, 1996), correlated sensory inputs lead to sensory disorganization and have the potential to produce motor dysfunction. Here we extended this work using a more realistic plasticity model with spike-timing dependent plasticity.

4.6 Author Contributions

Designed the experiment: WS CN. Performed the experiments: WS. Developed the hardware and visual software: WS. Analyzed the data: WS. Wrote the paper: WS. Presented by WS at the Annual Meeting of the Neural Control of movement (NCM) in April 2014 and April 2015. Reviewed the manuscript: WS CN TS.

5 Study 3: How does the constraint-induced therapy work?

Emergent phenomenon from a synaptic competition: Constraint-induced intervention as a way to escape from the suboptimal stable solution in biological systems

Won J. Sohn[1†], Terence D. Sanger[1,2,3*]

[1]Department of Biomedical Engineering, [2]Biokinesiology, and [3]Neurology, University of Southern California, 1042 Downey Way, Los Angeles, California, 90089

*** E-mail:** tsanger@usc.edu

Abstract. The principle of constraint-induced therapy is widely practiced in rehabilitation. In the animal model of hemiplegic cerebral palsy (CP), the impaired contralateral corticospinal projection due to postnatal unilateral injury was repaired after imposing temporary constraint in one of the less affected hemisphere. Despite some differences, such impairment in motor control by early brain injury bears a resemblance to amblyopia in that it involves inter-hemispheric activity-dependent synaptic plasticity. Previously, the mechanism for amblyopia, equivalent to hemiplegic CP in visual system, has been explained within the framework of BCM theory, a rate-based synaptic modification theory, but here we attempt to provide a fundamental explanation for the general biological phenomena that involve inter-hemispheric synaptic competition in spike-based theory. In this study, we choose to emulate the restoration of the postnatal hemiplegic CP in terms of the competition between ipsilateral and contralateral CST. The importance of the study comes from the fact that there is a considerable gap between clinical practice and the understanding of the neural mechanism underlying the therapeutic method due to the limited methodological availability in electrophysiology, despite the success in the many applications of constraint-induced therapy. We strive to overcome the limitation by leveraging our neuromorphic high-speed hardware emulation platform created in previous work to study the neural underpinning of constraint-induced therapy. We hypothesize that the mechanism of constraint-induced therapy can be demonstrated when a simplified neural descending tract with 2 layers of spiking neurons that represent cortical and spinal neural substrate are simulated with spike-timing-dependent

plasticity (STDP). In the 19-days of continuous emulation that includes periods of the development of hemiplegia and the recovery from it due to imposing an alternate constraint on the uninjured hemisphere, we observed the activity-dependent synaptic competition as a key mechanism that accounts for the formation of persistent deficits which is suboptimal due to transient developmental injury and learned the fact that a forced intervention is essential to transition into an improved state. Although our model is a highly simplified and limited representation of descending corticospinal system, it offers an explanation of how constraint as an intervention can help the system to escape from the suboptimal solution. This is a display of an emergent phenomenon from the synaptic competition.

Keywords: Spike-timing-dependent plasticity (STDP), Constraint-induced therapy, Constraint-induced movement therapy (CIMT), corticospinal development, suboptimal system.

5.1 Introduction

Recent discoveries regarding how the central nervous system responds to injuries have prompted development of rehabilitative training for the patient to reacquire lost function. For instance, new families of techniques called constraint-induced movement therapy (CIMT) have been developed and proven to be effective in producing large improvement in limb use of patients after cerebrovascular accidents (CVA) (Taub *et al.*, 1999), and sensory and motor CNS injuries (stroke, etc.). It is constraining the use of less-impaired upper extremities while intensive and repetitive training of motor activities are conducted for up to 6 hours per day, for 2-4 weeks with rewarding to the successive approximation to the target task (Taub *et al.*, 1999; Taub *et al.*, 2007; Brady and Garcia, 2009), and it became a 'paradigm shift' in rehabilitation of CNS injury.

Conceptually similar interventional strategy that promotes activity of the injured system or demotes the activity of uninjured system in the animal model of hemiplegic cerebral palsy (CP) has been shown to contribute to significant corticospinal tract (CST) repair and motor recovery. Martin *et al*. showed that temporarily imposed constraint in one of the less affected hemisphere and active stimulation in the affected hemisphere harness activity-dependent plasticity to repair the diminished connectional strength (Martin, 2005; Friel and Martin, 2007; Martin *et al.*, 2011). When activity in one motor cortex is blocked pharmacologically during an early sensitive period, CST axons withdraw their projections (Friel and Martin, 2007) and constraining the use of one limb during a similar period produced similar effect on the development of contralateral CST projections (Martin *et al.*, 2004).

Amblyopia is a unilateral reduction of visual acuity that bears a resemblance to the impairment in the corticospinal system by early brain injury, as it is referred as hemiplegic CP in the visual system. Amblyopia is the most common cause of lifelong monocular blindness (Attebo *et al.*, 1998), caused by abnormal visual experience during postnatal development. The commonly practiced intervention involves patching the dominant eye while forcing the child to use the weaker eye to revive the visual impairment of the weaker eye. In animal studies, the effect of monocular deprivation is reversible only if the treatment is applied during the critical period because the treatment causes changes in visual cortex for recovery (Movshon, 1976; Movshon & Van Sluyters, 1981). The classic idea is that the patching gives a competitive advantage to the amblyopic eye to overcome the dominance established by the other eye.

Although the underlying mechanisms behind the effect of the patching in the visual system may not identical to the effect of imposing a constraint in the corticospinal system, it is still evident that the principle of constraint-induced therapy can be highly effective across the modalities in the biological system as long as inter-hemispheric competition is present.

Previously, the treatment mechanism for amblyopia has been explained within the framework of BCM theory, a rate-based synaptic modification theory. Here, we attempt to provide a simple yet fundamental mechanism that accounts for the general biological phenomena that involve inter-hemispheric synaptic-competition using spike-based plasticity theory. Specifically in this study, we choose to emulate the development of and restoration from the abnormal corticospinal projections in postnatal hemiplegic CP. The importance of the current study comes from the fact that there is a considerable gap between clinical practice and the understanding of the neural mechanism underlying the therapeutic method due to the limited methodological availability in electrophysiology, despite the success in the many applications of constraint-induced therapy. We strive to overcome the limitation by leveraging our neuromorphic high-speed hardware emulation platform created in previous work to study the neural underpinning of constraint-induced therapy. We hypothesize that the mechanism of constraint-induced therapy can be demonstrated when simplified neural descending tracts with two layers of spiking neurons representing cortical and spinal neural substrate are simulated with spike-timing-dependent plasticity (STDP). With 19-days of continuous simulation of the effect of alternate constraints on the cortical neural substrate, we observe the formation of persistent deficits which is suboptimal due to transient problems and learn the fact that a forced intervention is essential to transition into an improved state.

5.1.1 Postnatal brain damage and its effect in corticospinal projection

If there is damage to the corticospinal tract (CST) in the postnatal period, there could be a substantial and long-term consequence for motor function. Unilateral brain injury of this kind can result in hemiplegic cerebral palsy (CP) (Farmer *et al.*, 1991; Carr *et al.*, 1993; Eyre *et al.*, 2001; Eyre, 2007). If the injury causes unilateral inactivation in the developing sensorimotor cortex, the reduced activity in the affected hemisphere could cause increased withdrawal of its existing contralateral corticospinal projection thus results in a weakened contralateral corticospinal projection from the affected cortex. In contrast, the uninjured cortex could develop

increased ipsilateral corticospinal projection, subsequently displacing the contralateral projection, developing suboptimal bilateral projections from the less affected side to the spinal cord, contributing to the persistence of the impairment in motor control due to the insufficiency of the ipsilateral projection from the less affected side to replace the contralateral projection from the affected side (Hendricks *et al.*, 2003; Vandermeeren *et al.*, 2003; Eyre, 2007).

In feline model of CP, Martin found that with hemiplegic CP, the impaired contralateral CST is at disadvantage early in development, compared with the ipsilateral CST that is undamaged, in forming a strong synaptic connection in the spinal cord (Martin *et al.*, 2011). It was proposed that activity-dependent synaptic plasticity is a key mechanism both in the development of hemiplegia and restoring a normal spinal termination pattern and restoring skilled motor function. It was shown that electrical simulation of the impaired CST and inactivation of unimpaired side (reverse inactivation) restored the normal CST termination and the normal motor control was recovered. The feline experiment was significant in understanding the development and treatment for postnatal hemiplegic CP because human CST development parallels closely that of the cat (Martin *et al.*, 2011).

5.1.2 Spike-based synaptic learning rule

Spike-timing-dependent plasticity (STDP) is a synaptic learning rule, based on biological evidences, that uses correlated spiking activity between pre- and postsynaptic neurons to implement synaptic plasticity effects and it is considered a good approximation to learning and information storage in the brain and also for the development and refinement of neuronal circuit in the brain. Depending on the temporal correlation between the spikes, either the synapse gets strengthened or weakened (Bi and Poo, 2001). If the presynaptic spike arrives a few milliseconds prior to the postsynaptic spike, then the pair will contribute to the long-term potentiation (LTP) of the synapses and vice versa for the long-term depression (LTD) of the synapses. The change of the synaptic weight according to the relative timing of pre- and postsynaptic spikes are shown in the STDP function or learning window (see Fig. 21). The curve is based on biological responses from previous studies (Froemke and Dan, 2002). The update of the synaptic weight follows additive, all-to-all scheme (Pfister and Gerstner, 2006).

A rate-based BCM synaptic modification theory (Bienenstock *et al.*, 1982) has shown success in providing an explanation for learning in the visual cortex, developed in 1982. It

proposes first order mathematical prediction of how synaptic plasticity stabilizes postsynaptic activity by a sliding threshold. Although useful to some extent, the explanation is superficial due to its poor biorealism and, therefore, its limitation is defined. The use of STDP over the rate-based models as a synaptic plasticity rule is an advance in terms of biorealistic property.

5.1.3 Benefit of simulating a biological system

We used programmable Very-Large-Scale-Integrated-circuit (VLSI) system, which allows us to create emulations of neurons that communicate using spikes, with the potential to increase the number of emulated neurons without sacrificing speed. A spike-based model is valuable because we want to understand the high-level process in the physiological system that arises from synaptic plasticity based on the neural spiking activity. In this way, we could use spike-based plasticity theory such as spike-timing-dependent plasticity (STDP) to account for the key experimental results. The system allows us to emulate the long-term effect of an intervention, a change in input characteristics to the neural structure, to the change in the synaptic weights in the network. The system further allows us to monitor the emergent phenomena of the STDP in the context of synaptic competition in the simplistic neural structure representing the descending corticospinal system. In this study, we emulate 19-days of continuous simulation of the effect of alternate constraints in the developing brain modeling the experiment on the animal model by Martin et al (Friel and Martin, 2007).

We observed the formation of persistent deficits that is suboptimal due to transient developmental injury and learned the fact that a forced intervention is essential to transition into an improved state. Specifically, our model demonstrates (1) how unilateral inactivation could create hemiplegic bilateral projection, which is suboptimal stable state, (2) the inability of the system to spontaneously restore the diminished contralateral projection after the unilateral inactivation stage has ended, and (3) how alternate inactivation enables the diminished contralateral projection to be restored back by using a principle of constraint-induced therapy. Although our model is a highly simplified and limited representation of descending corticospinal system, it allows us to understand how the principle of constraint-induced therapy can be explained in terms of synaptic competition by activity-dependent plasticity.

5.2 Materials and methods

We hypothesize that the mechanism of constraint-induced therapy can be demonstrated when a simplified neural descending tract with two layers of spiking neurons that represent cortical and spinal neurons are simulated with spike-timing-dependent plasticity (STDP). We customized this two-layer neuronal network from our recently developed neuromorphic hardware. We focus on using spike-based emulation to determine the functional role of constraint-induced intervention, especially their sufficiency for causing restoration of the diminished contralateral projection. The hardware emulation of the spiking neurons and the associated neural structure are constructed using field programmable gate arrays (FPGA, Xilinx Spartan-6), a programmable version of VLSI electronic chips. The emulation includes four spiking neurons using Izhikevich's approximation to the classic Hodgkin-Huxley neurons (Izhikevich, 2003a). Although the system is designed to easily increase the number of emulated neurons to hundredfold without sacrificing speed, current study limits the number of neurons to minimal such that we could focus on understanding the fundamental effect of the intervention in the context of synaptic competition in the simplistic setting.

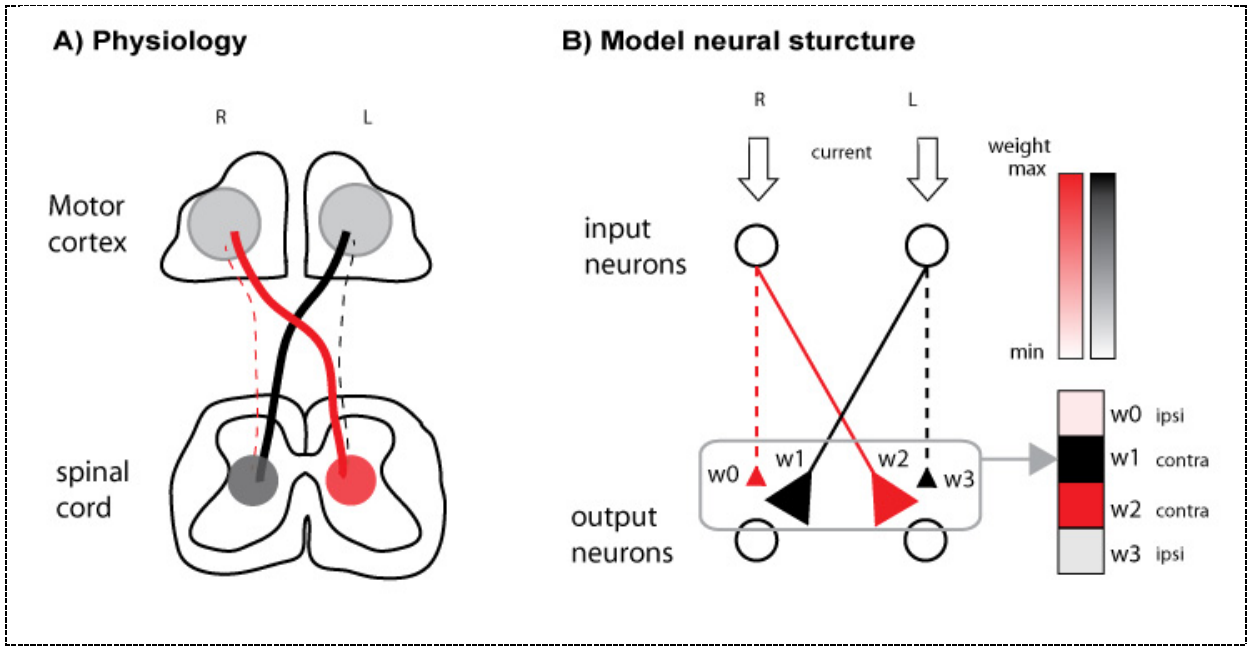

Figure 20. Model neural structure. A) Simplified schematic for descending CST. CSTs initiate from the motor cortex and terminate on the cervical gray matter in the spinal cord. The bold descending lines represent contralateral projection (e.g. right hemisphere to left spinal gray matter) and the dotted line represents ipsilateral projection. The projection strength of the descending tract is represented by the relative thickness of the lines. In normal development, contralateral projection dominates the ipsilateral projection. Distribution of CST projection within the gray matter is not considered for simplification. B) In the simulated neural structure, two layers of spiking neurons representing cortical neurons (input neurons) and output neurons (spinal neurons) are connected via synapses (triangles). A strength of the synapse is represented both by the relative size of the triangle in the structure and by the opacity of the colors in the color matrix. Red corresponds to the cortical projection from the right hemisphere and black for the left hemisphere.

5.2.1 Neural structure

We modeled the descending corticospinal system in two layers of neurons (Fig.20B). The two input neurons (R/L) in the input layer, representing cortical neurons in the right and left motor cortices, project to two output neurons in the output layer, representing neurons in the spinal gray matter (Fig.20A). Among the four synaptic connections present in the structure, the strength of the connection is represented by the size of the weight in the connecting synapses. Izhikevich neurons are used because they permit use of biologically realistic variables including transmembrane currents, yet they can be implemented much more efficiently in hardware than the more complex Hodgkin-Huxley equations that they approximate (Izhikevich, 2003a). In the network, all signals are encoded by neurons as spikes and the spikes pass through synapses. The timing of the presynaptic and postsynaptic spikes determines the strengthening and weakening of the connection according to the spike timing dependent plasticity (STDP) rule (Fig.21A). The standard additive STDP model with all-to-all algorithm where all pairwise combination of presynaptic and postsynaptic spikes contributes to plasticity is used (Fig.21C). In this implementation, maximum time difference between of spike pairs is 64ms due to hardware restriction. The number of points in the curve is adjusted to preserve the ratio of area under LTP

and LTD. In case of presynaptic spikes causing postsynaptic spikes to fire, causally correlated pre-post firing activity facilitates long-term potentiation (LTP) in the synapse under certain presynaptic frequency range (<20Hz) in the simulation**.** Stochastic current input to the input neuron is used as an activity generator. Input current to the neuron (I_input =[0.6*I_th, 1.7*I_th], I_th: neuron firing threshold) has a random variation centered around a mean value that causes presynaptic firing rate to be about 15Hz. The feeding of the current to the input neurons represents constant sensory activity over time.

The equations that govern the update of the postsynaptic current and the synaptic weight are as follows:

$$\tau_{SCD}\frac{dI(t)}{dt} = I(t) + \delta(t - t_0)g(t)$$

$$\tau_{SWD}\frac{dg(t)}{dt} = g(t) + f\left(t_{post} - t_{pre}\right)$$

First equation is a rule for updating the postsynaptic current. The postsynaptic current has an exponential decay ($\tau_{SCD} \cong 15ms$) and incoming presynaptic spike adds to a current the size of the strength of the synapse. Synaptic decay has a natural decay (τ_{SWD}) with a time constant of ~x ms. Synaptic strength ($g(t)$) is updated according to the STDP kernel (f) additively (Fig. 21A, C). The area under the STDP curve is larger in LTD curve than LTP curve by approximately 1.4 fold. In our implementation, discretized curve has a time resolution of 1ms. Fig. 1C is an illustration of the all-to-all algorithm in STDP(Kempter *et al.*, 1999; Song *et al.*, 2000). All pairwise combination of presynaptic and postsynaptic spikes contributes to plasticity. In this implementation, a maximum time difference between of spike pairs is 64ms due to hardware restriction. The number of points in the curve is adjusted to preserve the ratio of area under LTP and LTD.

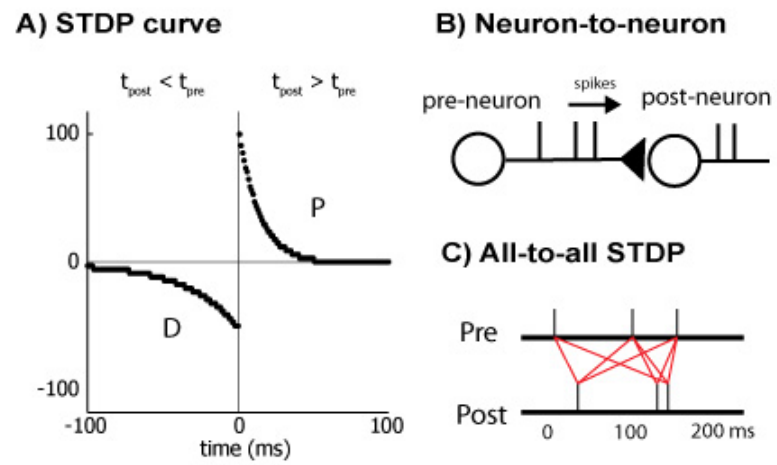

Figure 21. STDP model: the model includes standard all-to-all, additive STDP with synaptic decay and stochastic current input to the neuron as an activity generator. A) Spike timing dependent plasticity curve implemented on FPGA. Synapse potentiates when postsynaptic spike arrives a few milliseconds after presynaptic spike arrives and depresses if the order is reversed. The parameters A+= 103%, A- = -51%, tau+ = 0.014 sec, tau- = 0.034 sec are taken from Froemke and Dan (2002). The area under the curve is larger in LTD curve than LTP curve by approximately 1.4 fold. In our implementation, discretized curve has a time resolution of 1ms. B) Illustration of the spikes traveling from presynaptic neurons to postsynaptic neurons via synapses. The postsynaptic current generates postsynaptic spikes. C) Illustration of the all-to-all algorithm in STDP. All pairwise combination of presynaptic and postsynaptic spikes contributes to plasticity. In this implementation, a maximum time difference between of spike pairs is 64ms due to hardware restriction. The number of points in the curve is adjusted to preserve the ratio of area under LTP and LTD.

5.2.2 Experimental procedure

Experimental procedure of the emulating the constraint-induced therapy closely follows the original experimental procedure conducted by Martin in kittens. The initial stages represents (1) normal contralateral predominant structure ("initial state") and followed by (2) unilateral inactivation of one of the hemisphere by blocking the activity in one of the input neurons ("unilateral inactivation"), (3) normal bilateral activation by removing the blockade ("bilateral

activation”), (4) reverse inactivation of the other hemisphere by blocking the activity in the input neuron that wasn’t blocked before (“reverse inactivation”), and returning to (5) normal bilateral activation which is identical to the third stage (“bilateral activation”). The initial unilateral inactivation is to create a hemiplegic state from the normal contralateral-dominant state. In this stage bilateral projection is established from the activated side by the growth of initially weak ipsilateral connection. Subsequent bilateral activation is to prove that once the bilateral projection, which is suboptimal in terms of biological performance, is established, the state will not change spontaneously without an intervention. The reverse inactivation from the source of bilateral projection is applying a constraint as an intervention to escape from the otherwise consolidated (“*stuck”)* state. After keeping the constraint for a while, the constraint is removed to return to the normal bilateral activation for the hope that the intervention was effective and has a lasting effect. The synaptic decay rate of the synaptic weight of the contralateral connection is set to be lower than that of the ipsilateral connection (see discussion for more detail). We keep track of the change of synaptic weights from the four synapses during the dynamic changes in the input current profile to input neurons.

5.2.3 Constraint-induced therapy uses the property of synaptic competition.

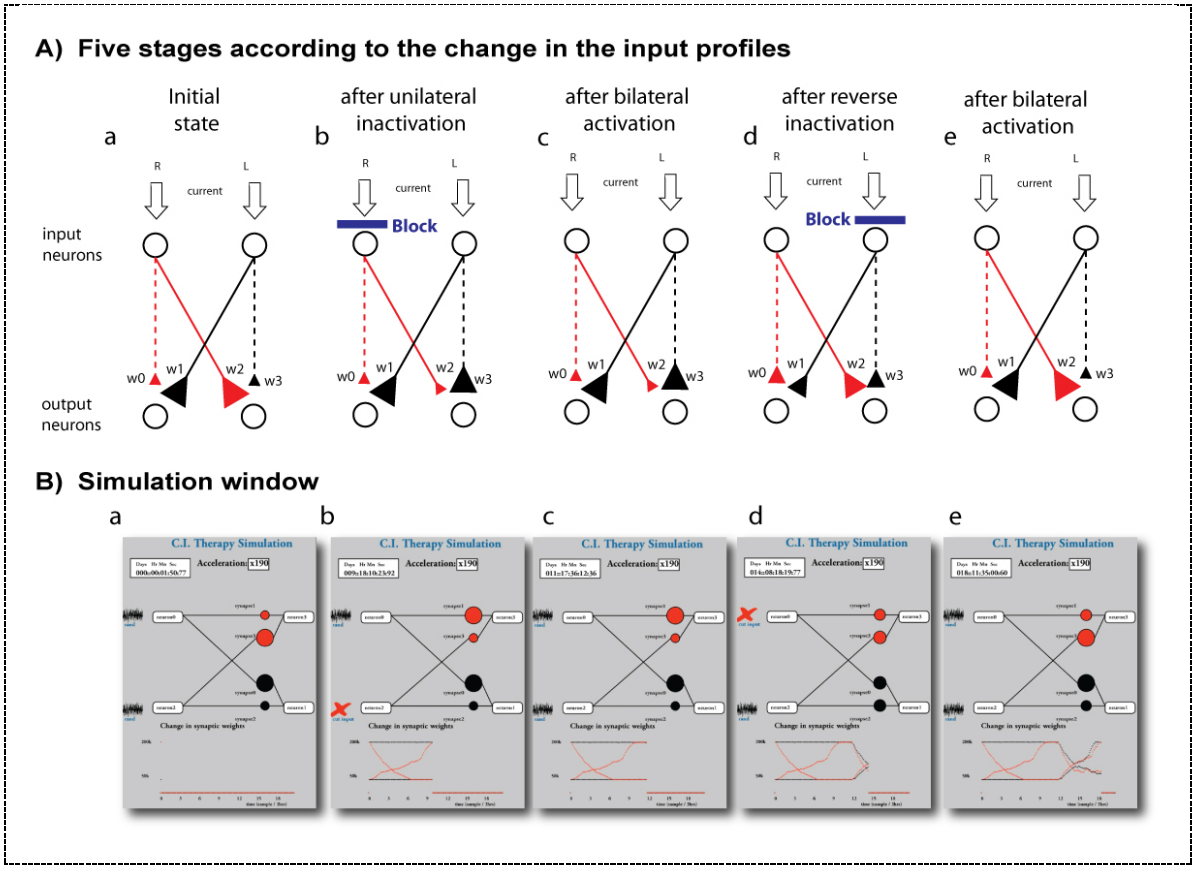

Figure 22. Simulating activity-dependent constraint-induced therapy by STDP in 4 neurons, 4 synapses neuronal structure. Schematic of five stages and corresponding simulation windows. The five stages parallels both the development of and the recovery from the hemiplegic CP in Martin's experiment (Friel and Martin, 2007). The sizes of synaptic weights (w1-w4) represent snapshots at the end of each phase. A) **a**. Initial stable state has normal predominant contralateral projection and weaker ipsilateral projection. **b**. Unilateral inactivation (blocking R) causes the inactive side to develop a diminished projection (w2), and the active side to develop bilateral connections (w1, w3). The ipsilateral projection in the active side (w3) is better able to compete with less active contralateral projection (w2) for synaptic connections with the output neurons. **c**. Bilateral activation after the removal of unilateral inactivation shows that the diminished contralateral projection (w2) could not be spontaneously restored. In other words, the state is *stuck* (fig. 3A) at bilateral projection. **d**. Reverse inactivation (blocking L) enables the diminished contralateral projection (w2) to be restored by inactivating the strong ipsilateral projection (w3), which has been preventing the recovery of w2. The duration of this stage is an experimental design choice. To ensure the effect of constraint therapy, this stage needs to be prolonged until w2 becomes comparable in size respect to w3. **e**. Bilateral activation after the reverse inactivation resumes the competition between contralateral and ipsilateral projection competing for the synaptic connection to the output neurons. If the reverse inactivation stage ended at contralateral connection being stronger than the ipsilateral connection, the competition leads to the contralateral dominant state with a high likelihood. B) Simulated windows for the five stages that correspond A. Note that the direction of the signals in this window is from left to right. The miniature plot in the bottom keeps track of the real-time change of the synaptic weights. The magnified version is in fig. 5.

5.3 Results

5.3.1 Illustration of activity-dependent synaptic competition

Fig. 23 shows illustrations of three contingencies for a synaptic competition according to STPD when two input neurons project to an output neuron. The outcome of the competition is dependent on the initial conditions of the synapses. The STDP rule dictates that the relationship between pre- and postsynaptic spikes will induce long-term potentiation (LTP) of the synapse if input and output are correlated, and long-term depression (LTD) if input and output are not correlated. In all cases, the input neurons (R/L) receive stochastic input current that are statistically independent to each other, and the synaptic weight sizes are capped (maximum weight is four times bigger than the maximum weight). When the synaptic strength of one has predominant initial condition, the predominant connection does not allow a chance for the weaker connection to grow, thus the states are kept *stuck* as they initial were (Fig. 23A). Even if the different in strength between two competing connection are small, the relatively stronger connection tends win and leads to the predominant connection with high likelihood (Fig. 23B). In order to escape from the *stuck* state, transient constraint of input activity in the dominant input neuron is useful. The transient constraint induces a switch in the predominant connection (Fig. 23C). In other words, the transient blockade of the activity to the predominant neuron provided a chance to the disadvantaged connection to overcome the dominance once established. The effective transient constraint will last until the relative weight of the two synaptic weights become comparable to each to other.

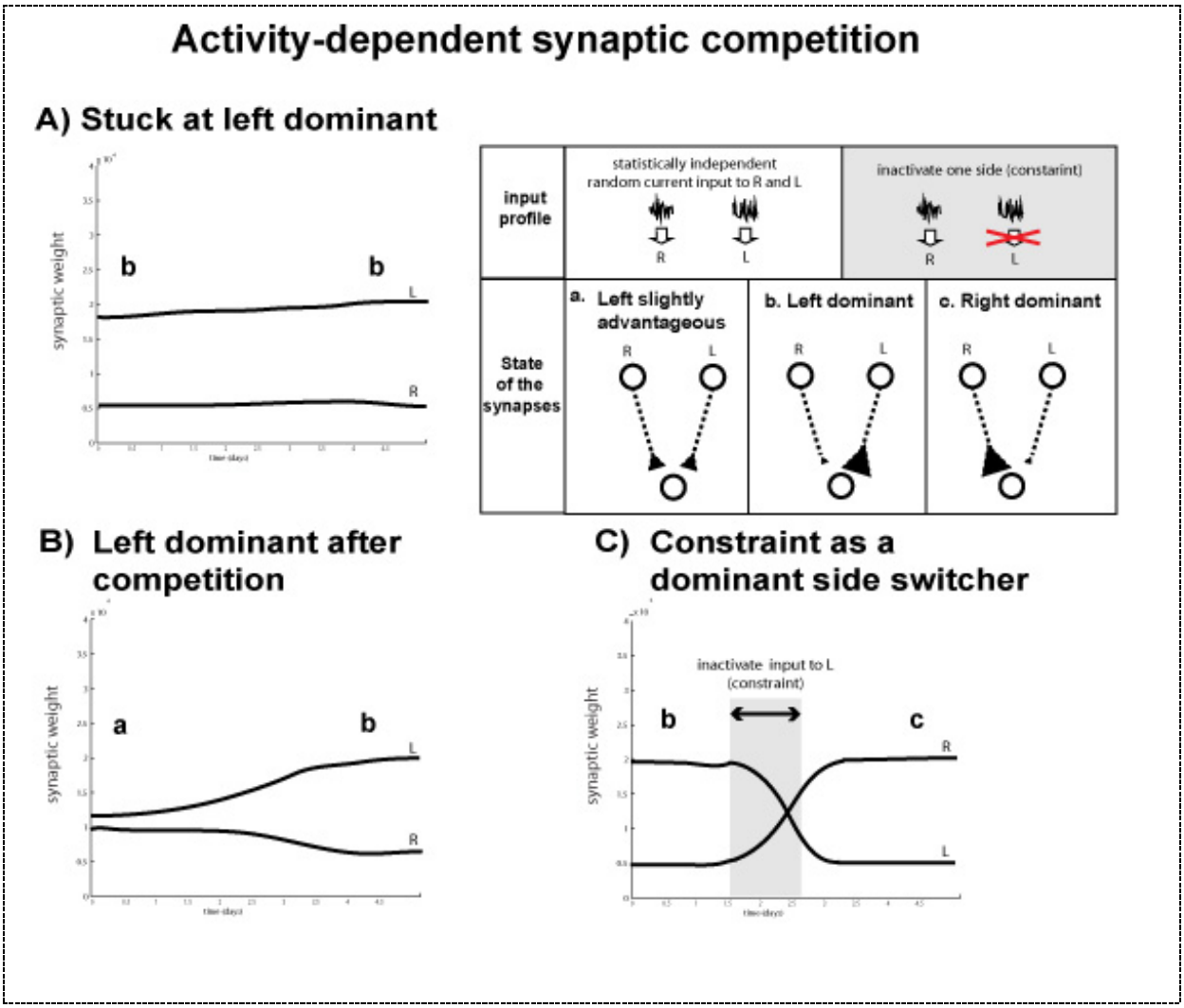
Activity-dependent synaptic competition
A) Stuck at left dominant
synaptic weight
b
b
L
R
input profile
statistically independent random current input to R and L
inactivate one side (constarint)
R
L
State of the synapses
a. Left slightly advantageous
b. Left dominant
c. Right dominant
B) Left dominant after competition
a
b
C) Constraint as a dominant side switcher
inactivate input to L (constraint)
b
c

Figure 23. Contingencies for a synaptic competition according to STPD when two input neurons project to an output neuron. The change in synaptic weights representing the connectional strengths between input and output neurons are plotted with different initial conditions. The results demonstrate how STDP affects potentiation and depression of the synapse over time when constant current activity is in the input neurons. The STDP rule dictates that the relationship between pre- and postsynaptic spikes will induce long-term potentiation (LTP) of the synapse if input and output are correlated, and long-term depression (LTD) if input and output are not correlated. In all cases, the input neurons (R/L) receive stochastic input current that are statistically independent to each other, and the synaptic weight sizes are capped (maximum weight is four times bigger than the maximum weight). A) When it starts with left predominant initial condition, the predominant connection does not allow a chance for the weaker connection to revive, thus the states are kept *stuck* as they initial were. B) When left is relatively stronger than the right, the synaptic competition leads to left predominant state with high likelihood. C) Transient constraint of input activity in the dominant input neuron induces a switch in the predominant connection. In other words, the transient blockade of the activity to the left predominant neuron (L) provided a chance to the disadvantaged connection (R) to overcome the dominance established by the other input neuron. The effective transient constraint will last until the relative weight of the two synaptic weights become comparable to each to other.

5.3.2 Simulating activity-dependent constraint-induced therapy by STDP

Change of synaptic weights of four synapses according to the five stages of input profiles are of key interests because the connectional strength of corticospinal tract is represented by their relative weights. The weight matrix helps to visualize the relative strength of the four synaptic connections (fig. 24A). Note that w0 and w1 are in competition and likewise w2 and w3 are in competition to gain synaptic connection to the output neurons. The normal state starts with predominant contralateral projections. Unilateral inactivation causes the inactive side to withdraw its projection (w2), and reciprocally causes active side to develop ipsilateral connections (w3) because the ipsilateral projection in the active side (w3) is advantageous to

compete with less active contralateral projection (w2) for synaptic connections with the output neurons. As a result, bilateral projection is developed from the active side (w1, w3). Bilateral activation after the removal of unilateral inactivation shows that the diminished contralateral projection (w2) could not be spontaneously restored. In other words, the state is *stuck* at pathological bilateral projection from the active side. Reverse inactivation enables the diminished contralateral projection (w2) to be restored by inactivating the strong ipsilateral projection (w3), which has been preventing the recovery of w2. The duration of this stage is an experimental design choice. To ensure the effect of the applying constraint, this stage is prolonged until w2 becomes comparable in size respect to w3 such that w2 is not overpowered by w3. If this condition were met, resumed competition between contralateral and ipsilateral projection in the following bilateral activation stage would provide setting favorable to the strengthening of the contralateral projection and reciprocally weakening of the ipsilateral projection.

5.3.3 What is the condition that the states will be consolidated?

Present study demonstrates the strengths of the two projections that are competing for the synaptic space in the output neuron are consolidated after a certain period of time as a result of competition by STDP. The question can be asked about the conditions of initial weights of the competing synapses that will decide the winner. Due to the fact that the presynaptic signals includes random noise, the stochastic nature of the result prohibits us to clearly mark the threshold of weights where one side will surely win the other side. However it is safe to state that when the weight of one side is significantly greater that the other side, the one with a greater weight will eventually displace the other and establish a predominant connection due to the nature of STDP. There ought to be a region of middle ground in which the development of predominance can go either way, which is highly unpredictable due to the stochasticity of the input stream. In this simulation, it is our design choice that the decay rate of the synaptic weight in the contralateral projection is set to be 50% higher than the decay rate of the synaptic weight of the ipsilateral projection to coarsely model the comparative advantage of the contralateral projection in forming a synaptic connection to the spinal neuron. This is because an axonal path with smaller decay rate will provide a survival advantage when competing with a path with higher decay rate. Although in real biology the winner between contralateral and ipsilateral

would form a denser projection that can be quantified from the relative number of synapses or the volume of axons projecting to the spinal neurons, we attempt to quantify this to an increase in synaptic weight size as a high-level rendering of the phenomenon. The level of advantage set here is arbitrary yet biologically plausible assumption and the ratio of decay rates would not affect the mechanism of constraint-induced intervention but it may affect how long it takes to restore the normal contralateral predominant projection.

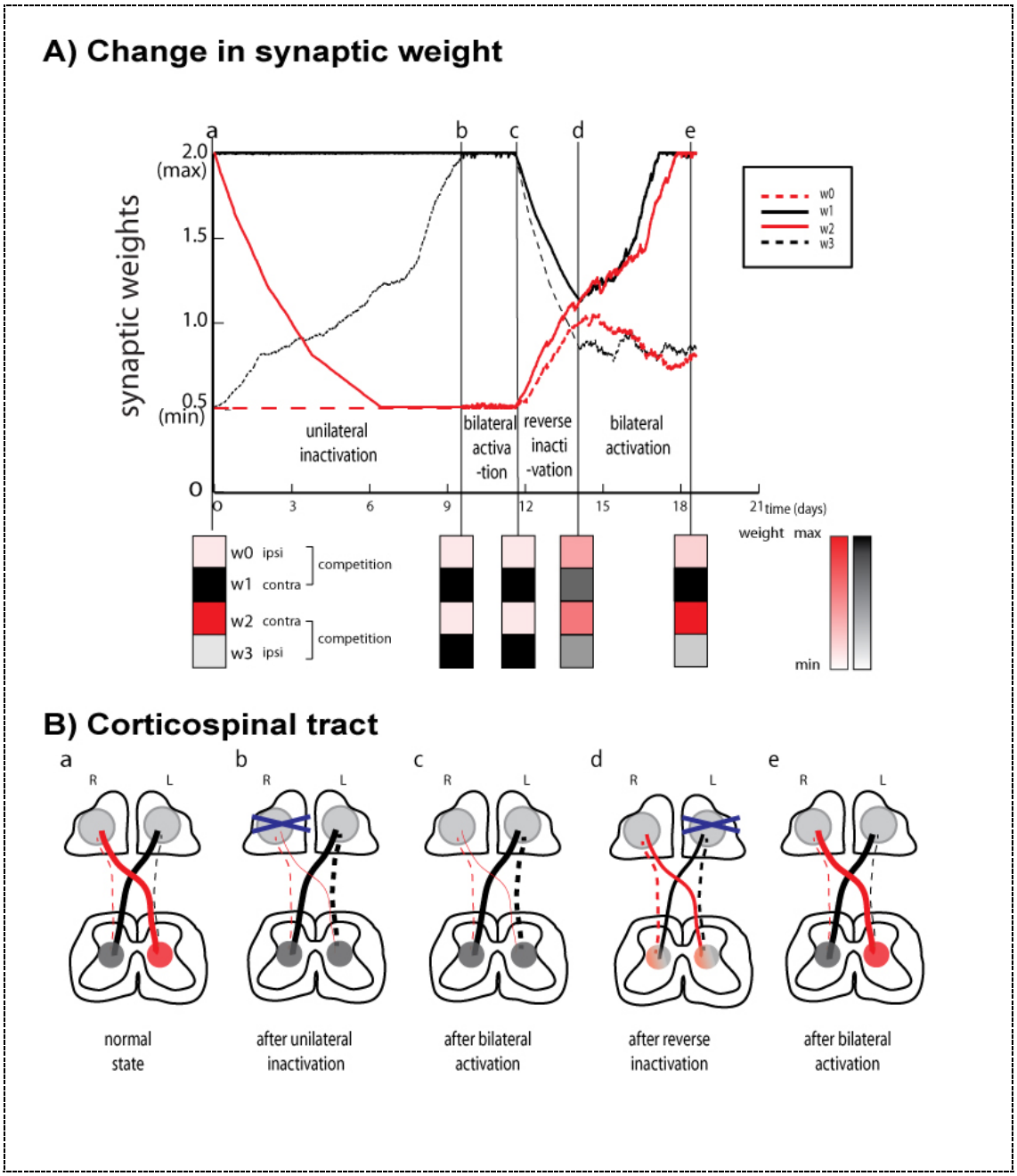
A) Change in synaptic weight
synaptic weights
2.0 (max)
1.5
1.0
0.5 (min)
0
a
b
c
d
e
w0
w1
w2
w3
unilateral inactivation
bilateral activa -tion
reverse inacti -vation
bilateral activation
0
3
6
9
12
15
18
21
time (days)
w0 ipsi
w1 contra
competition
w2 contra
w3 ipsi
competition
weight max
min
B) Corticospinal tract
a
b
c
d
e
R
L
normal state
after unilateral inactivation
after bilateral activation
after reverse inactivation
after bilateral activation

Figure 24. Simulating activity-dependent constraint-induced therapy by STDP: a change of synaptic weights of 4 synapses according to the five stages of input profiles. **A/B.** The weight matrix helps to visualize the relative strength of the four synaptic connections. Note that w0 and w1 are in competition and likewise w2 and w3 are in competition. **a**. The normal state with predominant contralateral projections. **b**. Unilateral inactivation (blocking R) causes the inactive side to develop a diminished projection (w2), and the active side to develop bilateral connections (w1, w3). The ipsilateral projection in the active side (w3) is better able to compete with less active contralateral projection (w2) for synaptic connections with the output neurons. **c**. Bilateral activation after the removal of unilateral inactivation shows that the diminished contralateral projection (w2) could not be spontaneously restored. In other words, the state is *stuck* (fig. 3A) at bilateral projection. **d**. Reverse inactivation (blocking L) enables the diminished contralateral projection (w2) to be restored by inactivating the strong ipsilateral projection (w3), which has been preventing the recovery of w2. The duration of this stage is an experimental design choice. To ensure the effect of the constraint therapy, this stage needs to be prolonged until w2 becomes comparable in size respect to w3. If this stage goes on longer, bilateral projection from R will develop reversely, which is why it is important to control the duration of this stage. **e**. Bilateral activation after the reverse inactivation resumes the competition between contralateral and ipsilateral projection competing for the synaptic connection to the output neurons. If the reverse inactivation stage ended at contralateral connection being stronger than the ipsilateral connection, the competition leads to the contralateral predominant state with a high likelihood (fig. 3B).

*The inherent decay rate of the synaptic weight of the contralateral connection is set to be lower than that of the ipsilateral connection.

5.4 Discussion

The purpose of this study was to use biologically realistic simulation tool to understand how biological system responds to injuries and also to find a fundamental and generalizable mechanism of constraint-induced therapy as a rehabilitative treatment after injuries. Although not identical in mechanism, constraint-induced movement therapy (CIMT) after central nervous system injury due to stroke or cerebrovascular accidents, constraint-induced intervention in hemiplegic cerebral palsy (CP), and restraining the use of unaffected eye in amblyopia all share a conceptually similar rehabilitative methodology, aiming to restore lost function in the affected side of the body. In this study, we hypothesize that the mechanism of constraint-induced therapy in the injured corticospinal system in hemiplegic CP can be demonstrated when simplified neural descending tracts with two layers of spiking neurons representing cortical and spinal neural substrate are simulated with spike-timing-dependent plasticity (STDP). Although we could have picked other injury, we chose an example from a study of kitten with hemiplegic CP (Martin, 2005; Friel and Martin, 2007; Martin *et al.*, 2011) to simulate in order to demonstrate the entire process—from the development of hemiplegic CP to restoration to the normal CST connectivity by constraint-induced therapy as a treatment.

5.4.1 Relevance of the simulated neural structure to the biology

The two-layer neural structure is used to represent a simplistic descending corticospinal system (Fig. 20). Four synaptic connections from input neuron substrate to output neuron substrate represent the contralateral and the ipsilateral corticospinal projection from left and right hemispheres to the spinal termination in gray matter. This structure forms competition sites at each output neurons, competitions between the contralateral projection from one hemisphere and the ipsilateral projection from the other hemisphere, which represents activity-dependent competition for spinal synaptic space based on physiological reports in primates including human (Nathan *et al.*, 1990; Lacroix *et al.*, 2004; Eyre *et al.*, 2007). The stages of development of and treatment from hemiplegic CP in simulation in present study (fig. 24B) are relevant to hemiplegic CP in human. Electrophysiological studies confirm that persistent unilateral abnormality by perinatal stroke is highly predictive of the development of hemiplegia (Kato *et al.*, 2004). Significant hypertrophy of the CST observed arising from the nonimpaired hemisphere (Scales and Collins, 1972), and a reciprocal relation between the diameter of

ipsilateral axons from the nonimpaired hemisphere and that of contralateral axons from the impaired hemisphere (Eyre *et al.*, 2007) supports the activity-dependent competition hypothesis at spinal cord termination (Martin and Lee, 1999).

5.4.2 Similarity to the treatment of amblyopia

Amblyopia is a unilateral reduction of visual acuity that bears a resemblance to the impairment in the corticospinal system by early brain injury, as it is referred as hemiplegic CP in the visual system. The neural architecture of binocular vision includes the binocular zone of visual cortex that responds to projection from both eyes via lateral geniculate nucleus (Casagrande and Boyd, 1996). It is known that monocular deprivation in the developmental period leads to reduction of neurons in the visual cortex driven by binocular eyes and also the reduction of neuron driven by amblyopic eye (Wiesel and Hubel, 1963, 1965; Shatz and Stryker, 1978). Therefore it can be said that the development of amblyopia due to monocular deprivation resembles the development of hemiplegic CP due to unilateral injury in the developing brain in that in both cases activity-dependent synaptic competition is taking place in the activity-receiving neuron: neuron in the spinal gray matter in hemiplegic CP and neuron in the visual cortex in case of amblyopia. The treatment for amblyopia is remarkably in sync with the concept of constraint-induced therapy. The patching of the dominant eye while forcing the child to use the weaker eye is essentially applying a transient constraint to the stronger side in order to revive the visual impairment of the weaker eye. The similar principle being effective demonstrates that the principle of constraint-induced therapy can be highly effective across the modalities in the biological system as long as inter-hemispheric competition is present.

Previously, the treatment mechanism for amblyopia has been explained within the framework of BCM theory, a rate-based synaptic modification theory (Cooper and Bear, 2012). Here, we attempt to provide a simple yet fundamental mechanism that accounts for the general biological phenomena, which includes the treatment of amblyopia, that involve inter-hemispheric synaptic-competition using spike-based plasticity theory.

5.4.3 Escaping from the suboptimal stable state

In the third stage of the experiment ("bilateral activation"), we observe a persistence of suboptimal stable solution due to hysteresis effect. The bilateral projection from one hemisphere

was due to a history of transient blockade of activity in the affected hemisphere. It is suboptimal because right intervention will move it to a better state. It is interesting phenomenon that traditional learning theories do not explain. Indeed, STDP could be the synaptic mechanism that allows the persistent suboptimal solution at a synapse level. Given that this competition mechanism proposed based on STDP is true, the same mechanism could be the thing that is operative everywhere when there is a persistent suboptimal solution in a biological system because spike-based plasticity proposed here is a generalizable mechanism.

5.4.4 Sensitivity of the result to other synaptic learning models

The question could be asked of how sensitive the result will be to the various synapse learning models. Although it is not of our interest in this study to test the different effects of various implementations of STDP update mechanisms, it can be said that the result is generalizable if 1) update mechanisms dictate that correlated pre- and postsynaptic spikes causes potentiation and uncorrelated pre- and postsynaptic spikes causes depression of the synaptic weight, 2) synaptic weight has upper limit to prevent infinite growth, 3) postsynaptic firing rates are *not* in the range that results in net depression and 4) synaptic decay is present to implement decrease in synaptic weight on inactivity. Our implementation has asymmetric STDP curve, and is all-to-all (Pfister and Gerstner, 2006) and standard additive. Variation in curve shape, nearest-neighbor implementation instead of all-to-all, multiplicative in stead of additive update will still generate the emergent phenomena of constraint-induced intervention in this study if the above conditions are met.

5.4.5 Caveats in the simulation of biological systems

Is the criticism "simulations doomed to succeed" valid in this study? If the simulation is attempting to explain the phenomena of a biological system, the statement is *not* true. In fact, simulation *do* fail if we do not account for the sufficient complexity of the neural circuit to explain a biological phenomenon, and studying the conditions that make it *doom to fail* is of scientific importance by itself. The statement simply reminds us the fact that there must be a verification of the simulation conditions and results when evaluating a simulation. The questions to ask in the verification process is whether the parameters used are biologically realistic, whether the theories used are well-established and sound, otherwise the simulation could be

deceptively manipulated to produce whatever result a researcher wants. In this study, we used well-established biologically realistic models of neurons (Izhikevich, 2003a), synapse with spike-based learning rule (Bi and Poo, 2001; Froemke and Dan, 2002), and realistic conditions, e.g. synaptic weight with lower and upper limits, the existence of synaptic decay, etc., as well as biologically realistic range of parameters that generate realistic output range using the models. The simulation failed to produce a valid synaptic competition due to STDP if the synaptic weight limit are not set, which will lead to unrealistic ever-growing synapse. Although our two-layer neuronal structure of the descending corticospinal system is clearly an over-simplification that does not compute the effects of other descending tracts, e.g. rubrospinal tract, it still provides a valuable insight of how constraint-induced therapy might work in minimal complexity using spike-based learning model. Provided that simulation is properly verified, it is useful in making prediction, explanation, retrodiction and in exploring emergent explanation (Grim *et al.*, 2013) that are otherwise impossible in real physiology due to practical and ethical reasons.

5.5 Conclusion

In this study we presented a simplified yet fundamental mechanism that provides explanation for some of the key phenomena in constraint-induced therapy by spike-based plasticity in synaptic level. By simulating the activity-dependent synaptic competition as a key mechanism that might harness synaptic plasticity to repair damaged coritocispinal system, this study suggests general principle of how biological system could escape from a suboptimal stable state by applying a forced transient constraint to a more competitive side of a system in order to transition into an improve state which otherwise could result in the suboptimal pathological deficit to become fixated.

5.6 Author Contributions

Designed the experiment: WS TS. Performed the experiment: WS. Developed the hardware and visual software: WS. Analyzed the data: WJ. Wrote the paper: WS. Presented by WS at the Annual Meeting of the Computational and Systems Neuroscience (Cosyne) in March 2015. Reviewed manuscript: WS TS.

6 Conclusions and future work

6.1 Conclusion

Movement disorders are neurological conditions that affect speed, fluency, quality, and ease of movement in a negative direction. In that regard, investigating the neurological underpinning of the cause of the movement disorder is desirable. The emulation study presented here is one of the alternative responses to overcome the limitation posed by human studies due to practical and ethical reasons. My study is centered on understanding the dystonia and the study is extended to understanding the neural mechanism of the constraint-induced rehabilitative intervention which is highly effective across multiple modalities in biological systems.

The first study proposes two plausible neurological mechanisms that lead to behavioral characteristics of dystonia and the outcomes from the emulation are compared with available data from subjects with dystonia (**chap 3**). The study has shown through neuromorphic emulation that there are at least two possible mechanisms of cortical abnormality that could cause increased long-latency stretch reflexes and result in the clinical phenomenon of dystonia. While an emulation of this type does not prove that this is the mechanism of dystonia, it does provide evidence that a mechanism of this type is sufficient to cause the clinical features of dystonia, and is, therefore, worthy of further study. We hope that these results provide both insight and guidance for future clinical studies to test whether reducing the long-latency stretch reflex may alleviate symptoms of dystonia.

The second study investigates the origin and development of motor overflow in focal hand dystonia in the context of spike-based plasticity mechanism (**chap 4**). The purpose of this study was to understand the pathology of developing focal hand dystonia by using biologically realistic neural structure to test our temporal correlation hypothesis. As predicted by Sanger and Merzenich (Sanger and Merzenich, 2000), and demonstrated by Merzenich and Byl (Byl *et al.*, 1996), correlated sensory inputs lead to sensory disorganization and have the potential to

produce motor dysfunction. Here we extended this work using a more realistic plasticity model with spike-timing-dependent plasticity.

The third study investigates the mechanism of constraint-induced therapy, a popular rehabilitative method in impaired biological systems with spike-based plasticity mechanism (**chap 5**). This study presents a simplified yet fundamental mechanism that provides an explanation for some of the key phenomena in constraint-induced therapy by spike-based plasticity in synaptic level. By simulating the activity-dependent synaptic competition as a key mechanism that might harness synaptic plasticity to repair damaged coritospinal system, this study suggests general principle of how biological system could escape from a suboptimal stable state by applying a forced transient constraint to a more competitive side of a system in order to transition into an improved state which otherwise could result in a suboptimal pathological deficit to become consolidated.

The second and the third study use the same neural structure that is assembled in a different way to emulate two different biological phenomena. The neurons in the input and output substrates represent sensory afferents to sensory representation in the cortex in the second study whereas they represent neurons on the motor cortex and spinal neurons in the corticospinal projection in the third study. The major difference between the studies is that the input current profile to the input substrate being different. The second study investigates the effect of *correlated* sensory inputs to the development of crosstalk and also shows transient correlated input could lead to perpetuated structural motor overflow. The third study investigates the effect of *differential* current input—on or off at times—in developing bilateral projection and producing a therapeutic effect from a constraint. The model in this study includes synaptic decay as a mean to diminish the strength of the synaptic connection when the input is inactivated. Synaptic decay is an essential assumption that leads to the result obtained by this study.

The studies required extremely fast and customizable hardware, which provides a unique benefit of accelerated emulation of the development of neurological system under relevant circumstances, at an affordable cost without having to spend on a system with extremely high computing power such as that of supercomputer. It required multi-scale emulation for the biological system both in time domain and space domain. Multi-scale in time domain accounts for the drastically different time scales that neural processes in developmental diseases usually operate on, e.g. spinal reflex in milliseconds versus learning in years, and multi-scale in space in

biological system accounts for the details, ranging from cellular level spiking activity to behavior level limb biomechanics. The spike level cellular activity was the highest level of abstraction essential to achieve sufficient biorealism in the neurological system that are still affordable to implement in the available hardware space. This daunting task was achieved both by highly customizing clock-level computation and efficient use of memory in commercially available field-programmable gate arrays (FPGAs), and also by carefully designing scientific studies using the built tool. The task was realized by our brilliant team members who are listed as authors in the three studies.

The potential importance of this project was to gain knowledge in complex interplay between development, plasticity, behavior and neurological injury because understanding the plastic mechanism of how early brain injury leads to developmental disorder could be used to guide early intervention such as in constraint-induced therapy. From the study of motor overflow and constraint-induced therapy, we observed plasticity can work in both way: adaptive plasticity taking place by transient inactivity (constraint) that facilitates the recovery of the injured function, and also maladaptive plasticity that consolidates the suboptimal pathological state which frustrates the recovery of the injured function unless effective intervention is applied.

The first study is published in Journal of Neural Engineering. The second and third studies will be submitted to relevant journals (undecided at this point). The engineering technique and general methodology behind the use of programmable hardware (**chap 2**) is published in neural information processing systems (NIPS).

6.2 Future studies

Future studies should further focus on the unique advantage of using emulation as a way to study and answer questions about finding the *sufficient* mechanism responsible for the movement disorders that have a neurological origin. Since we have built and modularized many neurological components that are proven to work, we can utilize the built library to test specific disease hypotheses by building a neural circuit around a structure that is relevant. We can conduct experiment that is generally prohibited in human studies due to practical and ethical reasons, especially by maximizing the high-speed acceleration that the technology provides to

study plasticity and learning effects that span several years for development. We have used the system around a sensorimotor reflex pathway to study the immediate effects of the change in physiological parameters but did not incorporate the "learning" synapse in the study of dystonia. The future study could strive to close the loop in the dystonia study to emulate the plasticity effect of many pharmacological treatments, deep brain stimulation, cell death, and behavior training. The general emulation platform is capable of opening a new line of projects that is non-dystonia studies. We could expand the currently available single joint system to multi-joint system to emulate the various postural and behavioral characteristics of tic, Parkinsonism, tremor, and ataxia, etc. Because we believe the only way to test and characterize the high-level behavior of a brain model is to actually build the closed loop system between the artificial nervous system and the body (plant) acting in an environment, by elaborating the brain model we can interrogate the system through a well-designed experiment to acquire a unique and practical knowledge about the mechanism of biological phenomena and become a step closer to treating the disorders by studying how the system breaks.

7 Bibliography

Air E L, Ostrem J L, Sanger T D and Starr P A 2011 Deep brain stimulation in children: experience and technical pearls *Journal of neurosurgery. Pediatrics* **8** 566-74

Albanese A, Bhatia K, Bressman S B, Delong M R, Fahn S, Fung V S, Hallett M, Jankovic J, Jinnah H A, Klein C, Lang A E, Mink J W and Teller J K 2013 Phenomenology and classification of dystonia: a consensus update *Movement disorders : official journal of the Movement Disorder Society* **28** 863-73

Attebo K, Mitchell P, Cumming R, Smith W, Jolly N and Sparkes R 1998 Prevalence and causes of amblyopia in an adult population *Ophthalmology* **105** 154-9

Bara-Jimenez W, Catalan M J, Hallett M and Gerloff C 1998 Abnormal somatosensory homunculus in dystonia of the hand *Annals of neurology* **44** 828-31

Bara-Jimenez W, Shelton P and Hallett M 2000a Spatial discrimination is abnormal in focal hand dystonia *Neurology* **55** 1869-73

Bara-Jimenez W, Shelton P, Sanger T D and Hallett M 2000b Sensory discrimination capabilities in patients with focal hand dystonia *Annals of neurology* **47** 377-80

Beck S, Richardson S P, Shamim E A, Dang N, Schubert M and Hallett M 2008 Short intracortical and surround inhibition are selectively reduced during movement initiation in focal hand dystonia *The Journal of neuroscience : the official journal of the Society for Neuroscience* **28** 10363-9

Bi G and Poo M 2001 Synaptic modification by correlated activity: Hebb's postulate revisited *Annual review of neuroscience* **24** 139-66

Bienenstock E L, Cooper L N and Munro P W 1982 Theory for the development of neuron selectivity: orientation specificity and binocular interaction in visual cortex *The Journal of neuroscience : the official journal of the Society for Neuroscience* **2** 32-48

Blake D T and Merzenich M M 2002 Changes of AI receptive fields with sound density *Journal of neurophysiology* **88** 3409-20

Brady K and Garcia T 2009 Constraint-induced movement therapy (CIMT): pediatric applications *Developmental disabilities research reviews* **15** 102-11

Brashear A and Elovic E 2010 *Spasticity: Diagnosis and Management*: Demos Medical)

Breakefield X O, Blood A J, Li Y, Hallett M, Hanson P I and Standaert D G 2008 The pathophysiological basis of dystonias *Nature reviews. Neuroscience* **9** 222-34

Byl N N, Merzenich M M and Jenkins W M 1996 A primate genesis model of focal dystonia and repetitive strain injury: I. Learning-induced dedifferentiation of the representation of the hand in the primary somatosensory cortex in adult monkeys *Neurology* **47** 508-20

Capaday C, Forget R, Fraser R and Lamarre Y 1991 Evidence for a contribution of the motor cortex to the long-latency stretch reflex of the human thumb *The Journal of physiology* **440** 243-55

Carpaneto J, Micera S, Galardi G, Micheli A, Carboncini M C, Rossi B and Dario P 2004 A protocol for the assessment of 3D movements of the head in persons with cervical dystonia *Clinical biomechanics* **19** 659-63

Carr L J, Harrison L M, Evans A L and Stephens J A 1993 Patterns of central motor reorganization in hemiplegic cerebral palsy *Brain : a journal of neurology* **116 (Pt 5)** 1223-47

Casagrande V A and Boyd J D 1996 The neural architecture of binocular vision *Eye* **10 (Pt 2)** 153-60

Ceballos-Baumann A O 1994 Overactivity of primary and associated motor areas in secondary hemi-dystonia (SHD) due to thalamic or basal ganglia lesions: a PET study. *Movement disorders : official journal of the Movement Disorder Society* **9** 238

Chen R, Cohen L G and Hallett M 2002 Nervous system reorganization following injury *Neuroscience* **111** 761-73

Colton C A, Brown C M, Czapiga M and Vitek M P 2002 Apolipoprotein-E allele-specific regulation of nitric oxide production *Annals of the New York Academy of Sciences* **962** 212-25

Cooper L N and Bear M F 2012 The BCM theory of synapse modification at 30: interaction of theory with experiment *Nature reviews. Neuroscience* **13** 798-810

De Luca C J and Hostage E C 2010 Relationship between firing rate and recruitment threshold of motoneurons in voluntary isometric contractions. *Journal of neurophysiology* **104** 1034-46

DeLong M R and Wichmann T 2007 Circuits and circuit disorders of the basal ganglia *Archives of neurology* **64** 20-4

Edwards M J, Huang Y Z, Mir P, Rothwell J C and Bhatia K P 2006 Abnormalities in motor cortical plasticity differentiate manifesting and nonmanifesting DYT1 carriers *Movement disorders : official journal of the Movement Disorder Society* **21** 2181-6

Edwards M J, Huang Y Z, Wood N W, Rothwell J C and Bhatia K P 2003 Different patterns of electrophysiological deficits in manifesting and non-manifesting carriers of the DYT1 gene mutation *Brain : a journal of neurology* **126** 2074-80

Elbert T, Candia V, Altenmuller E, Rau H, Sterr A, Rockstroh B, Pantev C and Taub E 1998 Alteration of digital representations in somatosensory cortex in focal hand dystonia *Neuroreport* **9** 3571-5

Emonet-Denand F, Laporte Y, Matthews P B and Petit J 1977 On the subdivision of static and dynamic fusimotor actions on the primary ending of the cat muscle spindle *The Journal of physiology* **268** 827-61

Evarts E V and Tanji J 1976 Reflex and intended responses in motor cortex pyramidal tract neurons of monkey *Journal of neurophysiology* **39** 1069-80

Eyre J A 2007 Corticospinal tract development and its plasticity after perinatal injury *Neuroscience and biobehavioral reviews* **31** 1136-49

Eyre J A, Smith M, Dabydeen L, Clowry G J, Petacchi E, Battini R, Guzzetta A and Cioni G 2007 Is hemiplegic cerebral palsy equivalent to amblyopia of the corticospinal system? *Annals of neurology* **62** 493-503

Eyre J A, Taylor J P, Villagra F, Smith M and Miller S 2001 Evidence of activity-dependent withdrawal of corticospinal projections during human development *Neurology* **57** 1543-54

Fahn S 1988 Concept and classification of dystonia *Advances in neurology* **50** 1-8

Farmer S F, Harrison L M, Ingram D A and Stephens J A 1991 Plasticity of central motor pathways in children with hemiplegic cerebral palsy *Neurology* **41** 1505-10

Friel K M and Martin J H 2007 Bilateral activity-dependent interactions in the developing corticospinal system *The Journal of neuroscience : the official journal of the Society for Neuroscience* **27** 11083-90

Froemke R C and Dan Y 2002 Spike-timing-dependent synaptic modification induced by natural spike trains *Nature* **416** 433-8

Fuglevand A J, Winter D A and Patla A E 1993a Models of recruitment and rate coding organization in motor-unit pools *Journal of neurophysiology* **70** 2470-88

Fuglevand A J, Winter D A and Patla A E 1993b Models of recruitment and rate coding organization in motor-unit pools. *Journal of neurophysiology* **70** 2470-88

Gelfan S, Kao G and Ruchkin D S 1970 The dendritic tree of spinal neurons. *The Journal of comparative neurology* **139** 385-411

Ghez C, Gordon J and Hening W 1988 Trajectory control in dystonia *Advances in neurology* **50** 141-55

Glowatzki E and Fuchs P A 2002 Transmitter release at the hair cell ribbon synapse *Nature neuroscience* **5** 147-54

Godde B, Spengler F and Dinse H R 1996 Associative pairing of tactile stimulation induces somatosensory cortical reorganization in rats and humans *Neuroreport* **8** 281-5

Gordon L M, Keller J L, Stashinko E E, Hoon A H and Bastian A J 2006 Can spasticity and dystonia be independently measured in cerebral palsy? *Pediatric neurology* **35** 375-81

Grim P, Rosenberger R, Rosenfeld A, Anderson B and Eason R 2013 How simulations fail *Synthese* **190** 2367–90

Hallett M 2006 Pathophysiology of writer's cramp *Human movement science* **25** 454-63

Hallett M 2011 Neurophysiology of dystonia: The role of inhibition *Neurobiology of disease* **42** 177-84

Hashimoto T, Naito K, Kitazawa K, Imai S and Goto T 2010 Pallidotomy for severe tardive jaw-opening dystonia *Stereotactic and functional neurosurgery* **88** 105-8

Hendricks H T, Pasman J W, van Limbeek J and Zwarts M J 2003 Motor evoked potentials in predicting recovery from upper extremity paralysis after acute stroke *Cerebrovascular diseases* **16** 265-71

Henneman E 1957 Relation between size of neurons and their susceptibility to discharge. *Science (New York, N.Y.)* **126** 1345-7

Henneman E, Somjen G and Carpenter D O 1965 Functional Significance of Cell Size in Spinal Motoneurons *Journal of neurophysiology* **28** 560-80

Hill A V 1938 The heat of shortening and dynamics constants of muscles. *Proc. R. Soc. Lond. B* **126** 136-95

Hoon A H, Jr., Stashinko E E, Nagae L M, Lin D D, Keller J, Bastian A, Campbell M L, Levey E, Mori S and Johnston M V 2009 Sensory and motor deficits in children with cerebral palsy born preterm correlate with diffusion tensor imaging abnormalities in thalamocortical pathways *Developmental medicine and child neurology* **51** 697-704

Imer M, Ozeren B, Karadereler S, Yapici Z, Omay B, Hanagasi H and Eraksoy M 2005 Destructive stereotactic surgery for treatment of dystonia *Surgical neurology* **64 Suppl 2** S89-94; discussion S-5

Izhikevich E M 2003a Simple model of spiking neurons *IEEE transactions on neural networks / a publication of the IEEE Neural Networks Council* **14** 1569-72

Izhikevich E M 2003b Simple model of spiking neurons. *IEEE transactions on neural networks / a publication of the IEEE Neural Networks Council* **14** 1569-72

Jankovic J 2001 Can peripheral trauma induce dystonia and other movement disorders? Yes! *Movement disorders : official journal of the Movement Disorder Society* **16** 7-12

Kaas J H and Florence S L 1997 Mechanisms of reorganization in sensory systems of primates after peripheral nerve injury *Advances in neurology* **73** 147-58

Kahn J, Anderton B H, Gibb W R, Lees A J, Wells F R and Marsden C D 1985 Neuronal filaments in Alzheimer's, Pick's, and Parkinson's diseases *The New England journal of medicine* **313** 520-1

Kato T, Okumura A, Hayakawa F, Kuno K and Watanabe K 2004 Electroencephalographic aspects of periventricular hemorrhagic infarction in preterm infants *Neuropediatrics* **35** 161-6

Kempter R, Gerstner W and von Hemmen J L 1999 Hebbian learning and spiking neurons *Phys Rev E* **59** 4498-514

Kojovic M, Parees I, Kassavetis P, Palomar F J, Mir P, Teo J T, Cordivari C, Rothwell J C, Bhatia K P and Edwards M J 2013 Secondary and primary dystonia: pathophysiological differences *Brain : a journal of neurology* **136** 2038-49

Konczak J and Abbruzzese G 2013 Focal dystonia in musicians: linking motor symptoms to somatosensory dysfunction *Frontiers in human neuroscience* **7** 297

Krauss J K 2010 Surgical treatment of dystonia *European journal of neurology : the official journal of the European Federation of Neurological Societies* **17 Suppl 1** 97-101

Krutki P, Ciechanowicz I, Celichowski J and Cywinska-Wasilewska G 2008 Comparative analysis of motor unit action potentials of the medial gastrocnemius muscle in cats and rats *Journal of electromyography and kinesiology : official journal of the International Society of Electrophysiological Kinesiology* **18** 732-40

Kukke S N and Sanger T D 2011 Contributors to excess antagonist activity during movement in children with secondary dystonia due to cerebral palsy *Journal of neurophysiology* **105** 2100-7

Lacroix S, Havton L A, McKay H, Yang H, Brant A, Roberts J and Tuszynski M H 2004 Bilateral corticospinal projections arise from each motor cortex in the macaque monkey: a quantitative study *The Journal of comparative neurology* **473** 147-61

Lebiedowska M K, Gaebler-Spira D, Burns R S and Fisk J R 2004 Biomechanic characteristics of patients with spastic and dystonic hypertonia in cerebral palsy *Archives of physical medicine and rehabilitation* **85** 875-80

Lee R G, Murphy J T and Tatton W G 1983 Long-latency myotatic reflexes in man: mechanisms, functional significance, and changes in patients with Parkinson's disease or hemiplegia *Advances in neurology* **39** 489-508

Levin M F and Feldman A G 1994 The role of stretch reflex threshold regulation in normal and impaired motor control. *Brain research* **657** 23-30

Lomont C 2003 Fast inverse square root. In: *Technical Report*: Available at http://www.lomont.org/Math/Papers/2003/InvSqrt.pdf)

Martin J H 2005 The corticospinal system: from development to motor control *The Neuroscientist : a review journal bringing neurobiology, neurology and psychiatry* **11** 161-73

Martin J H, Chakrabarty S and Friel K M 2011 Harnessing activity-dependent plasticity to repair the damaged corticospinal tract in an animal model of cerebral palsy *Developmental medicine and child neurology* **53 Suppl 4** 9-13

Martin J H, Choy M, Pullman S and Meng Z 2004 Corticospinal system development depends on motor experience *The Journal of neuroscience : the official journal of the Society for Neuroscience* **24** 2122-32

Martin J H and Lee S J 1999 Activity-dependent competition between developing corticospinal terminations *Neuroreport* **10** 2277-82

Matthews P B 1991 The human stretch reflex and the motor cortex *Trends in neurosciences* **14** 87-91

McIntyre C C, Savasta M, Kerkerian-Le Goff L and Vitek J L 2004 Uncovering the mechanism(s) of action of deep brain stimulation: activation, inhibition, or both *Clinical neurophysiology : official journal of the International Federation of Clinical Neurophysiology* **115** 1239-48

Mileusnic M P, Brown I E, Lan N and Loeb G E 2006a Mathematical models of proprioceptors. I. Control and transduction in the muscle spindle *Journal of neurophysiology* **96** 1772-88

Mileusnic M P, Brown I E, Lan N and Loeb G E 2006b Mathematical models of proprioceptors. I. Control and transduction in the muscle spindle. *Journal of neurophysiology* **96** 1772-88

Morimoto C, Distaso J A, Cheney J J, Reinherz E L and Schlossman S F 1984 Cellular interaction between subsets of T8 population for maximal suppression of antigen-specific antibody response *Cellular immunology* **88** 75-84

Murray W M, Delp S L and Buchanan T S 1995 Variation of muscle moment arms with elbow and forearm position *Journal of biomechanics* **28** 513-25

Nathan P W, Smith M C and Deacon P 1990 The corticospinal tracts in man. Course and location of fibres at different segmental levels *Brain : a journal of neurology* **113 (Pt 2)** 303-24

Nelles G, Spiekermann G, Jueptner M, Leonhardt G, Muller S, Gerhard H and Diener H C 1999 Reorganization of sensory and motor systems in hemiplegic stroke patients. A positron emission tomography study *Stroke; a journal of cerebral circulation* **30** 1510-6

Niu C M, Nandyala S K and Sanger T D 2014 Emulated muscle spindle and spiking afferents validates VLSI neuromorphic hardware as a testbed for sensorimotor function and disease *Frontiers in computational neuroscience* **8** 141

Nudo R J 2013 Recovery after brain injury: mechanisms and principles *Frontiers in human neuroscience* **7** 887

Palmer E and Ashby P 1992 Evidence that a long latency stretch reflex in humans is transcortical *The Journal of physiology* **449** 429-40

Pfister J P and Gerstner W 2006 Triplets of spikes in a model of spike timing-dependent plasticity *The Journal of neuroscience : the official journal of the Society for Neuroscience* **26** 9673-82

Playford E D, Fletcher N A, Sawle G V, Marsden C D and Brooks D J 1993 Striatal [18F]dopa uptake in familial idiopathic dystonia *Brain : a journal of neurology* **116 (Pt 5)** 1191-9

Prescott I A, Dostrovsky J O, Moro E, Hodaie M, Lozano A M and Hutchison W D 2013 Reduced paired pulse depression in the basal ganglia of dystonia patients *Neurobiology of disease* **51** 214-21

Pruszynski J A, Kurtzer I, Nashed J Y, Omrani M, Brouwer B and Scott S H 2011 Primary motor cortex underlies multi-joint integration for fast feedback control *Nature* **478** 387-90

Quartarone A, Bagnato S, Rizzo V, Siebner H R, Dattola V, Scalfari A, Morgante F, Battaglia F, Romano M and Girlanda P 2003 Abnormal associative plasticity of the human motor cortex in writer's cramp *Brain : a journal of neurology* **126** 2586-96

Raphael G, Tsianos G A and Loeb G E 2010 Spinal-like regulator facilitates control of a two-degree-of-freedom wrist. *The Journal of neuroscience : the official journal of the Society for Neuroscience* **30** 9431-44

Ridding M C, Sheean G, Rothwell J C, Inzelberg R and Kujirai T 1995 Changes in the balance between motor cortical excitation and inhibition in focal, task specific dystonia *Journal of neurology, neurosurgery, and psychiatry* **59** 493-8

Rodriguez I, Gila L, Malanda A, Gurtubay I G, Mallor F, Gomez S, Navallas J and Rodriguez J 2007 Motor unit action potential duration, I: variability of manual and automatic measurements *Journal of clinical neurophysiology : official publication of the American Electroencephalographic Society* **24** 52-8

Sanger T D 2010 Neuro-mechanical control using differential stochastic operators. In: *Engineering in Medicine and Biology Society (EMBC), 2010 Annual International Conference of the IEEE,* pp 4494-7

Sanger T D 2011a Distributed control of uncertain systems using superpositions of linear operators *Neural computation* **23** 1911-34

Sanger T D 2011b Distributed control of uncertain systems using superpositions of linear operators. *Neural computation* **23** 1911-34

Sanger T D, Delgado M R, Gaebler-Spira D, Hallett M, Mink J W and Task Force on Childhood Motor D 2003 Classification and definition of disorders causing hypertonia in childhood *Pediatrics* **111** e89-97

Sanger T D and Merzenich M M 2000 Computational model of the role of sensory disorganization in focal task-specific dystonia *Journal of neurophysiology* **84** 2458-64

Sanger T D, Tarsy D and Pascual-Leone A 2001 Abnormalities of spatial and temporal sensory discrimination in writer's cramp *Movement disorders : official journal of the Movement Disorder Society* **16** 94-9

Scales D A and Collins G H 1972 Cerebral degeneration with hypertrophy of the contralateral pyramid *Archives of neurology* **26** 186-90

Scheidt R A and Ghez C 2007 Separate adaptive mechanisms for controlling trajectory and final position in reaching *Journal of neurophysiology* **98** 3600-13

Scontrini A, Conte A, Defazio G, Fiorio M, Fabbrini G, Suppa A, Tinazzi M and Berardelli A 2009 Somatosensory temporal discrimination in patients with primary focal dystonia *Journal of neurology, neurosurgery, and psychiatry* **80** 1315-9

Shadmehr R and Wise S P 2005 (Cambridge, MA: MIT Press) pp 1-18

Shatz C J and Stryker M P 1978 Ocular dominance in layer IV of the cat's visual cortex and the effects of monocular deprivation *The Journal of physiology* **281** 267-83

Sitburana O and Jankovic J 2008 Focal hand dystonia, mirror dystonia and motor overflow *Journal of the neurological sciences* **266** 31-3

Song S, Miller K D and Abbott L F 2000 Competitive Hebbian learning through spike-timing-dependent synaptic plasticity *Nature neuroscience* **3** 919-26

Soska K C, Galeon M A and Adolph K E 2012 On the other hand: overflow movements of infants' hands and legs during unimanual object exploration *Developmental psychobiology* **54** 372-82

Suminski A J, Rao S M, Mosier K M and Scheidt R A 2007 Neural and electromyographic correlates of wrist posture control *Journal of neurophysiology* **97** 1527-45

Taub E, Griffin A, Nick J, Gammons K, Uswatte G and Law C R 2007 Pediatric CI therapy for stroke-induced hemiparesis in young children *Developmental neurorehabilitation* **10** 3-18

Taub E, Uswatte G and Pidikiti R 1999 Constraint-Induced Movement Therapy: a new family of techniques with broad application to physical rehabilitation--a clinical review *Journal of rehabilitation research and development* **36** 237-51

Tinazzi M, Frasson E, Bertolasi L, Fiaschi A and Aglioti S 1999 Temporal discrimination of somesthetic stimuli is impaired in dystonic patients *Neuroreport* **10** 1547-50

Trompetto C, Avanzino L, Marinelli L, Mori L, Pelosin E, Roccatagliata L and Abbruzzese G 2012 Corticospinal excitability in patients with secondary dystonia due to focal lesions of the basal ganglia and thalamus *Clinical neurophysiology : official journal of the International Federation of Clinical Neurophysiology* **123** 808-14

Valero-Cuevas F J, Yi J-W, Brown D, McNamara R V, Paul C and Lipson H 2007 The tendon network of the fingers performs anatomical computation at a macroscopic scale. *IEEE transactions on biomedical engineering* **54** 1161-6

van Doornik J, Kukke S and Sanger T D 2009 Hypertonia in childhood secondary dystonia due to cerebral palsy is associated with reflex muscle activation *Movement disorders : official journal of the Movement Disorder Society* **24** 965-71

Vandermeeren Y, Bastings E, Fadiga L and Olivier E 2003 Long-latency motor evoked potentials in congenital hemiplegia *Clinical neurophysiology : official journal of the International Federation of Clinical Neurophysiology* **114** 1808-18

Vidailhet M, Vercueil L, Houeto J L, Krystkowiak P, Benabid A L, Cornu P, Lagrange C, Tezenas du Montcel S, Dormont D, Grand S, Blond S, Detante O, Pillon B, Ardouin C, Agid Y, Destee A, Pollak P and French Stimulation du Pallidum Interne dans la Dystonie Study G 2005 Bilateral deep-brain stimulation of the globus pallidus in primary generalized dystonia *The New England journal of medicine* **352** 459-67

Weise D, Schramm A, Stefan K, Wolters A, Reiners K, Naumann M and Classen J 2006 The two sides of associative plasticity in writer's cramp *Brain : a journal of neurology* **129** 2709-21

Wiesel T N and Hubel D H 1963 Single-Cell Responses in Striate Cortex of Kittens Deprived of Vision in One Eye *Journal of neurophysiology* **26** 1003-17

Wiesel T N and Hubel D H 1965 Comparison of the effects of unilateral and bilateral eye closure on cortical unit responses in kittens *Journal of neurophysiology* **28** 1029-40

Young S J, van Doornik J and Sanger T D 2011 Finger muscle control in children with dystonia *Movement disorders : official journal of the Movement Disorder Society* **26** 1290-6